DISS. ETH NO. 21804

Adaptive-twist airfoils based on variable stiffness

A thesis submitted to attain the degree of
DOCTOR OF SCIENCES of ETH ZURICH
(Dr. sc. ETH Zurich)

presented by
WOLFRAM RAITHER
MSc ETH in Mechanical Engineering
born on 14th August 1984
citizen of Germany

accepted on the recommendation of
Prof. Dr. Paolo Ermanni, examiner
Prof. Dr.-Ing. Horst Baier, co-examiner
Dr. Andrea Bergamini, co-examiner

2014

Abstract

This doctoral thesis presents a new structural concept for shape-adaptable airfoils based on adjustable elastic twist. The adaptive-twist concept rests upon the idea that stiffness changes in the load-carrying structure of an airfoil put into effect by an integrated smart material can be utilised to induce variations in the airfoil's shear centre location and torsional stiffness that allow for controllable bending-twist coupling. No actuators are required in such a system, since aerodynamic loads are exploited to realise shape adaptations. This semi-passive approach, in which energy has to be spent only for the activation of the smart material that effects the changes in stiffness, promises high energy and lightweight efficiency, not least by the high degree of structural integration resulting from its compliant and smart nature.

Theoretical and experimental investigations of this dissertation evolve from the local level of the smart material and interface, carrying over the findings to the level of the adaptive wing box and, finally, to the global one of the adaptive airfoil. Two different smart material systems relying on temperature-controlled polymeric glass transition and voltage-regulated electrostatic adhesion are considered.

Based on the analytical foundation of the structural concept and on the examination of the smart materials and interfaces, a comprehensive analytical, numerical and experimental investigation of adaptive wing box structures, which represent the constitutive element of the adaptive-twist concept, is performed, showing the effectiveness of the elastic working principle. Building upon the results of this study, a structural design for the adaptive-twist airfoil is devised. The results obtained by numerical simulation and static testing of experimental airfoil structures based on this design demonstrate the structural concept to be effective when applied in a realistically sized wing structure. By numerical scalability investigations on the basis of aeroelastic simulations considering the dimensions and flight conditions of a wing of a glider plane the proof of concept in an application-oriented environment is accomplished. For certain upscaled configurations changes in lift coefficient of the same order of magnitude as the ones of conventional wing attachments can be achieved by the novel airfoil concept, for which also the

feasibility of aeroelastically stable designs is demonstrated.

An applicability survey highlights the strong dependence of the performance of the adaptive-twist airfoil on the smart material system employed. Very different, contrary characteristics of the two materials investigated are revealed. Regardless of this, an application of the adaptive-twist concept for functions that either require only few adaptations under constant loading or allow for lift alleviation during operation is considered feasible.

Implying a design philosophy of variable, and notably reduced, stiffness for lightweight structures, the proposed structural concept represents an alternative conception to the paradigm of stiffness maximisation of classical lightweight design.

Zusammenfassung

Die vorliegende Dissertation behandelt ein neuartiges Strukturkonzept für formveränderliche Tragflügel, welches auf elastischer Verdrillung basiert. Dieses Konzept baut auf der Idee auf, dass Steifigkeitsänderungen in der lasttragenden Struktur einer Tragfläche, die mittels eines integrierten smarten Werkstoffes realisiert werden, für eine variable Schubmittelpunktlage und Torsionssteifigkeit und damit für eine adaptive Biegetorsionskopplung eingesetzt werden können. Ein solches System benötigt keine Aktuatoren, da aerodynamische Lasten für die Formänderungen genutzt werden. Dieser semipassive Ansatz, bei welchem nur für die Aktivierung des smarten Materials zur Steifigkeitsänderung Energie aufgewandt werden muss, verspricht eine hohe Energie- und Leichtbaueffizienz, nicht zuletzt durch den mit der Nachgiebigkeit und dem smarten Werkstoff einhergehenden hohen Integrationsgrad.

Die theoretischen und experimentellen Untersuchungen dieser Doktorarbeit gehen von der lokalen Ebene des smarten Werkstoffes und der smarten Schnittstelle aus. Von dort werden die Ergebnisse auf die Ebene des adaptiven Flügelkastens und schliesslich auf die globale Ebene des adaptiven Tragflügels übertragen. Zwei verschiedene smarte Materialsysteme werden betrachtet: Während das eine auf dem temperaturgesteuertem Glasübergang polymerer Werkstoffe basiert, besteht das Wirkprinzip des anderen in spannungsgesteuertem, elektrostatisch induziertem Kraftschluss.

Aufbauend auf der analytischen Begründung des Strukturkonzepts und auf der Charakterisierung der smarten Werkstoffe und Schnittstellen wird eine umfangreiche analytische, numerische und experimentelle Untersuchung der adaptiven Flügelkastenstrukturen durchgeführt, welche das konstitutive Element des vorgeschlagenen Konzeptes darstellen. Auf diese Weise kann die Wirksamkeit des elastischen Wirkprinzips aufgezeigt werden. Auf der Grundlage der Ergebnisse dieser Studie wird die Konstruktion einer adaptiven Tragfläche ausgearbeitet. Die Resultate numerischer Simulationen und statischer Strukturversuche an Flügelstrukturen, in welchen diese Konstruktion realisiert ist, zeigen die Effektivität des Strukturkonzepts für eine realistisch ausgelegte Tragfläche. Numerische Skalierbarkeitsuntersuchungen

mittels aeroelastischer Simulationen, welchen die Abmessungen und Flugbedingungen des Tragflügels eines Segelflugzeugs zugrunde liegen, erlauben den Machbarkeitsnachweis unter anwendungsnahen Bedingungen. Für bestimmte hochskalierte Konfigurationen erreicht das neuartige Flügelkonzept Auftriebsänderungen, die in ihrer Grössenordnung denjenigen konventioneller Klappensysteme entsprechen. Auch die Machbarkeit aeroelastisch stabiler Auslegungen wird in diesem Zusammenhang gezeigt.

Eine Untersuchung der Anwendbarkeit des Konzepts hebt hervor, dass die Leistungsfähigkeit der Tragfläche mit adaptiver Verdrillung stark vom verwendeten smarten Materialsystem abhängt, wobei die beiden untersuchten Werkstoffe sehr verschiedene, gegensätzliche Eigenschaften erkennen lassen. Unabhängig hiervon wird ein Einsatz des Strukturkonzeptes für Anwendungen, die entweder eine geringe Zahl von Aktivierungen unter Last erfordern oder eine Entlastung während des Betriebs erlauben, als realisierbar erachtet.

Das vorgeschlagene Strukturkonzept impliziert eine Konstruktionsphilosophie, für die Änderungen und insbesondere Minderungen der Struktursteifigkeit konstitutiv sind. Auf diese Weise repräsentiert es einen Gegenentwurf zum Paradigma der Steifigkeitsmaximierung, welches den klassischen Leichtbau auszeichnet.

Preface

The work summarised in this doctoral thesis was carried out between September 2010 and December 2013 at the Centre of Structure Technologies (now Laboratory of Composite Materials and Adaptive Structures) of ETH Zurich. I would like to express my gratitude to those that contributed, in that environment as in others, to make the work contained in this book possible.

My sincere thanks go to Prof. Dr. Paolo Ermanni, my doctoral father, for the strong and continuous support he dedicated to this dissertation. I am grateful to Dr. Andrea Bergamini who supervised my project in the most committed way and to whom I owe many inspiring suggestions and discussions. Also, I want to thank Prof. Dr.-Ing. Horst Baier for his interest in my work and his valuable advice as a co-examiner.

Many thanks go as well to my colleagues at ETH for their appreciated help and for the good time spent together. Moreover, the students that contributed to this project by their theses shall be acknowledged.

Finally, I want to mention those that stand out in the list of this section and that shall receive my most personal thanks: My parents—and Caroline, my beloved companion.

Contents

Symbols and abbreviations

Symbols

Latin characters[1]

A	Area
$\mathbf{A}_\mathrm{D}$	Aerodynamic damping matrix
$\mathbf{A}_\mathrm{K}$	Aerodynamic stiffness matrix
$\widehat{\mathbf{A}}_\mathrm{K}$	Modal aerodynamic stiffness matrix
$\mathbf{A}_\mathrm{M}$	Aerodynamic inertia matrix
$\mathbf{a}$	Vector containing degrees of freedom
$\widehat{\mathbf{a}}$	Modal displacement vector
B	Primary width
$\mathbf{B}$	Modal matrix
b	Secondary width
C	Specific heat capacity, or constant (with subscripts "1" and "2")
C_el	Electric capacitance
c	Chord length
c_L	Lift coefficient of a wing
c_l	Lift coefficient of a wing section
c_{M_roll}	Roll moment coefficient of a wing
c_m	Moment coefficient of a wing section
c_{m0}	Zero-lift moment coefficient of a wing section
d	Offset
E	Young's modulus
$\mathbf{E}$	Electric field
$\hat{E}$	Relative interface modulus
$\widetilde{EC_\mathrm{W}}$	Warping stiffness
$\widetilde{EI_y}$	Flexural stiffness
e	Euler's number
F	Tension force

[1] Subscripts attached to characters are listed separately below.

G	Shear modulus
$\widetilde{GI_t}$	Torsional stiffness
g	Gravitational acceleration
H	Primary height
h	Secondary height
I	Moment of inertia
i	Imaginary unit
K	Stiffness matrix
$\widehat{\mathsf{K}}$	Modal stiffness matrix
k	Number of selected eigenmodes
L	Length
l	Lift per unit span
l_w	Warping length
M	Moment
M	Mass matrix
$\widehat{\mathsf{M}}$	Modal mass matrix
m	Mass
m_x	Pitching moment per unit span
n	Number of degrees of freedom
p	Eigenvalue
Q	Transverse shear force
Q_{el}	Electric energy
Q_{th}	Thermal energy
q	Dynamic pressure
S	Static moment
s	Circumferential coordinate
T	Temperature
t	Thickness
U	Voltage
u	Displacement in x-direction
V	Volume
v	Flow speed
w	Displacement in z-direction
$\bar{w}$	Sectorial area
x, y, z	Cartesian coordinate directions

Greek characters[2]

α	Angle of attack
β	Laminate stiffness
ε	Permittivity
θ	Lamination angle
μ	Coefficient of friction
ν	Poisson's ratio
σ	Normal stress
τ	Shear stress
ρ	Mass density
Φ	Tip twist angle ratio
ϕ	Twist angle

Subscripts

0	Enclosed, or centre, or vacuum
11	Flexural
22	Torsional
a	Antimetric
b	Bending
CP	Centre of pressure
c	Closed
d	Dielectric
div	Divergence
e	Electrode
f	Flange
fs	Front spar
flut	Flutter
g	Glass transition, or gap
i	Inner, or interface
j	Integer variable
M	Maxwell
m	Mean
max	Maximum
min	Minimum

[2]Subscripts attached to characters are listed separately below.

NP	Neutral point
o	Open, or outer, or overlap
p	Protrusion
r	Relative, or rib
rs	Rear spar
SC	Shear centre
s	Shear, or symmetric, or skin
t	Twist
te	Trailing edge
w	Warping, or web
wb	Wing box

Abbreviations

AFRP	Aramide-fibre-reinforced polymer
CF	Carbon fibre
CFRP	Carbon-fibre-reinforced polymer
DMA	Dynamic mechanical analysis
EBL	Electro-bonded laminate
ETH	Eidgenössische Technische Hochschule
FE	Finite element
GFRP	Glass-fibre-reinforced polymer
NACA	National Advisory Committee for Aeronautics
PVC	Polyvinyl chloride

1 Introduction

1.1 At once compliant, strong and lightweight—the design conflict of shape-adaptable airfoils

The design space of shape-adaptable airfoils is characterised by pronounced constraints originating from conflicting requirements on these structures: On the one hand, they have to provide sufficient compliance in order to enable utilisable shape variations, and, on the other, a certain minimum stiffness is required to carry operational loads without excessive deformation. Besides the two opposed specifications of stiffness and compliance, being lightweight—a general need for aerospace structures—constitutes an additional contrary requirement, exacerbating the conflict of aims in the design of shape-adaptable airfoils.

This design problem can be illustrated by means of a requirement triangle [1] as shown in figure 1.1, whose vertices represent the three mentioned crucial requirements. Each of the triangle's edges represents a group of design solutions which respectively fulfil two of the requirements but do not meet the third one. They can be recognised in three established classes of structural design, which even have to be considered as design philosophies in this context: *lightweight structures*, which are usually optimised for low mass and high stiffness and which thus cannot provide articulate compliance, conventional *rigid-body mechanisms*, that combine shape adaptivity with load-carrying capability but generally suffer from high weight, and *compliant mechanisms*, which are shape-adaptable and light but lack good load-carrying qualities.

While lightweight structures and rigid-body mechanisms represent the industrial standard for the design of airfoils and their discrete attachments for shape changes, respectively, compliant systems have been widely proposed as solutions for less conventional designs of shape-adaptive airfoils. Based on the previous discussion, it has to be stated however that, from a conceptional point of view, none of the three design strategies permits to find solutions effectively close to the optimum given by a design reconciling all the three specifications. Indeed, the compromise-driven nature of many design con-

cepts proposed for shape-adaptable airfoils has its origin in this fact.

Overcoming the limitations of conventional approaches to the solution of the design problem of shape-adaptable airfoils calls for a novel design philosophy, and in the present doctoral thesis, *variable-stiffness design* is proposed as such. It can be directly concluded from the problem statement above that, in principle, a lightweight structure with time-variable stiffness, adapting its rigidity to varying operating conditions, allows to meet all of the three crucial requirements, justifying its placement in the centre of the requirement triangle.

As the establishment of a design philosophy based on intentional variations, and particularly reductions, in structural stiffness of primary components would constitute a kind of paradigm shift in the culture of lightweight design, which bases upon the concept of equivalence of minimising weight and maximising stiffness [2–4], the adaptive-stiffness idea will be further motivated in the following chapters.

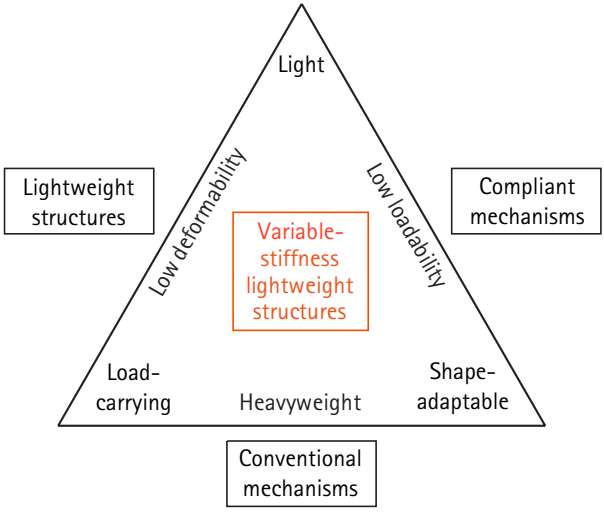

Figure 1.1: Requirement triangle (extended based on [1])

1.2 State of research

1.2.1 Design of shape-adaptable airfoils

Figure 1.2: Examples for the difference in shape adaptivity of birds and state-of-the-art airplanes: Brant goose (Branta bernicla) during flight [5] contrasted with flaps and ailerons of an Airbus A380 [6]

Up to date, the industrial state of the art of shape adaptation in wings of airplanes and rotor blades of helicopters and wind turbines is represented by rigid-body attachments (figure 1.2, right). Motivated by their aerodynamic and lightweight potential and often inspired by the flight of birds (figure 1.2, left) [7–9], design concepts relying on continuous geometrical changes have been proposed as alternative designs for airfoils for a long time. While early conceptions of smoother shape adaptation were relying on classical metal structures with differential design and rigid-body mechanisms, this kind of machinery was progressively abandoned in favour of composite, more integral, compliant and smart designs and the term "*morphing*" has been coined to characterise these novel strategies. Figure 1.3 gives an impression of the historical development of the technological state undergone by the conceptions of shape-adaptable airfoils. To some extent, this development goes along with the general progress in aerospace technology, to another it seems to go far beyond, leading to an increasing technological difference between commercial wing design and morphing wing research.

Originating from "metamorphosis", morphing generally refers to changes "of the form or nature of a thing (...) into a completely different one" [10] and, in the particular context of adaptive airfoils, to "any nontraditional method" providing "large changes in span, wing area, chord, etc." of "the

order of 100%" [11]. The analysis of the state of research in this chapter focuses on these morphing airfoils.

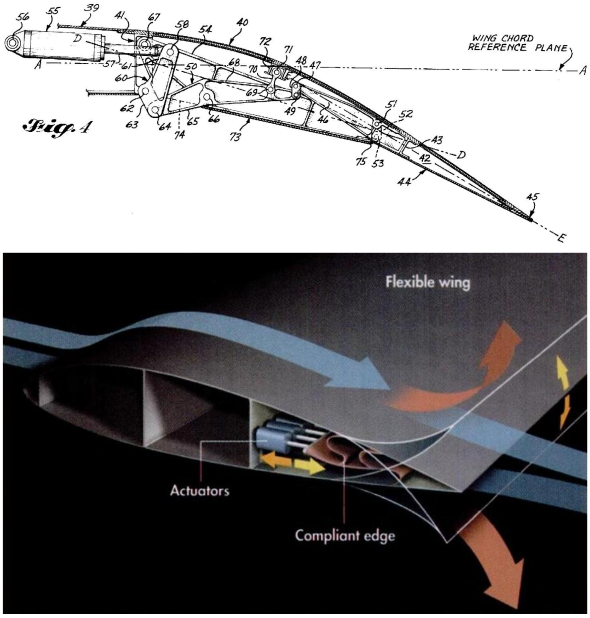

Figure 1.3: Examples for the historical development of conceptions of shape-adaptable airfoils: patent drawing of camber mechanism from 1977 [12] and visualisation of a flexible morphing wing from 2003 [13]

In literature reviews or taxonomies dealing with morphing airfoils [14–21] the usual classification criteria consist in the adaptive properties (span, chord, sweep, camber, twist, dihedral, etc.), in the respective superordinate classes of these (in-plane, out-of-plane, profile, etc.) and in the purposes of morphing (performance, control, propulsion). Instead of these criteria relevant at the flight vehicle's system level, the crucial characteristics from a point of view of structural design, for which the aforementioned properties are often fixed, are the three following ones: *energy concept* (active or passive), *kinematics* (rigid or compliant) and *effectuator* (conventional or smart) [22]. Like there are three decisive requirements for the design of shape-adaptable airfoils, there

are thus also three crucial criteria for their classification which are introduced and explained in the following paragraphs.

Active structures have been characterised as containing "sensors and/or actuators that are highly integrated into the structure and have structural functionality" [23]. At this point, however, they are clearly defined as structures whose properties can be changed by supply of energy from a designated supply. For the special case of active structures with adaptable shape this applies to the energy that has to be spent for the change in shape. On the other hand, *passive structures* are characterised by the absence of a designated energy supply for a change in their properties (particularly in shape), which means that they extract energy from the environment. Finally and correspondingly, *semi-active* or *semi-passive structures*—depending on the speaker's intention to relate them more to the one or the other class—draw energy partly from a provided supply and partly from the environment.[1]

In contrast to *conventional kinematics*, which are based on relative rigid-body motion between assembled parts, *compliant kinematics*, which have already been spoken of in section 1.1, rely on material strain. While these two active principles can be clearly distinguished from each other and a certain mechanism can thus be uniquely attributed to one of the two kinds of kinematics, this attribution is often more difficult for the whole structural system, as some structural concepts involve mechanisms of both classes. It is therefore appropriate to refer to this latter kind of kinematics as *hybrid* when speaking about the way of shape adaptation of a certain design.[2]

The *effectuator*, the third of the crucial criteria for the characterisation of a shape-adaptable airfoil, denotes the entity that induces a change in the properties of an adaptive structure. In case of an active system, it is usually constituted by the actuator. A distinction between the two expressions is needed, however, as the term "actuator" cannot be applied for passive and some semi-passive/semi-active structures due to its implication of an active nature. Generally, the effectuator transforms energy from a certain domain into—mainly—the mechanical one and for variable-stiffness effectuators these

[1] Naturally, this energetic consideration may depend on how the system boundaries are drawn: Whereas for example, following this definition, a system consisting of an energy-harvesting device and an actuator driven by the harvester has to be called passive at the system level, as it is energetically autonomous, it has to be characterised as active when considering the subsystem level of the actuator, for which the harvester's energy output represents a designated energy supply.

[2] As an example, the kinematics of the airfoil design known as horn concept [24,25] or eccentuator concept [26] would have to be characterised as hybrid, since they rely on both rigid-body rotation and structural strain.

domains will be elaborated on in section 1.2.2. However, a transition between energy domains is not a sine qua non for effectuators, especially when passive systems are concerned. The decisive criterion for the assessment of an effectuator from the design point of view is related to its nature which can be conventional or *smart*.

In 1996, the results of a survey among researchers on the definition of the terms "smart material" and "smart structure" have been published, showing "that there is a wide range of sometimes incompatible viewpoints that all consider themselves to be consistent with smart materials and structures" [27]. Also the literature analysis presented in this terminological contribution has shown the variety of definition attempts and up to date no clear consensus seems to be established in this matter. Instead of applying the general definition proposed in [27] based on this analysis, in the doctoral thesis on hand, a smart effectuator is therefore explicitly—and intentionally focussing on structural design aspects—defined as an effectuator which causes a change in mechanical properties by transducing energy from a certain non-mechanical domain to the mechanical one and which is highly integrated in the structure in the sense of an adoption of structural functionality. Accordingly, the term "smart structure" refers to a structure in which at least one smart effectuator is applied to fulfil a main function. Non-smart effectuators are called conventional. Due to the integrability specification in the definition above, "smart effectuator" and "smart material" can be considered as equivalent terms.

Some important general characteristics of adaptive structural systems can be deduced from the classification according to the three presented criteria. First, the active or passive character of a structural concept largely influences its energy consumption. Here, passive or semi-active systems have an advantage over active ones due to their capability of utilising energy from the environment. Moreover, their smaller dependence from an external energy supply has a favourable effect on the reliability and the degree of complexity of passive and semi-active designs. On the other hand, active systems provide more flexibility and often also higher adaptation authority [28].

Second, compliant mechanisms have several conceptional advantages over conventional ones, which result from their integrated design instead of a differential one: They are lightweight, provide smooth kinematics, are characterised by the absence of wear, play, noise and particle release, and they allow not only for lower costs for manufacturing and assembly but also for a reduced complexity and need of maintenance with respect to their rigid-body competitors. On the other hand, conventional mechanisms benefit from es-

pecially high compliance in direction of their degrees of freedom, from load-independent kinematics and from their ability to provide high stroke [1, 29].

Third, smart materials permit a higher lightweight efficiency when compared to conventional effectuators, since they are more integrated in the load-carrying structure and, furthermore, integration permits a multifunctional design of the smart effectuators in some cases. Not all of the smart materials are competitive to conventional solutions in terms of stress, energy and power density, maximum strain, bandwidth, energy efficiency or load-carrying capability, but, when making such comparisons, the substantial difference in the technological level of maturity of both classes of effectuators should be kept in mind.

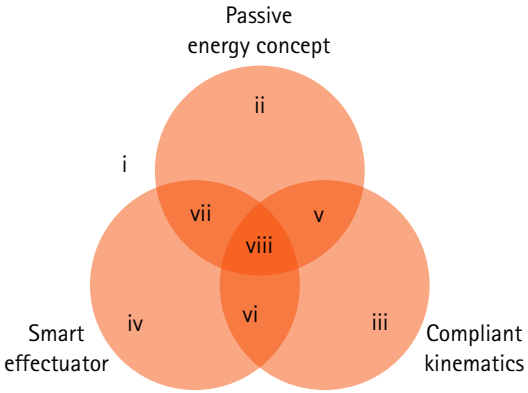

Figure 1.4: Diagram for the classification of the structural design of shape-adaptable airfoils

The diagram in figure 1.4 illustrates the classification scheme based on the described three criteria. It rests upon three circles which display the status of the three criteria for a certain design. If a design exhibits the—for the case of shape-adaptable airfoils—less conventional property with regard to one of the criteria, i. e. passive energy concept, compliant kinematics or smart effectuator, it belongs to the subset of designs represented by the respective circle. Accordingly, the intersections of two and three circles contain designs displaying two and all three of the mentioned properties, respectively. Some distinct classes of shape-adaptable airfoil designs can be identified in this diagram: Class i does not belong to any of the subsets defined by the three

circles. This class comprises active systems with rigid-body kinematics and conventional actuators, which are placed outside the diagram's circles and represent the most conventional kind. Classes ii–iv, three groups of concepts which differ from the ones of class i in a single criterion, can each be represented by one circle. Classes v–vii, three kinds of systems that have only one of the criteria in common with the ones of class i, can be attributed to an intersection of two circles. Correspondingly, passive designs with compliant kinematics and smart materials, which are farthest away from traditional airfoil structures in terms of the decisive properties and which thus represent the least conventional solutions, are placed in the intersection of all three circles as class viii. All in all, the degree of conventionality of a certain structural design is related to the colour intensity of its representation in the diagram, if it is illustrated, like in figure 1.4, in the intuitive way known from the overlay of colour filters.

Many of the design concepts which have been proposed in reality for shape-adaptable airfoils can be attributed to one of these abstractly introduced classes: Class i represents the industrial state of the art. Class ii can be identified, for example, in structural concepts in which (semi-)passive morphing is achieved by a stiffness change resulting from rigid-body motion of internal structural elements which is induced by conventional actuators [30–44]. As examples of class iii, airfoil structures with compliant skin and/or internal structure as presented in [45–47] can be mentioned, if they are equipped with a conventional actuator. Segmented airfoil concepts with smart actuation as, for example, proposed in [48] represent class iv, and class v can be recognised in compliant wing and rotor blade structures with passive, purely mechanical shape adaptation (so-called *aeroelastic tailoring*) [49] as well as in some of the concepts preliminarily investigated in [50]. Class vi, on the other hand, has become manifest in the numerous design proposals (e. g. [51, 52]) for compliant morphing airfoils with smart actuation. Smart, compliant airfoils that exploit aeroelastic coupling effects (and particularly aeroelastic instabilities) and thus contain a passive component can be attributed to class viii, which is farthest away from common solutions in terms of the considered criteria and represented by the intersection of all three circles in the centre of the design diagram. From the aeroelastic point of view, this usually semi-active approach is paradoxically referred to as *active aeroelasticity* [53, 54].[3] Being semi-passive, compliant and smart, the structural concept investigated in the dissertation on hand also belongs to this most

[3] Accordingly, non-compliant and non-smart "active aeroelastic" concepts like the one reported in [55] should also be mentioned as semi-passive approaches belonging to class ii.

unconventional class.

1.2.2 Adaptive structural stiffness

Whereas the idea of time-variable stiffness originates from structural dynamics [56, 57], where it has been and is being utilised for vibration control, more and more variable-stiffness applications for shape adaptation in general and airfoil morphing in particular are being observed. The literature analysis contained in the following discussion is limited to the latter group related to variable static stiffness that is of interest for this dissertation.

The effectuators which come into consideration for controlling a structure's mechanical properties are—besides conventional actuators and passive mechanical effectuators—given by the subset of smart materials related to the mechanical domain. These are illustrated, as a specialisation of the considerations in [58, 59], in figure 1.5. In general, variations in a certain elastic stiffness component of a structural system can be achieved by affecting at least one of the following properties: the material's elastic properties, the structure's topology, its geometry and its elastic boundary conditions.[4] Since all the smart materials shown in figure 1.5 have effects in the mechanical domain, all of them can in principle be applied to influence certain of these characteristics and can thus be considered as candidate effectuators for variable structural stiffness.

A comprehensive literature review of scientific contributions dealing with adaptive stiffness is not within the scope of this introductory chapter and can be left, at least as far as morphing applications are concerned, to a recent review article [60]. Instead, the approach of structural design with variable stiffness, which has already been motivated in section 1.1, shall be introduced by means of selected examples from the field of shape adaptation, situating the structural concepts proposed in the present doctoral thesis in a broader context.

Beginning from purely mechanical, passive approaches to adaptive structural stiffness, the design of a ski with progressive flexural rigidity (figure 1.6) can be quoted as an example for the commercial application of variable static stiffness. This ski is based on a stiffener ("upper deck") which is connected to

[4] This consideration holds for linear elastic structures, while in nonlinear systems the stiffness depends also on the deformation. For structures with variable stiffness based on static instabilities this amendment is relevant, since in such systems the instabilities' nonlinear nature is utilised. As stiffness variations resulting from structural nonlinearities are however tied to shape changes, they can be subsumed under the geometry category, so that the given list does not have to be extended.

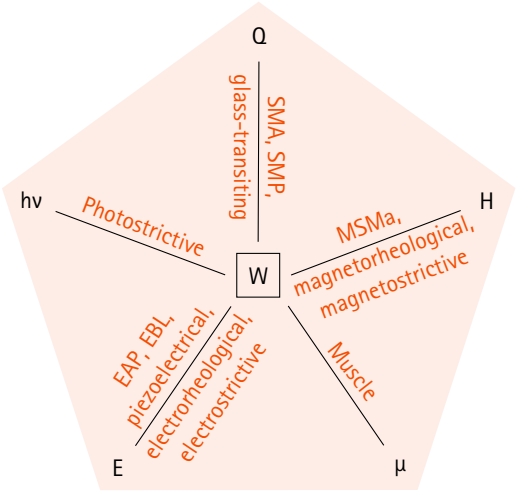

Figure 1.5: Diagram (modified based on [58, 59]) for the classification of smart materials exploiting the interaction of certain physical domains (E: electrical, H: magnetical, hv: optical, μ: chemical, Q: thermal) with the mechanical one (W).

the base ski ("lower deck") by means of sliders allowing for a certain longitudinal play. Above a certain curvature of the ski, the sliders, which are fixed to the lower deck, interlock with the stiffener, resulting in an increased bending stiffness which is desired at higher deflections for performance reasons. This concept is characterised by hybrid kinematics, since it relies both on elastic strain in base ski and stiffener and on relative motion between these components. In terms of its adaptive shear load transfer between the two decks, it can be considered as similar to some of the smart variable-stiffness approaches introduced later.

Another class of variable-stiffness concepts within the mechanical domain is constituted by systems utilising static instabilities. While a decrease in stiffness can be usually reached passively (by exploiting external loads), active parts are sometimes added for controlling the structure and, particularly, resetting it to a stable state. Varying widely in scale and applications envisaged, proposed solutions reach from material concepts like so-called fluidic flexible matrix composites [62, 63] or adaptively pressurised sandwich cores

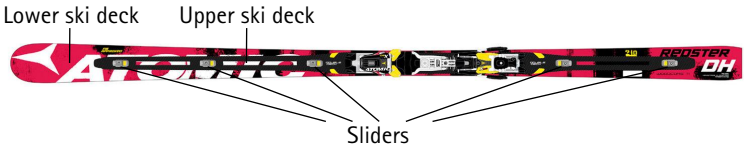

Figure 1.6: Example for the commercial use of a variable-stiffness technology: Ski with passively adaptive bending rigidity (image modified based on [61])

[64,65] to the structural design of a compliant shape-adaptable wing involving actuators with buckling beams and pneumatic reset [66] or morphing concepts based on multistability of structural elements, like the compliant bistable flap presented in [67].

As a concept which is more closely related to the approach pursued in this dissertation, the idea of stiffness control by means of adaptive shear stress transfer between the plies of a multilayer material has to be mentioned, which has been investigated in an electromechanical as well as in a thermomechanical configuration. Referring to the first one, capacitor-like stacks of electrodes and dielectrica have been proposed [59,68–70]. In this smart material termed "electro-bonded laminate" (EBL), controlling the voltage between the electrodes allows to influence the interlaminar adhesion, thus the topology and finally stiffness components like the laminate's bending stiffness. The corresponding thermomechanical system is given by a laminate consisting of structural layers spaced out by polymeric plies of variable temperature and has been investigated in [71–73]. In this case, the driving influence is, instead of the topology, the temperature-dependent modulus of the polymer (especially around the glass transition). Both kinds of multilayer materials, which can be applied for semi-passive shape adaptation and which can be considered as smart, compliant and more continuous versions of the concept the ski mentioned before is based on, are explained in greater detail in sections 4.1 and 5.1.

A group of structural concepts for semi-active shape control of aerodynamic surfaces by means of variable stiffness rests upon the application of rigid-body mechanisms: Triggered by findings on the potential of stiffness variation for flight control [74], wing structures with controllable elastic characteristics (like shear centre location and torsional stiffness) by virtue of rotary [30,32–35] or movable [32–35,40–43] spars have as well been proposed as a vertical tail equipped with a mechanism with adjustable twisting rigidity

[31, 35, 75, 76]. Using machinery like hinges, bearings or linear guides, all these approaches suffer from the general drawbacks of rigid-body kinematics explained in the context of the requirement conflict in sections 1.1 and 1.2.1. Moreover it should be mentioned that in these concepts, except from some based on spar rotation, the airfoil's topology remains unchanged, so that only relatively low changes in torsional stiffness are obtained.

The working principle which the design of a wing box for semi-passive twist reported in [36–39, 44] is based on has close similarities to the one investigated in the dissertation on hand: Both concepts utilise the variations in torsional stiffness and twisting moment evolving from changes in the topology of an airfoil structure, namely from opening and (re-)closing of spars. Instead of the integrated smart materials suggested for the latter, however, the former relies on a clutch actuated by conventional pneumatic jacks.

Potential applications of controllable twist, which is the objective of most of the presented variable-stiffness airfoils, range from flight control to load alleviation and adaptive lift-to-drag ratio. Concerning the last item, it has been pointed out e. g. in [77] that, due to the continuous change in wing loading by fuel consumption, an airplane with wing tanks and a bending-twist coupled wing can operate at its design lift coefficient only for a single instant during a flight. Already this fact motivates time-variable elastic properties and calls for an "*adaptive aeroelastic tailoring*" as proposed in the present dissertation.

"Stiffer is better" [78]—this title of a lecture on automotive structural design is representative of the importance of rigidity as a major design criterion in many industrial sectors, and also the historical development of structural engineering has shown the continuous striving for higher (specific) stiffness to be constitutive especially for the design of lightweight structures. For many structural applications with constant geometry, a design with high stiffness is actually appropriate. For shape-adaptable lightweight structures, on the other hand, the requirement conflict characterised in section 1.1 motivates intentional reductions in stiffness, as the lightest design is not anymore generally given by the most rigid one in this case. The presented variable-stiffness approaches, like the contribution of the thesis on hand, ultimately also represent an alternative conception to the classical design philosophy described just before and should be understood also in this cultural context.

1.3 Objective and outline

From the analysis of the current state of research performed in the previous section, an explicit need for research on (semi-)passive shape-adaptable airfoils can be derived, since neither the integration of smart materials instead of differential conventional actuators nor the implementation of compliant kinematics replacing rigid-body mechanisms—not to mention the combination of both—have been addressed by preceding scientific work. It can further be concluded from the previous general discussion that an application of such alternative design strategies promises considerable advances with respect to state-of-the-art solutions in terms of performance, energy consumption and lightweight efficiency.

Certain steps towards the closure of these research gaps are thus approached by the present dissertation which aims at the development and demonstration of a compliant structural concept for a semi-passive morphing airfoil and contains for this purpose analytical, numerical and experimental investigations of the respective structural systems, implementing two kinds of smart materials.

The problem statement and the discussion of the current state of research of chapter 1 have lead to the identification of a research need on which, in turn, the formulation of the objectives of this doctoral thesis has been based. While chapter 2 is devoted to the analytical foundation of the working principle applied in this research project, chapter 3 is about the implementation of this idea in an airfoil structure. Chapters 4 and 5 present the numerical and experimental characterisation of the structural concept, investigating two kinds of smart variable-stiffness materials. The first of the considered adaptive material systems is based on the changes in elastic modulus that are induced by temperature variations in polymers in proximity of their glass transition. The second one aims at changes in mechanical topology which are put into effect by controllable electrostatic forces at a lap interface.

In both chapters on the implementation of adaptive-twist airfoils based on the proposed structural concept, the considerations follow the order of the steps taken for the implementation of the basic idea of this work: Beginning from the understanding of the working principle of the respective material concept, the local phenomena on the level of the smart interface can be investigated. This analysis, in turn, allows to conceive the meso behaviour of the wing box as the structural element which is constitutive for the adaptive capability of the novel wing design. Based on the findings on this level, the integration of the concept in a wing structure can be performed

and the airfoil's global characteristics can be analysed. The results obtained in this study are presented in chapter 6 with respect to the applicability of the adaptive-twist airfoil concept, before the dissertation concludes with the closing remarks and prospects of chapter 7.

2 Concept of adaptive twist by variable cross-sectional properties—working principle and analytical foundation

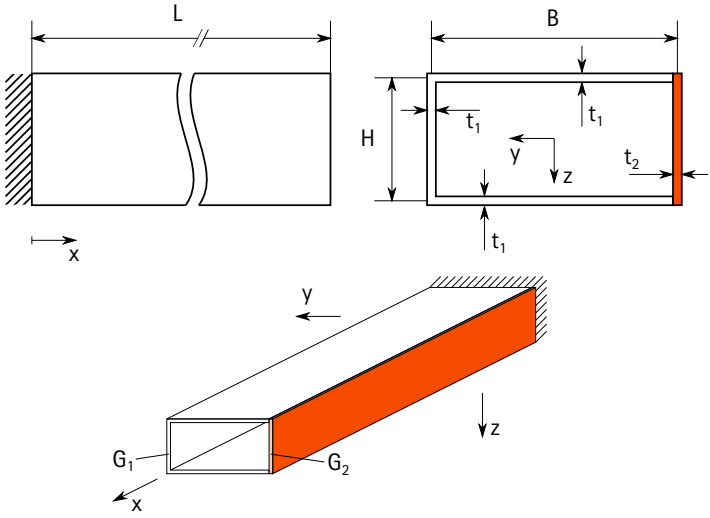

Figure 2.1: Geometry and coordinate system for beams with adaptive bending-twist coupling

The variable-stiffness approach to adaptive twist pursued in this research project is based on variations of a structure's cross-sectional properties resulting in changes in the twist angle when the structure is loaded. This concept of adaptive bending-twist coupling[1] is illustrated for the fundamental case

[1] The common, though actually imprecise, usage of the term "bending-twist coupling" also for the coupling of *transverse shear* and twist is adopted here.

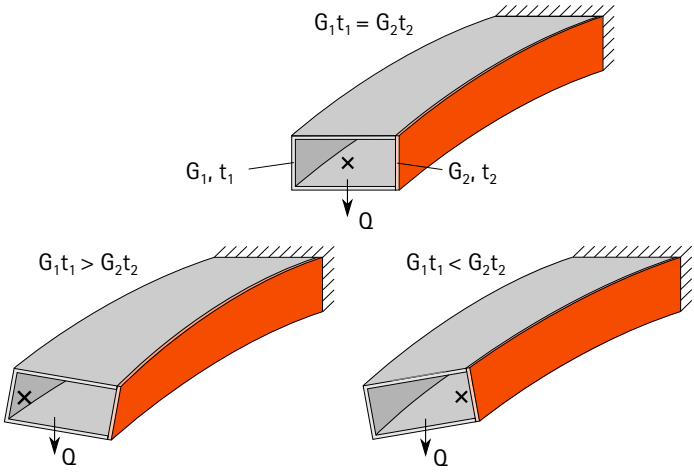

Figure 2.2: Working principle of profile beam with adaptive bending-twist coupling (shear centre location indicated by "x")

of a thin-walled profile beam with rectangular cross section (cf. [79]) in the following paragraphs.[2]

While the basic geometric quantities and the system of coordinates which will be referred to in the subsequent discussion are defined in figure 2.1, figure 2.2 presents the working principle for such a beam equipped with one variable-stiffness web and loaded by a transverse force Q in the centroid. The decisive property for the bending-twist coupling behaviour is given by the distribution of shear stiffness Gt over the cross section: For the case shown at the top of figure 2.2, in which the shear stiffness $G_2 t_2$ of the adaptive web on the right side of the profile (shown in orange) is equal to the shear stiffness $G_1 t_1$ of the rest of the profile, the section is doubly symmetric in terms of its elastic properties, its shear centre coincides with its centroid and no twist occurs for the considered loading. If, on the other hand, $G_1 t_1 > G_2 t_2$ as illustrated at the bottom left in the figure, the profile's shear centre is shifted along the y-axis and a torsional deformation of the beam in negative x-direction is observed. Accordingly, the beam is twisted in the opposite di-

[2] The considerations of this chapter are based on the usual assumptions of the theory of thin-walled beams. For a detailed specification see [79].

rection for the situation depicted at the bottom right, for which $G_1 t_1 < G_2 t_2$.

Varying the adaptive web's shear stiffness hence allows to tune the beam's bending-twist coupling behaviour, the limiting cases for infinitely low and infinitely high web stiffness (relative to the rest of the structure) being given by the open c-profile and the web itself, respectively. If instead of a continuous change in shear stiffness the topology of the web can be affected such that the profile can be opened and closed, a similar change in the coupling characteristics can be realised. In this case the discrete states of adaptation are given by the symmetrical rectangular box (if $G_1 t_1 = G_2 t_2$) and the opened section. For both ways, the one based on variable stiffness and the one based on variable topology, the shear centre location is not the only elastic property affected by changes of the web's state: Opening the cross section as well as sufficiently lowering the web stiffness also lead to a large drop in torsional stiffness, which is evident from a comparison of the respective expressions from the theory of thin-walled beams for a closed [80] and an open [81] cross section:

$$\widetilde{GI_{\mathrm{t,c}}} = \frac{4A_0^2}{\oint \frac{\mathrm{d}s}{Gt}}, \quad \widetilde{GI_{\mathrm{t,o}}} = \frac{1}{3}\sum_j G_j b_j t_j^3 \tag{2.1}$$

This reduction in torsional stiffness can be beneficially combined with the change in torsional moment induced by the shear centre shift in order to generate large twist angles. Further relevant stiffness characteristics like the flexural rigidity $\widetilde{EI_y} = \iint Ez^2 \,\mathrm{d}A$, in contrast, are much less dependant on the activation of the adaptive web, which explains the concept's promising character for controlling the bending-twist coupling.

In order to evaluate the bending-twist coupling behaviour of a beam, the deformation has to be separated in the deflection components related to bending (w_{b}), transverse shear (w_{s}) and twist about the shear centre (w_{t}), as shown in figure 2.3. The flexural contribution can be expressed by the following solution of the Bernoulli-Euler equation [82, 83]:

$$w_{\mathrm{b}} = \frac{QL^3}{6\widetilde{EI_y}}\left(-\frac{x^3}{L^3} + \frac{3x^2}{L^2}\right) \tag{2.2}$$

The shear component, on the other hand, is given by ([84])

$$w_{\mathrm{s}} = \frac{Q}{I_y^2}\int_s \frac{S_y^2}{Gt}\,\mathrm{d}s \cdot x \tag{2.3}$$

—where $S_y = \int_0^s zt\,\mathrm{d}s$ denotes the first moment of area—and the relation for the deflection due to a twist ϕ reads

$$w_\mathrm{t} = -\left(y_\mathrm{SC} - y\right)\tan\phi \tag{2.4}$$

In this expression y_SC represents the shear centre's horizontal location.

The twist of a beam resulting from a torsional moment M_t under presence of warping constraints can be described by the differential equation ([85,86])

$$\widetilde{EC_\mathrm{w}}\frac{\mathrm{d}^3\phi}{\mathrm{d}x^3} - \widetilde{GI_\mathrm{t}}\frac{\mathrm{d}\phi}{\mathrm{d}x} + M_\mathrm{t} = 0 \tag{2.5}$$

where $\widetilde{EC_\mathrm{w}} = \int_s E\bar{w}^2 t\,\mathrm{d}s$ denotes the section's warping stiffness and $\bar{w}$ is called sectorial area.

For a cantilever beam loaded by a transverse force at the horizontal position y_Q at the tip, the solution of equation 2.5 is given by

$$\begin{aligned}\phi \;=\; & \frac{Q\left(y_Q - y_\mathrm{SC}\right)}{\widetilde{GI_\mathrm{t}}}\left[x - l_\mathrm{w}\tanh\left(\frac{L}{l_\mathrm{w}}\right)\right. \\ & \left. + l_\mathrm{w}\tanh\left(\frac{L}{l_\mathrm{w}}\right)\cosh\left(\frac{x}{l_\mathrm{w}}\right) - l_\mathrm{w}\sinh\left(\frac{x}{l_\mathrm{w}}\right)\right]\end{aligned} \tag{2.6}$$

in which $l_\mathrm{w} = \sqrt{\widetilde{EC_\mathrm{w}}/\widetilde{GI_\mathrm{t}}}$.

These fundamental elastic relations form the basis for the analytical calculations and the evaluation of numerical simulations and experiments with structures having adaptive cross-sectional properties which are presented in chapters 4 and 5.

The considerations of the previous paragraphs assume that variations in bending-twist coupling are put into effect by continuous changes in shear stiffness of one of the profile's webs. Similar characteristics can however also be obtained by affecting a web's topology, i. e. by opening and (re-)closing the section, and under certain conditions the states resulting from these discontinuous changes in properties are equivalent to the limiting cases of the continuous system for infinitely low and infinitely high web stiffness, respectively. Whereas the first concept is applied in the dissertation on hand in the thermomechanical implementation reported in chapter 4, the second one can be recognised in the electromechanical approach of chapter 5.

In terms of their elastic couplings, unsymmetrical profile beams can be compared to anisotropic laminates that have been proposed for shape adapta-

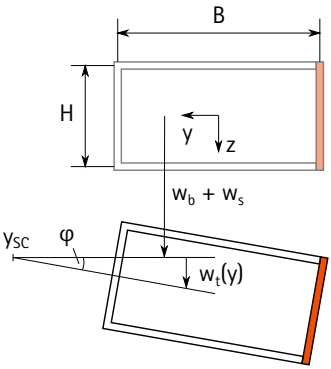

Figure 2.3: Deflection components related to bending, transverse shear and twist

tion based for example on bending-twist or extension-twist coupling [73,87]. In figure 2.4 the stiffness changes of a laminated plate with layup $[\theta_o;\theta_i]_s$ are contrasted to the ones of a non-symmetrical cross section like introduced before. In this diagram, the torsional stiffnesses β_{22} and $\widetilde{GI_t}$ of a CFRP laminate with material properties according to [73] and of a thin-walled profile beam with square cross section, respectively, as well as the respective ratios of torsional and flexural stiffness, β_{22}/β_{11} and $\widetilde{GI_t}/\widetilde{EI_y}$, are plotted against the outer lamination angle θ_o and the shear stiffness ratio G_2/G_1, respectively, that have a strong influence on the respective stiffness components. Concerning the laminate's inner ply angle, the value of $\theta_i = -56°$, which yields the highest torsional stiffness, has been selected for this plot, while the profile beam is assumed to have a homogeneous thickness.

Although this general consideration neglects important effects like shear deflection and warping constraints of the beam or a possible influence of the laminate's coupling stiffness, the following basic conclusions can be drawn: First, the relative changes in torsional stiffness that can be achieved with the profile beam in the chosen parameter range are much larger than the ones of the laminate; and, second, for the profile beam, the considered parameter affects the torsional stiffness much more than the flexural one, while the opposite holds for the laminated plate. It should be stressed that only the changes in cross-sectional stiffness of the profile have been accounted for in this analysis, while in a three-dimensional beam structure a considerable

twist due to the mentioned shear centre shift can be additionally exploited, which increases the difference between the two approaches even more. For an application like the adaptive-twist airfoil, in which substantial changes in torsional stiffness are required, while at the same time the bending rigidity may not vary too much, the profile beam with adaptive cross section can thus be regarded as the more promising of the two structural concepts. The results of a more complete analytical characterisation of the adaptive-beam approach can be found in chapter 4.3.

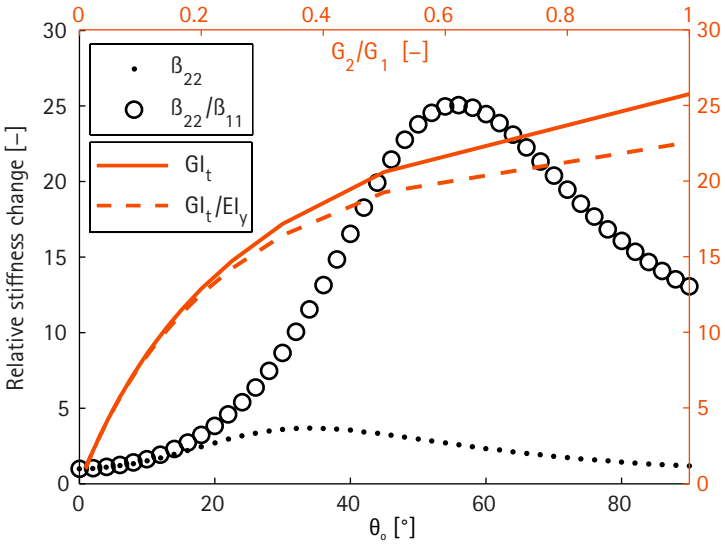

Figure 2.4: Comparison of the stiffness changes achievable with anisotropic laminated plates and with unsymmetrical thin-walled cross sections. Torsional stiffnesses (β_{22} and $\widetilde{GI_t}$) and ratios of torsional and flexural stiffness ($\beta_{22}/\beta_{11}$and $\widetilde{GI_t}/\widetilde{EI_y}$) as a function of outer lamination angle θ_o and shear stiffness ratio G_2/G_1, respectively

While the present section is devoted to the most fundamental case of a beam with rectangular cross section featuring one adaptive web, an application of the general idea in an airfoil calls for various extensions: Re-

versible twisting requires torsional moments of different signs and hence a second variable-stiffness web; additional adaptive interfaces in the flanges or other structural components that do not primarily carry transverse shear permit to lower the torsional stiffness without noteworthily inducing twisting moments; composite laminates with inherent coupling of deformation components can be applied to enhance the desired elastic effect, and many more design adjustments are possible. Not only in terms of continuity of stiffness change but also of these aspects, the considered structural systems move more and more away from the fundamental case introduced in the present section towards more realistic designs as the thesis progresses. The enhancements required for an implementation of the discussed basic concept for twist control of airfoils are presented in the following chapter.

3 Implementation of adaptive twist in airfoils

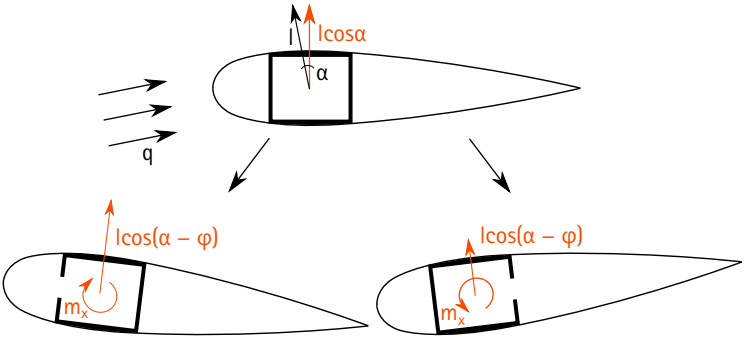

Figure 3.1: Schematic of the aeroelastic working principle of adaptive twist in an airfoil based on shear centre shifting

Controlling the aerodynamic forces and moments on the airfoil represents the major objective of shape adaptation of wings and rotor blades. As the lift force does not only constitute—under normal operating conditions—the largest component of the aerodynamic loads on an airfoil, but also it strongly depends on the local angle of attack of each spanwise section of a wing or blade, controlling an airfoil's twist constitutes an effective way of shape adaptation.

For a two-dimensional airfoil section, the lift force per unit span is given by

$$l = c_l q c \tag{3.1}$$

where c_l, q and c denote the section's lift coefficient, the incident flow's dynamic pressure and the airfoil's chord length, respectively. For this case, thin-airfoil theory predicts the following linear relation between lift coeffi-

cient c_l and angle of attack α [88][1], [90], [91][2], [89, 92]:

$$c_l = 2\pi\alpha + c_{l,0} \tag{3.2}$$

Although for a three-dimensional lifting surface the lift coefficient $c_L = \int c_l \mathrm{d}x / \int \mathrm{d}x$ varies over the span, and in reality the drag force as well as—depending on the operating conditions—viscous, compressible and stall effects have to be additionally taken into account, this basic two-dimensional consideration can be used to explain the fundamental aeroelastic working principle of airfoils with adaptive twist based on structural components with variable cross section. For reasons of simplicity an uncambered profile is considered here, for which not only the position y_{CP} of the centre of pressure, in which the lift force acts, is independent from the angle of attack but also $c_{l,0} = 0$.

It is intuitive that the presented structural concept is especially effective if a drop in torsional stiffness is exploited to generate an increment in twist. If, on the other hand, for methodical reasons, a cross section like introduced in chapter 2, whose shear centre coincides with its centroid in the stiff state, is chosen, it is clear that this state should represent the neutral reference configuration, for which no twisting moment is caused by the lift force. In order to meet this condition, the airfoil's shear centre has to coincide with its centre of pressure when the interface is closed (or in the stiffest state). This situation is shown at the top in figure 3.1, which schematically illustrates the aeroelastic working principle of adaptive twist in an airfoil with variable cross section. The opening or softening of an interface in the spar located more upstream leads to a shift of the shear centre in y-direction (in the coordinate system introduced in chapter 2 and assuming the transverse shear component of the lift force to point in z-direction) and thus to a torsional moment (per unit span) $m_x = -l\cos(\alpha)(y_{\mathrm{SC}} - y_{\mathrm{CP}})$, as depicted at the bottom left in figure 3.1. Consequently, a wash-in twist and finally an increment in lift occur, amplified not only by the drop in torsional stiffness resulting from opening the structure but also by the aeroelastic coupling in the sense that the lift and hence also the torsional moment increase with the twist angle. The airfoil twists until a state of equilibrium between elastic and aerodynamic loads is reached. The same behaviour in the opposite direction is obtained if an interface in the spar closer to the trailing edge is activated in the described way instead of the first one (bottom right image in figure 3.1).

[1] Quoted after [89].
[2] Quoted after [89].

As already brought up in section 1.2.2, there are several potential applications of this aeroelastic concept: First of all, airplane flight control relies on variations of aerodynamic forces. The changes in lift put into effect, for example, by deflections of an aileron or an elevator in order to roll or pitch a plane could in principle also be obtained replacing these discrete control surfaces with adaptively twisting aerodynamic surfaces. Similarly, adaptive-twist airfoils can be considered as an alternative to high-lift devices like flaps, slats or droop noses. In both cases, the general advantages of a compliant solution over rigid-body attachments introduced in 1.2.1 can expectedly be exploited. Moreover, the already mentioned idea of "adaptive aeroelastic tailoring" aims at adjusting, during operation, an airfoil's twist, such that the optimal lift distribution can be set for every operating condition. In designs of rotor blades of wind turbines, load alleviation measures prevent the blades from failure due to gusts or high wind speeds. Whereas the passive aeroelastic tailoring strategies that have been proposed for this purpose [93] introduce elastic couplings under all operating conditions, and especially also under conditions under which they are unwanted, variably twisting blades can be adapted online to the mechanical characteristics that are desired for a certain operation point, which can presumably increase a wind turbine's overall efficiency.

Besides these potential applications of quasi-static nature, employing adaptive twist dynamically can be considered for vibration control in airfoil structures. Not only allow the pure stiffness changes for state switching and thus for vibration attenuation, but also can sliding variable-stiffness interfaces be utilised for friction damping [94, 95]. Moreover, aerodynamic damping can be exploited by means of well-directed aeroelastic coupling.

As a matter of course, the requirements on the adaptive structural system vary widely according to these different applications. Concerning for example bandwidth specifications, a vibration management task with high dynamic requirements or a flight control implementation with activation frequencies of up to around 10 Hz [96] is much more demanding than a high-lift function which is—under usual operation of a transport airplane—activated only twice per flight and for which hence activation times of several seconds are tolerable. In a similar way, the requirements of repeatability and durability differ considerably, depending on the specific application. On the other hand, the required adaptation range (in terms of changes in stiffness and loads) is generally expected to be higher for quasi-static implementations. Furthermore, a fundamental difference in the required spanwise distribution of adaptive elements is obvious when the approach of adaptive aeroelas-

tic tailoring is compared to other airplane applications: Whereas for flight control and high-lift features a prismatic extension over a certain part of the span can be considered, adjusting the spanwise lift distribution requires an optimised placement of adaptive material along the span. For the latter application, a variable-stiffness material concept is generally superior over a variable-topology one due to the continuous adjustability of a tunable-stiffness material in contrast to the limitation of a variable-topology system to discrete states.

In view of the variety of potential applications, the research in the frame of this dissertation has to be confined to a certain type of implementation. Therefore, the considerations of the present chapter on the integration of the basic working principle in airfoil structures, as well as the ones of the two following chapters, which are directed towards the realisation of experimental airfoils, focus on the application of adaptive twist for quasi-static lift control in fixed wings.

The proposed structural concept is based on intentional reductions in an airfoil's torsional stiffness and—in case of increases in lift force—on shifts of the shear centre towards the trailing edge. These unconventional measures attract attention in the context of aeroelastic instabilities, as they both make the airfoil tend in the divergence-critical direction, and as the drop in torsional rigidity can potentially cause flutter problems. In light of these particular characteristics of airfoils based on the suggested concept, their safety against static and aeroelastic instabilities receives special consideration in the simulation parts of this doctoral thesis, which are discussed in chapters 4.4.1 and 5.4.1.

It has been explained how the concept of shear centre shifting can be applied to obtain wash-in or wash-out twist of a wing or rotor blade, but the question how an adaptive-twist airfoil can be brought back to its initial geometry once a shape adaptation has been performed has not been addressed in the previous discussion, and, in fact, the reversibility of semi-passive structures under loading represents a general key challenge. It is easy to see that a return of the twisted airfoil to its initial state is always possible by relieving the loads, but this would imply the necessity of special alleviation manoeuvres, if the reverse twist shall be performed in flight. Theoretically, a rethinking of the one-way relation between desired flight condition and according configuration of the control surfaces is possible, and manoeuvres like entering a zero lift flight path in order to reset the airfoil are imaginable. Such measures would however be unpractical for the operation of an airplane and would probably cancel out the benefit in efficiency that can potentially

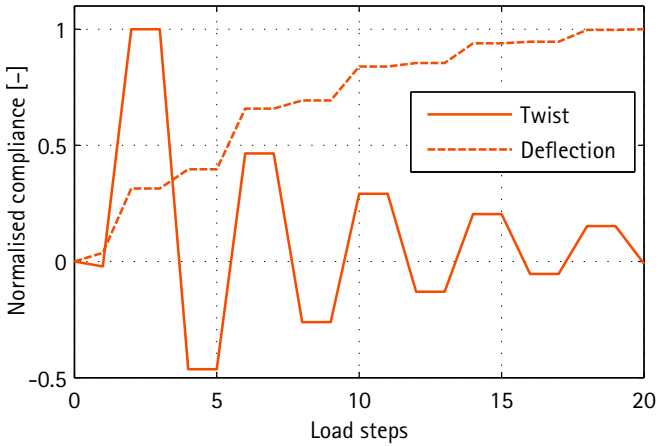

Figure 3.2: Reversibility investigation based on thin-airfoil theory and nonlinear finite element simulation of a beam with rectangular cross section. Normalised tip twist and deflection for cyclic shape adaptation (opening of interfaces in the webs). B/H = 2, L/B = 10, $t_1 = t_2 = t$, H/t = 10. Wash-in twist angles are positive.

be attained by the lightweight and aerodynamic qualities of the morphing wing.

A more conventional possibility of reverse shifting, which makes use of a second adaptive interface in the airfoil structure, is thus introduced in the following. In order to adapt the airfoil in the way described before, an adaptive interface in one of the two spars is softened or opened, causing a twist until an aeroelastic equilibrium is reached. In this state, the interface is closed again and a second interface in the other spar is activated in the same way as the first one. As a consequence, the equilibrium is lost, which leads to a redistribution of stresses in the structure, such that a twisting moment of opposite sign results, and the airfoil twists back. Apart from nonlinear effects, the effective twisting moments for both directions have the same value[3] and also for the torsional stiffness it does not make any difference which of both

[3] Since the lift changes with the twist angle, the twisting moment in the state when the second interface is activated is different from the one when the first one is opened. Integrated over the whole range confined by initial zero twist and twist angle in the deformed equilibrium state, this difference cancels out, however.

interfaces is open. This gives rise to the assumption that the system's revertive behaviour is symmetric. An asymmetry is however introduced by the fact that, due to the different location of both interfaces, the elastic stresses that are frozen when the first interface is re-closed (or re-stiffened) are not ideally released by opening (or softening) the second one, so that the elastic deformation is not recovered completely. As it is shown in figure 3.2, this influence results in an asymptotically decreasing amplitude of the twist angle under cyclic activation of the concept. Furthermore, it is evident from this figure that the deflection asymptotically approaches a maximum value, which can be easily understood by the fact that the twisting structure's cross sections are in each step rotated about the shear centre which is cyclically shifted. For the calculations on which the diagram of figure 3.2 is based, the fundamental aerodynamic model introduced before has been used, and the relations reported in the figure's caption have been assumed for the main structural parameters.

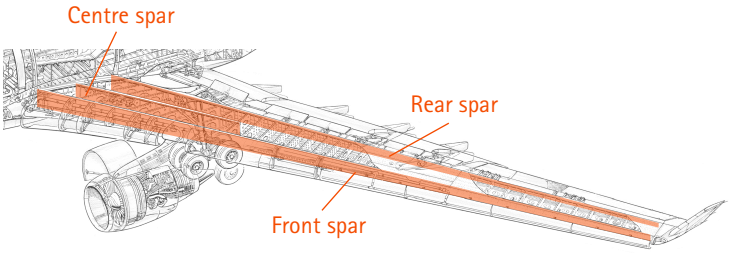

Figure 3.3: Cutaway illustration of the wing structure of an Airbus A330 as an example for a conventional wing design. The spars are highlighted.

As already indicated by the previous considerations, the nature of the presented structural concept suggests an integration of the adaptive interfaces in the spars of an airfoil structure. This kind of implementation is, from a structural point of view, well compatible with many conventional designs of airplane wings that rely on a main load-carrying wing box in whose webs the adaptive elements can be placed. In certain regions, the wing box can be subdivided into multiple cells by additional spars, as shown for an example of a transport aircraft wing in figure 3.3. Although the wing box usually contributes decisively to the airfoil's overall elastic properties, also the skin and further structural elements like ribs have an influence which has been

neglected in the previous considerations. Especially the skin though is of major importance for the implementation of the proposed structural concept in a wing structure: As explained precedingly, a substantial proportion of the effectiveness of the elastic working principle relies on changes in torsional stiffness due to (quasi-)opening of a closed cross section. Even if the stiffness or topology of all the internal spars of an airfoil can be modified in this way, the skin constitutes a remaining closed cell with relatively high torsional rigidity. In order to fully exploit the potential of the structural concept, either additional adaptive interfaces or openings have thus to be introduced in the skin.

The special attention that has to be dedicated to the airfoil's aeroelastic stability in the states of low torsional stiffness as well as to its aerodynamic quality in view of the local reductions in the skin's shear and bending stiffness should be emphasised at this point. The latter point can be considered as a matter of the detailed design of the skin openings. Closing these gaps by a soft material that still provides a quasi-open global behaviour, but at the same time an acceptably smooth local shape in order to maintain good flow conditions can be proposed as a general possible solution which is however not investigated deeper in the frame of this dissertation.

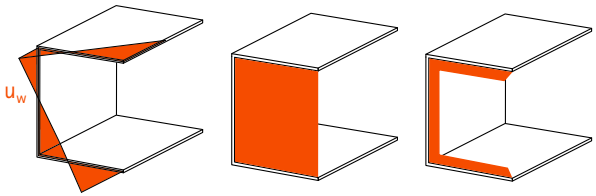

Figure 3.4: Importance of warping in the compliant state of an adaptive-twist airfoil for the rib design. Warping deflection u_w of an open profile (left), schematic of conventional plate-like rib design (centre), schematic of improved frame-like rib design (right)

In this context, also the particular implications of the novel wing concept on the rib design have to be mentioned. Ribs are generally used to prevent the wing's cross sections from excessive shear deformation, to increase buckling stability, to introduce concentrated loads and to attach components. Conventionally designed ribs would not allow for enough twisting compliance in the airfoil's soft states, as in the quasi-open configurations the twist behaviour is dominated by warping. It is evident from the example of fig-

ure 3.4 that the warping deflection u_w of an open cell leads to differential bending of the profile (with a bending moment in y-direction) which would be constrained too much by ordinary plate-like ribs. Therefore, segmented frame-like rib geometries are proposed which maintain the ribs' reinforcing function but do not noteworthily impede the warping deformation.

If an adaptive-twist airfoil has to adopt the neutral state introduced before, its shear centre has to coincide with its centre of pressure when both adaptive interfaces are stiff or closed. Assuming the wing box to dominate the airfoil's shear centre location and a wing box cross section that is approximately symmetric with respect to the z-axis, the wing box has to be centred around about a quarter of the chord, where many common profiles have their centre of pressure (at least for small angles of attack). Although the placement depends on the actual stiffness distribution of a certain airfoil design, it can be generally concluded from the relation between shear centre and centre of pressure that, firstly, in an adaptive-twist airfoil the wing box tends to be placed closer to the leading edge than in a conventional one and, secondly and as a consequence, the wing box of an adaptive-twist airfoil is characterised by an especially low width (in chordwise direction).

In order to exploit as much as possible the lightweight potential of the smart-material based design concept proposed in this work, the adaptive interfaces should be highly integrated in the load-carrying structure. In the passages of the following two chapters dedicated to the construction of adaptive wing spars relying on two different kinds of smart materials, particular attention will be paid to this aspect.

As a summary of the considerations on the placement of interfaces and wing box and on the design of skin and ribs, figure 3.5 contrasts the structural layout of an adaptive-twist airfoil with the one of a conventional fixed wing.

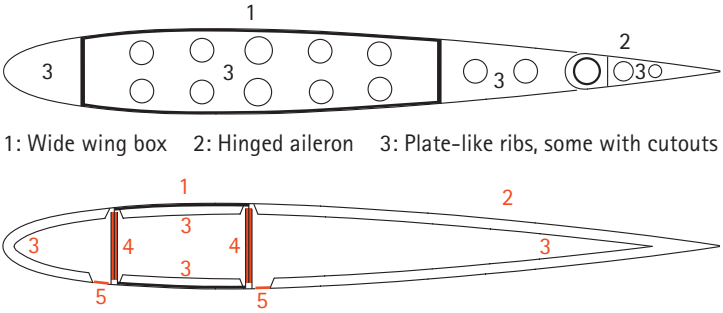

Figure 3.5: Comparative illustration of the design characteristics of a conventional wing cross section (top) and of a cross section of an adaptive-twist wing (bottom)

4 Adaptive-twist airfoil based on thermomechanical coupling

4.1 Material concept: glass transition–based stiffness variation

The smart material approach applied in the first implementations of beams and airfoils with adaptive cross section is based on the strong temperature dependence of the mechanical properties of polymers.

In the mechanical characteristics of an amorphous polymer, five distinct regimes can be identified which appear depending on the material's temperature T. As a mechanical quantity that varies considerably over temperature and that is accordingly constitutive for the distinction of the five temperature regions, the *complex modulus* E^* [97] shall be defined first:

$$E^* = E + iE' \tag{4.1}$$

In equation 4.1, E represents the *storage modulus*, the elastic component of the complex modulus, and E' denotes the *loss modulus*, the viscous contribution.

Based on this fundamental quantity, the left image of figure 4.1 contains an idealised illustration of the characteristic regimes: At low temperatures, the complex modulus of an amorphous polymer shows the highest values and is almost constant with respect to temperature. Under these conditions, the molecular motion is dominated by vibrations and small-angle rotations, so that the material behaves brittly and this region is referred to as *"glassy state"* (1 in figure 4.1). Increasing the temperature lets the polymer enter the region of *glass transition* (2), which is characterised by a large and rapid drop in modulus, typically by about three orders of magnitude within a temperature range of 20–30 K [98]. The higher mechanical compliance in this regime is due to the temperature-induced activation of the rotational degrees of freedom of the polymer chains which enable long-range motions on the molecular scale involving about ten times more atoms than in the glassy region [98]. At even higher temperatures, another regime characterised by

lower temperature dependence of the complex modulus can be identified. In this range called *"rubbery plateau region"* (3), reptation and diffusion of molecular chains lead to rubber elastic macromechanical characteristics. When the material has entered the following range, the further increase in temperature has lead to mobility of entire assemblies of polymer chains, so that the polymer flows under mechanical load. As still some extent of rubber elasticity is present, this regime is referred to as *"rubbery flow region"* (4). Raising the temperature even more activates the flow of individual polymer molecules and thus causes a liquid behaviour at the macro scale. The region of *liquid flow* (5) is reached, in which the complex modulus rapidly decreases to zero.

In contrast to this behaviour observed for amorphous thermoplasts, semicrystalline (dashed line) and (lightly) cross-linked (dotted line) thermoplastic polymers show different characteristics: While the first exhibit a less pronounced glass transition which is followed by a wide rubbery plateau up to the melting temperature, the latter are characterised by a rubbery plateau extending to their decomposition.

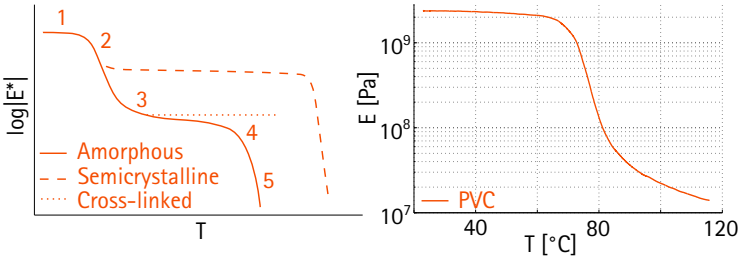

Figure 4.1: Left: idealised temperature-dependence of the complex modulus of polymers according to [98]. The numbers denoting the temperature regimes are explained in the text. Right: temperature plot of the storage modulus of hard polyvinyl chloride (PVC) determined by dynamic mechanical analysis (DMA) and offset calibration at room temperature by results of tensile tests [99]

At this point, the absence of a definition consensus for the glass transition temperature T_g, which is often used as a single quantity representative of the glass transition region, should be mentioned: While the step in the temperature plot of a polymer's thermal expansion coefficient is reported as the most common defining criterion for T_g [98, 100], other widespread def-

initions equalise the glass transition temperature with the temperatures of maximum loss modulus or loss tangent[1] [101]. The nature of these "definitions" [98, 100] to be based on certain manifestations of physical processes observed in different kinds of experiments instead of the processes themselves is noticeable.

The right image of figure 4.1 presents the temperature plot of the storage modulus of the hard polyvinyl chloride (PVC) which has been applied for the variable-stiffness interfaces of the experimental wing box and airfoil structure discussed in sections 4.3 and 4.4, respectively. This plot, which has been recorded by means of dynamic mechanical analysis (DMA) and calibration with results of tensile tests at room temperature as described in [99], verifies the preceding general and idealised considerations for the specific example of the amorphous polymer which is of interest in the experimental part of this dissertation.

The characterisation of the temperature-dependent mechanical behaviour of polymers points out the eligibility of the glass transition phenomenon as the working principle of a variable-stiffness material: If the material's temperature can be controlled, large changes in elastic modulus can in principle be put into effect by relatively small control inputs due to the high sensitivity of the modulus on the temperature.

Utilising the temperature-induced stiffness change requires energy to be spent for heating (or cooling) of (at least) the polymer and for compensation of losses. Neglecting the latter for the present general explanations, the energy demand for a temperature change from T_1 to T_2 is given by

$$Q_{\mathrm{th}} = m \int_{T_1}^{T_2} C \,\mathrm{d}T \tag{4.2}$$

if m denotes the mass of the material to be heated and C the specific heat capacity of this material. Based on experimental data reported for PVC (for example in [102, 103]), an idealised and qualitative temperature plot of C can be drawn as in figure 4.2. It can be deduced from this consideration that investing the step-like increment in thermal energy related to the glass transition has to be put up with when applying the proposed thermomechanical variable-stiffness concept, since the gain in terms of change in modulus between glassy and rubbery state is much higher than the expense in terms of change in heat capacity in the glass transition regime.

[1] The loss tangent is defined as the ratio of loss modulus and storage modulus.

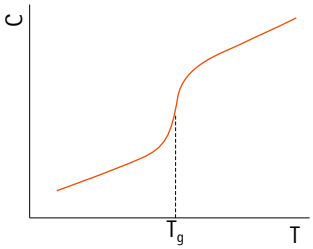

Figure 4.2: Idealised temperature plot of the specific heat capacity of PVC across its glass transition (cf. [102, 103])

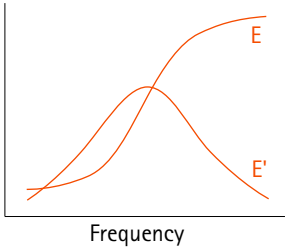

Figure 4.3: Idealised frequency dependence of storage modulus and loss modulus of a viscoelastic solid according to [104]

Concerning the selection of an appropriate polymer material, some general conclusions can already be made based on the previous conceptual discussion on the thermomechanical material concept: First, with regard to well controllable and reversible stiffness variations, the changes in modulus across the glass transition region, which is surrounded by two "stable" plateaus, should be used. Exploiting the regimes of melting or liquid flow, on the other hand, can be expected to be unfavourable in these respects. Second, if the range of stiffness adaptation is to be maximised, amorphous thermoplasts are preferable over thermosets and, especially, semicrystalline thermoplasts, due to the more pronounced change in modulus of amorphous polymers around T_g. Third, when it comes to material selection or material development for a particular application, two aspects should especially be considered:[2] In order to avoid redundant heating (and cooling) *up to* (and *down to*) the onset of glass transition, this onset temperature should be chosen higher but as close as possible to the polymer's highest operating temperature. In order to avoid redundant heating (and cooling) *across* the glass transition, the change in modulus should be chosen as large and rapid as possible.

The described viscoelastic behaviour of polymers implies that the complex modulus varies with frequency, as qualitatively illustrated in figure 4.3. Comparability of experimental results has therefore to be ensured by requiring the frequencies to have the same value (or at least very similar values) in all the respective experiments. In particular, this has been provided for in the

[2] At this point, a state of high stiffness is assumed to be the primary state of operation, as it can be expected for many applications.

material characterisation and structural testing performed in this work.

4.2 Local behaviour—the smart interface

As introduced in chapters 2 and 3, the main function of the adaptive interface consists in providing reversible changes in shear stiffness of airfoil components which affect the airfoil's shear centre location and its torsional stiffness. In order to apply the idea of thermomechanical coupling presented in section 4.1 for this purpose, a polymer element with controllable temperature has to be introduced in the load path of the respective structural component.

Before the conceptual design and certain characteristics of the mechanical behaviour of the smart interfaces can be discussed, some technological aspects have to be addressed which delimit the design space of the interfaces.

In the present research project, only active heating of polymer parts has been investigated, while cooling has been assumed to occur passively, by heat transfer to the environment. Although in a technical application active cooling might be required under certain conditions, only heating elements are considered in the following discussion. Concerning heating technologies, only heat conduction from integrated ohmic heating elements to the variable-stiffness polymer has been applied. While there are many more heating concepts which are generally eligible,[3] the mentioned one has been selected for its promising structural integrability.

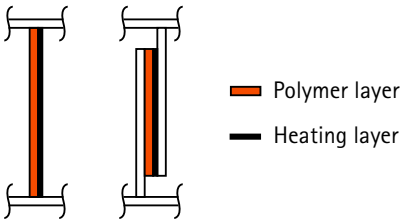

Figure 4.4: Schematics of the cross sections of monolithic interface design (left) and overlap-based one (right). Adaptive polymer layers are shown in orange, heating layers are shown in black.

[3] For example Peltier elements, which also offer active cooling capabilities and fairly good integrability.

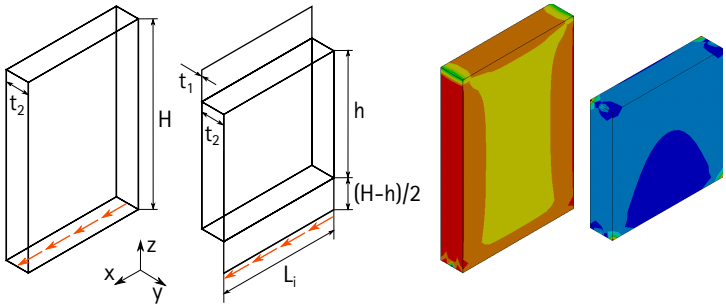

Figure 4.5: Left: geometry and loading of the finite element (FE) models of monolithic and overlapping interface design. Right: normalised shear stress (τ_{xz}) distribution in the polymer layer resulting from the FE calculations for both configurations

Under these conditions, the two design concepts shown in figure 4.4 for the integration in a wing spar can in principle be considered for the variable-stiffness interface: a monolithic representation or a design based on overlapping spar parts. These alternatives differ in some fundamental aspects: First, an immediate integration of heating layers in the load-carrying structure can only be realised with the overlap approach, where the series connection of elastic elements permits to place a heating element which is directly connected to the polymer material in the spar's shear load path. In the monolithic design, in contrast, polymer and heating are inevitably arranged in parallel. Here, a load-carrying and thus stiff heating element would compromise the state of low stiffness, in which it would still represent a relatively rigid load path. As a consequence, only compliant heating layers or stiffer layers that are elastically decoupled from the polymer come into consideration, which are both characterised by a low degree of integration. Similar arguments can be made on the integrability of designated thermal insulation layers.

Second, a substantial difference in the influence of the polymer thickness on the interface design is tied to the general elastic characteristics of both design alternatives: While the monolithic layout, which exhibits large free surfaces if the heating layer is assumed to be effectively compliant, requires a thin polymer layer for the shear stiffness of the softened interface to be low, the opposite is observed for the overlap design: Here, the surface of

the softening polymer is supported by overlapping spar parts which remain stiff, so that a pronounced shear compliance in the soft state can only be realised by a thick polymer layer. In order to confirm this intuitive description of the thickness influence, both interface variants have been investigated by finite element (FE) modelling. The left two images in figure 4.5 show the geometries and the loading assumed for these calculations. As it is obvious from these sketches, heating layers are neglected in the model. The interfaces have been simulated as clamped at the top edge and supported in y- and z-direction at the bottom edge. These boundary conditions—together with the x-wise loading—can be considered as representative of the conditions in the soft state of the integrated interface, in which the twisting behaviour is dominated by warping. A stiffness ratio of $G_2/G_1 = 1/1000$ has been assumed for the overlap design in the FE model.

As a result of this simulation, the x-wise displacement u of the front (highest x-value) corner of the load introduction edge normalised by the value u_0 recorded for the lowest thickness $t_{2\,\mathrm{min}}$ is plotted with respect to the thickness ratio t_2/t_1 in figure 4.6. The mentioned contrariness of the thickness dependence of both design concepts is evident from the respective curves.

The two plots on the right in figure 4.5 present the shear stress (τ_{xz}) distribution in the polymer layer resulting from the FE modelling for a thickness ratio of $t_2/t_1 = 4$. For both interfaces, large shear stress gradients are observed, and in both distributions a similarity to the hyperbolic analytical solution of the two-dimensional problem of a lap joint under tension ([105, 106], formula quoted after [4])

$$\tau(\bar{x}) = \tau_\mathrm{m}\frac{C_1}{2}\left[\frac{\cosh\left(\frac{C_1\bar{x}}{l_\mathrm{o}}\right)}{\sinh\left(\frac{C_1}{2}\right)} - \frac{\left(1-C_2\right)\sinh\left(\frac{C_1\bar{x}}{l_\mathrm{o}}\right)}{\left(1+C_2\right)\cosh\left(\frac{C_1}{2}\right)}\right] \tag{4.3}$$

can be recognised.

In equation 4.3, $C_1 = \sqrt{(1+C_2)G_3 l_\mathrm{o}^2/(E_1 t_1 t_3)}$ and $C_2 = E_1 t_1/(E_2 t_2)$; τ_m denotes the mean shear stress in the adhesive, and l_o represents the overlapping length; indices "1" and "2" denote the adherends, and index "3" denotes the adhesive.

The substantially different thickness effect on the shear compliance of both interface layouts is also directly reflected in their structural stability: In case of the monolithic solution the buckling stability in soft system states is low due to the fact that the comparably slender web is only supported by

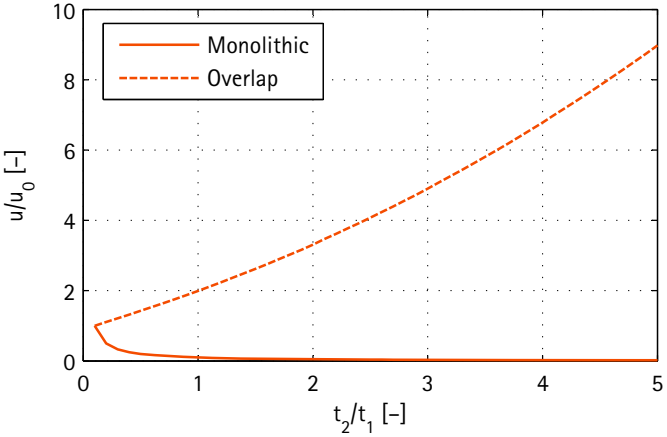

Figure 4.6: Normalised shear displacement with respect to relative thickness of polymer layer for both interface designs resulting from FE calculations. $L_i/h = 1$, $h/t_1 = 20$, $h/(H - h) = 2$

stiff structural members at its edges. The adjacent spar parts of the overlap-based design, on the other hand, support the surface of the softened material from both sides, which strongly increases the buckling stability. This stability behaviour has been confirmed by finite element calculations based on the conditions specified previously for the investigation related to shear compliance. The plot in figure 4.7 shows that, in accordance with the results reported for the shear compliance, the shear buckling stability shows a much more pronounced thickness dependence in case of the monolithic design. It should be noted here that, under the considered conditions, the absolute buckling factors of the monolithic design are much lower than the ones of the lap design for all analysed thickness ratios. It is self-evident that these characteristics limit the applicability of monolithic interfaces in soft states, for which the requirement conflict introduced in chapter 1 is observed.

4.3 Meso behaviour—the wing box

From a structural analyst's point of view, the monolithic interface configuration presented in the previous chapter can in principle be treated analytically,

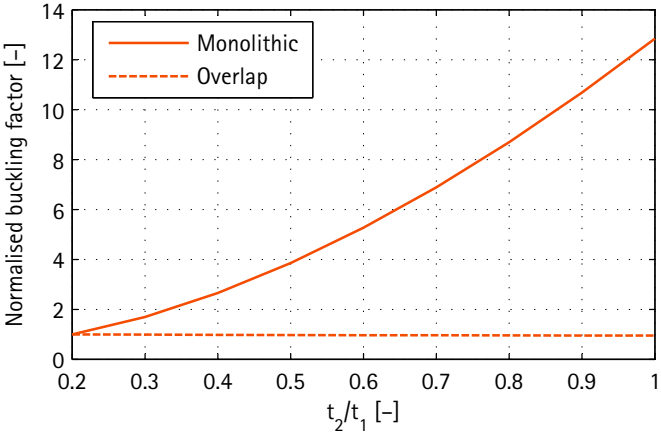

Figure 4.7: Buckling load factor normalised by the respective value at the minimum thickness ratio for both interface designs resulting from FE analysis. $L_i/h = 1$, $h/t_1 = 20$, $h/(H - h) = 2$

applying the theory of thin-walled profiles quoted in chapter 2. Therefore, and, as a second systematic reason, in order to stay as close as possible to the fundamental beam structure of chapter 2 in this general investigation of the wing box behaviour, the monolithic web design has been selected for the considerations of the present section—despite its aforementioned practical problems.

However, an analytical description of the elastic properties of adaptive beams with monolithic web is only possible for moderate stiffness ratios (G_2/G_1 not much smaller or much bigger than one) and for the limiting case of the open c-profile in which $G_2/G_1 = 0$ (cf. 4.3.1). In a wide transition region between (quasi-)closed and (quasi-)open sections, on the other hand, no standard closed-form solution of the elastic problem exists, which thus has to be approached numerically.

4.3.1 Numerical investigation

With a view to the development of a comprehensive understanding of the trends in the mechanical behaviour of wing box structures with adaptive

Table 4.1: Geometric properties (in mm) assumed for the different parts of the parameter study

Parameter	L	B	H	t_1	t_2
B/H	1'000	50–200	50–200	1	1
t_2/t_1	500	50	50	4/13–16/13	4/13–40/13
L/B	250–2'000	50	50	1	1

bending-twist coupling, a parametric study of cantilevered profile beams as depicted in figure 2.1 has been conducted, applying the analytical relations of chapter 2.

The effect of variations in the stiffness ratio G_2/G_1, the cross-sectional aspect ratio B/H, the wall thickness ratio t_2/t_1 and the beam slenderness L/B—all of them representing parameters of major influence on the beams' elastic behaviour—has been investigated in this study. Table 4.1 gives an overview of the geometric properties that have been varied or held constant in the different parts of the parameter study. Concerning the cross-sectional quantities, changes in the aspect ratio B/H and in the thickness ratio t_2/t_1 have been performed under the condition of constant cross-sectional area[4].

Besides the purely cross-sectional properties of relative shear centre location y_{SC}/B, torsional stiffness $\widetilde{GI_t}$ and flexural stiffness $\widetilde{EI_y}$, the twist and deflection compliance of the tip of the three-dimensional beams (ϕ_{tip}/Q and $w_{0\,tip}/Q$, respectively[5]) have been chosen as quantities of interest for the evaluation of the parametric study. For the investigation of the slenderness effect, also the maximum warping stress at $x = L/2$ has been evaluated. In case of the three-dimensional properties, the analytical results are compared to the ones of FE calculations based on quadratic shell elements[6].

The results of the parameter study, further details on which are reported in [79], are presented in figures 4.8 to 4.23. Two main conclusions can be drawn from this investigation: The structural concept is highly effective for controlling the bending-twist coupling, and its elastic behaviour can be adjusted in a wide range by variation of the main design parameters. Referring

[4] Defined as the area of the profile's walls in the cross section.

[5] $w_{0\,tip}$ denotes the deflection at the beam's tip, in its centroid (in $x = L$, $y = 0$).

[6] The eligibility of quadratic elements also for the variable-stiffness web, which is subjected to pronounced shear deformation in the states of low modulus, has been validated by comparison of the results with results from solid models.

to the first point, the expected characteristic of the adaptive beam to exhibit a sensitivity to stiffness changes that is much higher in twist than in deflection is verified by the respective results. Not only the curves of the cross-sectional stiffness components, but also the ones of the three-dimensional compliance quantities—which account also for transverse shear deflection and for deflection due to twist of points different from the shear centre—reflect this behaviour.

The characteristic, convex dependence of the twist compliance on the cross-sectional aspect ratio directly results from the nature of the torsional stiffness to adopt its maximum value for an elastically doubly-symmetric configuration. The minimum value of twist compliance is however observed at smaller B/H values due to the influence of the shear centre shift which increases with increasing relative widths of the cross section. As expected, the flexural stiffness, which is hardly influenced by adaptations of the variable-stiffness web, depends inversely on the cross-sectional aspect ratio. The fact that the deflection compliance is not only affected much more by variations in the stiffness ratio than the purely flexural rigidity but is also characterised by a substantially different dependence on the aspect ratio, shows the predominance of twist and transverse shear for the deflection of the section's centroid.

Concerning the influence of the thickness ratio, different effects are present. The torsional stiffness peaks again for the cross section that is symmetric in terms of its shear stiffness distribution. The flexural stiffness, on the other hand, is mainly affected by the changes in thickness of the flanges coming along with variations in thickness ratio, since the cross-sectional area of the profile's walls is assumed to be constant, as mentioned before. This effect of the variation in thickness of the non-adaptive parts of the beam with the thickness ratio is also reflected in the curves reporting the compliance of the limiting case of the open c-profile. The strong dependence of the shear centre location on the thickness ratio that is observed for relatively stiff states of the adaptive web fades for higher stiffness ratios, at which the profile is quasi open and the influence of the adaptive web has virtually disappeared. Due to the antagonistic thickness dependences of shear centre shift and torsional stiffness, the effect of the relative web thickness on twist and deflection compliance is smaller than the one of the aspect ratio.

In the results of the investigation of the slenderness effect, the well-known nature of the warping stresses caused by the clamping to decay along the beam length becomes manifest. This influence leads to a higher compliance and a lower influence of warping stresses for higher L/B ratios. Because

of the cubic dependence of the deflection on the beam length, in contrast to the linear one of the twist angle[7], more slender beams are however characterised by lower ϕ/w ratios.

All in all, analytical and FE results of the parameter study agree well, although an overestimation of the twist compliance by the analytical model is observed at lower stiffness ratios. Under these conditions, the theory for closed sections is not applicable anymore. For even lower web moduli, the analytical solution for the open c-profile represents an appropriate description of the elastic behaviour, but in a relatively wide transition region between a quasi-closed and quasi-open configuration no closed-form solutions are known, so that one has to fall back on numerical results in these cases.

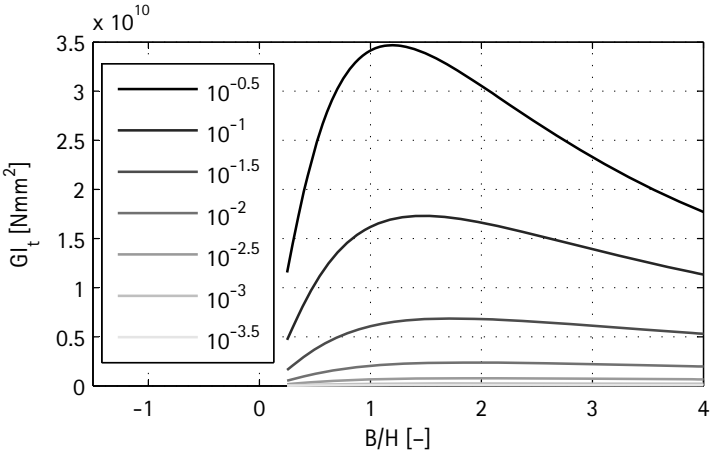

Figure 4.8: Influence of cross-sectional aspect ratio on torsional stiffness. Array parameter: stiffness ratio G_2/G_1

[7] Sufficiently distant from the clamping, the twist angle is linearly depending on the lengthwise coordinate.

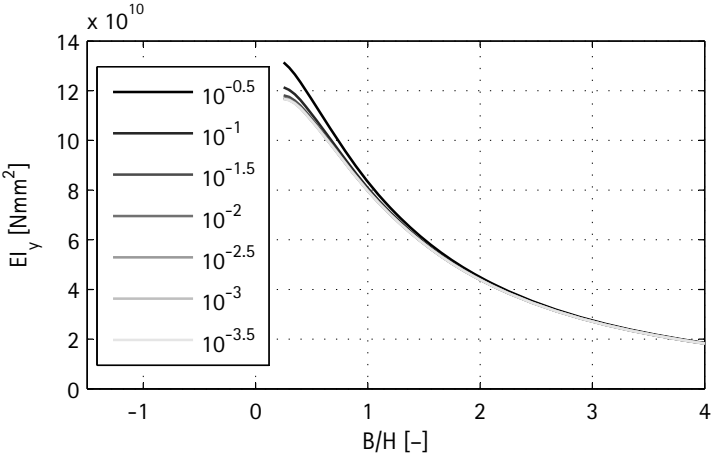

Figure 4.9: Influence of cross-sectional aspect ratio on flexural stiffness. Array parameter: stiffness ratio G_2/G_1

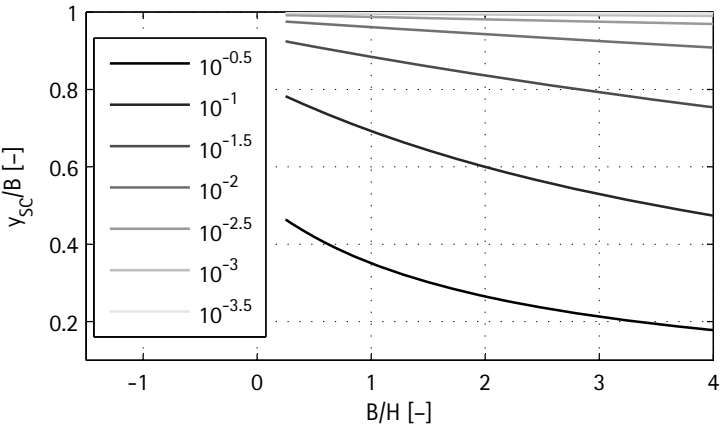

Figure 4.10: Influence of cross-sectional aspect ratio on relative shear centre location. Array parameter: stiffness ratio G_2/G_1

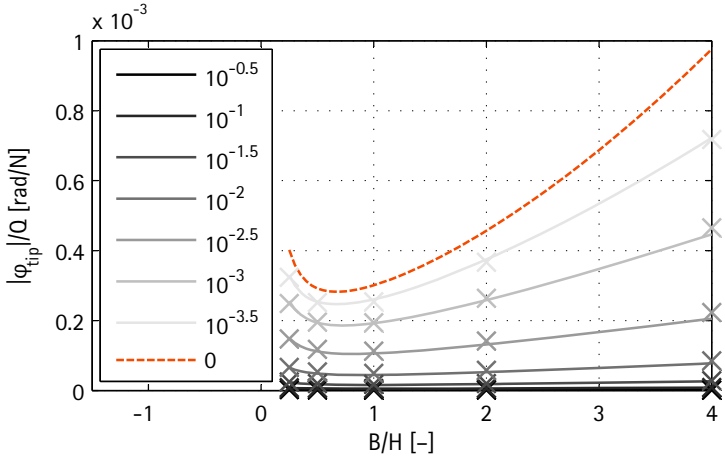

Figure 4.11: Influence of cross-sectional aspect ratio on twist compliance. Array parameter: stiffness ratio G_2/G_1. Crosses denote FE results.

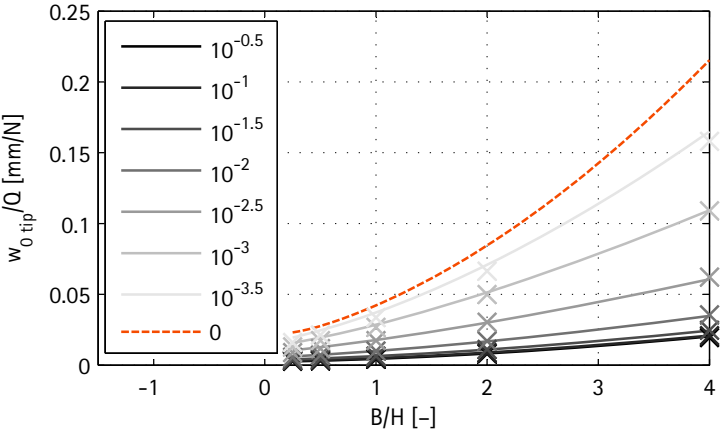

Figure 4.12: Influence of cross-sectional aspect ratio on deflection compliance. Array parameter: stiffness ratio G_2/G_1. Crosses denote FE results.

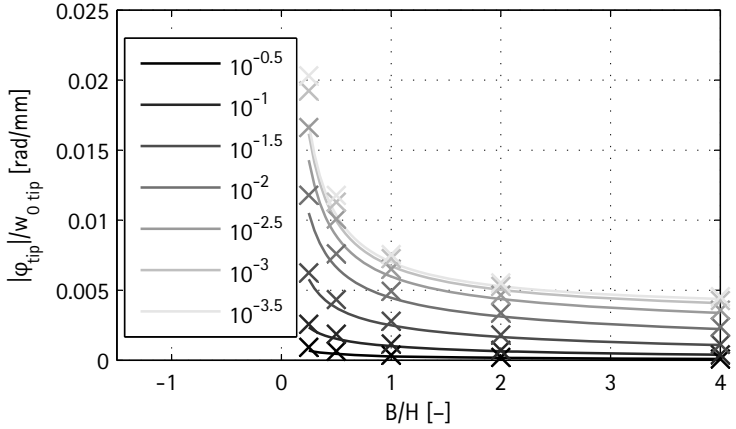

Figure 4.13: Influence of cross-sectional aspect ratio on the ratio of twist compliance and deflection compliance. Array parameter: stiffness ratio G_2/G_1. Crosses denote FE results.

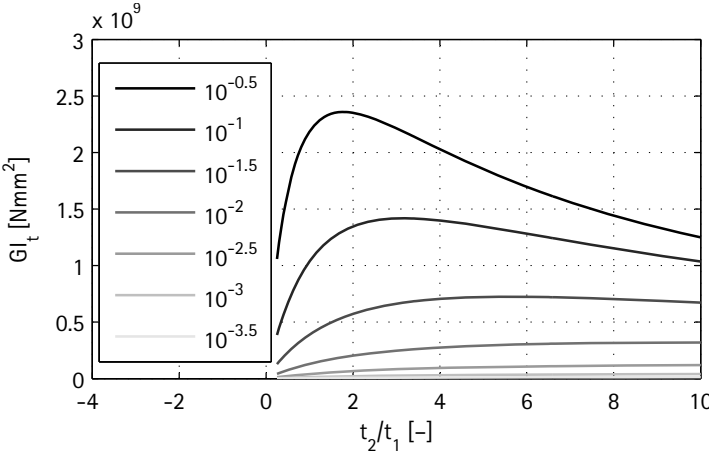

Figure 4.14: Influence of relative web thickness on torsional stiffness. Array parameter: stiffness ratio G_2/G_1

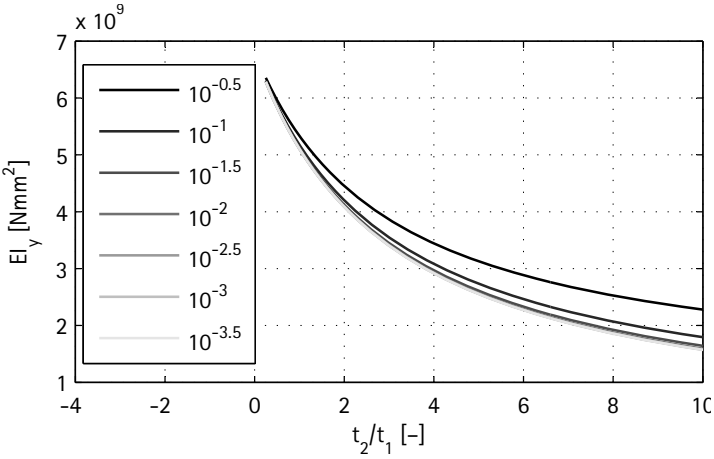

Figure 4.15: Influence of relative web thickness on flexural stiffness. Array parameter: stiffness ratio G_2/G_1

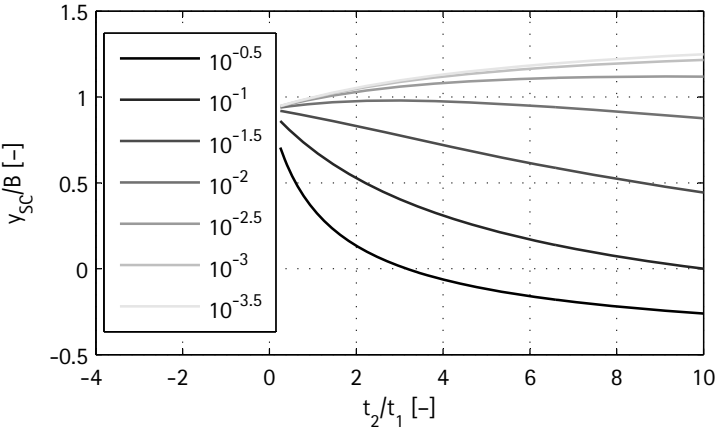

Figure 4.16: Influence of relative web thickness on relative shear centre location. Array parameter: stiffness ratio G_2/G_1

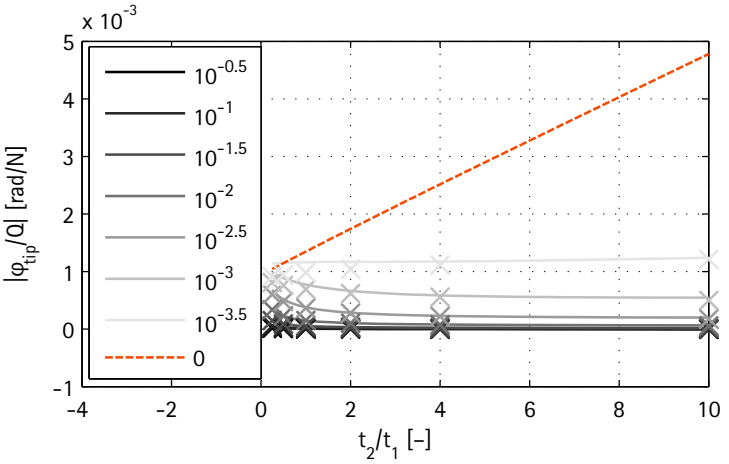

Figure 4.17: Influence of relative web thickness on twist compliance. Array parameter: stiffness ratio G_2/G_1. Crosses denote FE results.

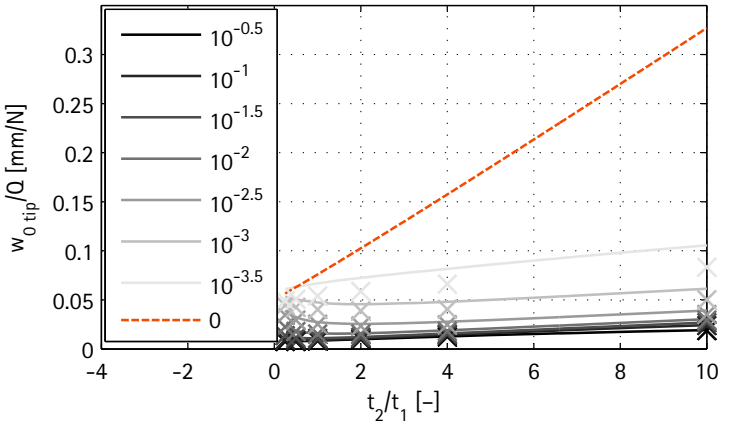

Figure 4.18: Influence of relative web thickness on deflection compliance. Array parameter: stiffness ratio G_2/G_1. Crosses denote FE results.

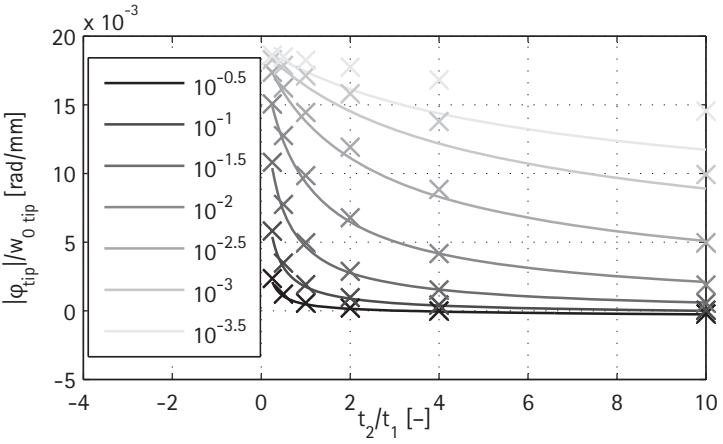

Figure 4.19: Influence of relative web thickness on the ratio of twist compliance and deflection compliance. Array parameter: stiffness ratio G_2/G_1. Crosses denote FE results.

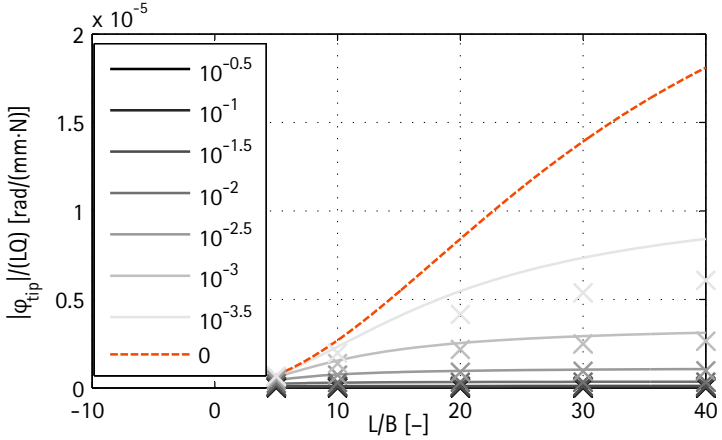

Figure 4.20: Influence of slenderness ratio on normalised twist compliance. Array parameter: stiffness ratio G_2/G_1. Crosses denote FE results.

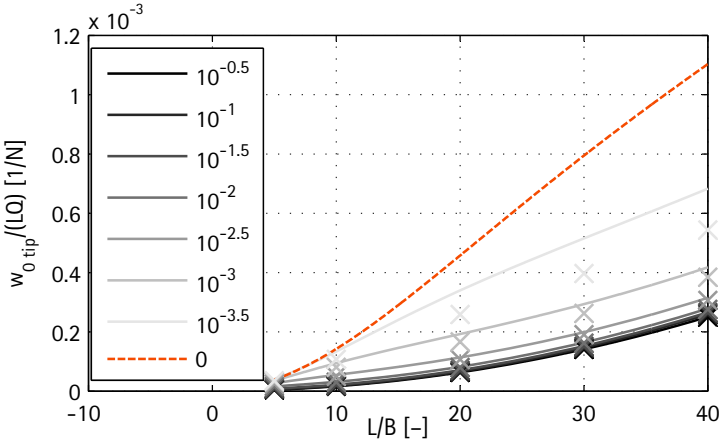

Figure 4.21: Influence of slenderness ratio on normalised deflection compliance. Array parameter: stiffness ratio G_2/G_1. Crosses denote FE results.

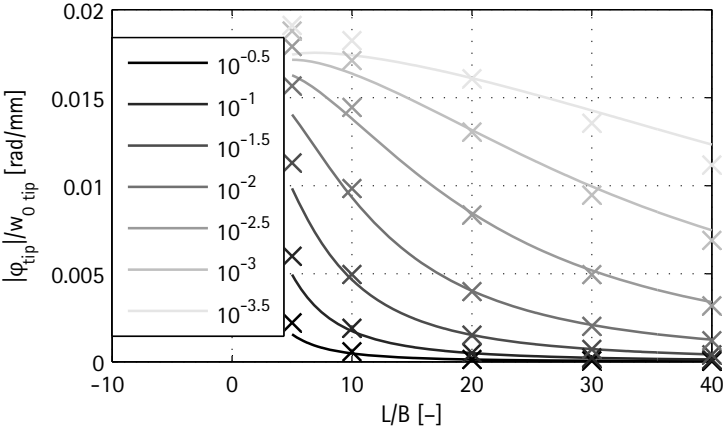

Figure 4.22: Influence of slenderness ratio on the ratio of twist compliance and deflection compliance. Array parameter: stiffness ratio G_2/G_1. Crosses denote FE results.

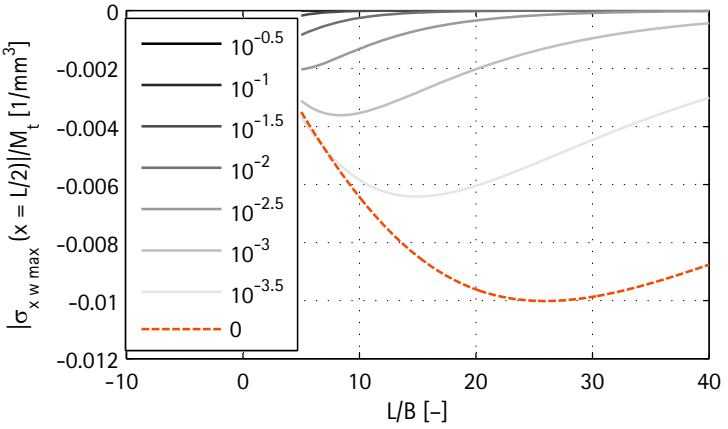

Figure 4.23: Influence of slenderness ratio on normalised warping stress. Array parameter: stiffness ratio G_2/G_1.

As an additional parameter investigation, the potential of utilising elastic couplings of the profile beam's walls to enhance the effect of adaptive bending-twist coupling has been investigated. For this purpose, the limiting cases of the adaptive wing box, i. e. the closed rectangular cross section and the open c-profile, have been simulated by means of finite elements, allowing for anisotropy in the flanges as an additional design parameter.

As it is evident from the illustrations of figure 4.24, the shear flow distributions of open and closed sections under torsion are fundamentally different. In view of these characteristics and of the fact that, under flexure of the wing box, the flanges are mainly exposed to stress states of extension and compression, the design strategy for the flanges becomes apparent: In order to realise a bending-twist coupled behaviour of the wing box for both cross sections, extension-shear coupled flanges have to be employed for the closed profile, while extension-twist coupled flanges have to be chosen for the c-profile.

In order to put the desired elastic couplings into effect, each of the extension-shear coupled flanges is composed of a laminate with $[\theta_o;\theta_i]_S$ layup, while the extension-twist coupled flanges possess $\pm[\theta_o;\theta_i]_a$[8] layups.

[8]The c-profile features the following laminate layups: $[\theta_o;\theta_i;-\theta_i;-\theta_o]$ for the upper flange and $[-\theta_o;-\theta_i;\theta_i;\theta_o]$ for the lower one.

Quasi-isotropic laminates have been assumed for the webs in both cases, and the material properties reported for a unidirectional CFRP ply in appendix A.1 have been used. Loading and further boundary conditions are the same as in the parameter study.

The results, which are presented in terms of twist angle plots in figures 4.25 and 4.26[9], show that, first, the effect of elastic couplings by anisotropy cannot compete with the one of a variable-stiffness web in terms of achievable changes in bending-twist coupling. This has already been demonstrated in the frame of the introduction of the working principle proposed in this dissertation in chapter 2. Second, the laminate properties have to be regarded as design parameter with an influence on the coupling behaviour of the order of the quantities considered in the parametric study, and they can be utilised in this way in the structural design of adaptive beams and airfoils. However, it is obvious from the results that laminate coupling can be exploited to enhance the twist effect only in case of the closed section. For the c-profile, in contrast, the twist compliance is maximised for a unidirectional 90° layup which does not induce any bending-twist coupling but rather minimises the warping stiffness. If the adaptation range for the twist of a variable-stiffness wing box is to be maximised, a design without layup-induced elastic coupling has thus to be chosen.

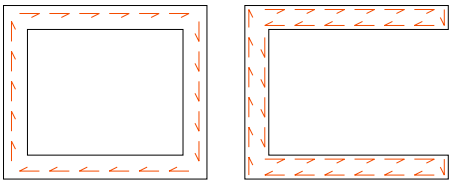

Figure 4.24: Qualitative illustration of the shear flow in thin-walled profiles under torsion: closed rectangular cross section vs. open c-profile

[9]The value ranges of these plots for negative inner lamination angles follow directly from the symmetry of the plotted surfaces with respect to the origin.

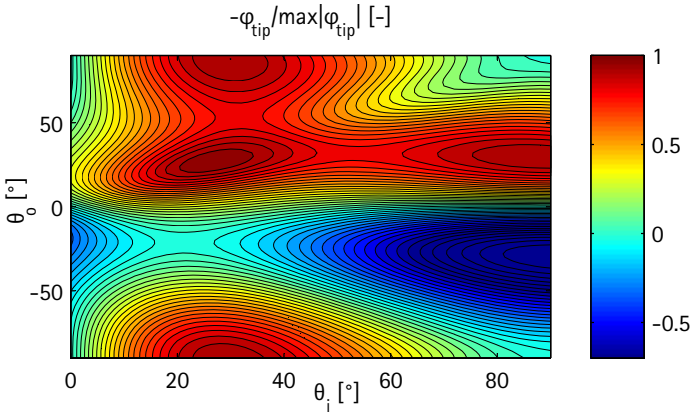

Figure 4.25: Normalised twist compliance at the tip of a profile beam with rectangular cross section and laminated flanges with respect to ply angles. B/H = 2, L/B = 10, $t_f/t_w = 3/2$ (t_f flanges' thickness, t_w webs' thickness), $H/t_f = 16$

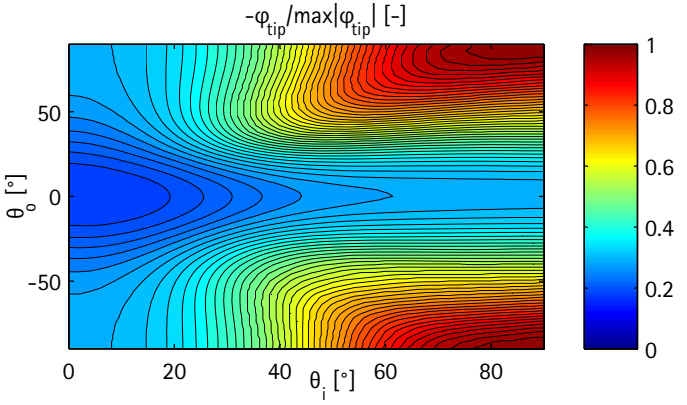

Figure 4.26: Normalised twist compliance at the tip of a c-profile beam with laminated flanges with respect to ply angles. B/H = 2, L/B = 10, $t_f/t_w = 3/2$ (t_f flanges' thickness, t_w web's thickness), $H/t_f = 16$

Besides the parametric study, the experimental wing box structure discussed in 4.3.2 has been simulated by means of a finite element model, wherein the material properties reported in appendix A.1 for aluminium have been used. The results of this simulation are compared to the according analytical and experimental findings in the following section 4.3.2.

4.3.2 Experimental investigation

With a view to a validation of the theoretical results and to a proof of the presented wing box concept under laboratory conditions, a beam structure with variable-stiffness web based on polymer glass transition has been manufactured and investigated experimentally. In this section, the most important findings related to this experiment and the respective calculations shall be mentioned, while a more detailed report is included in [79] and [99].

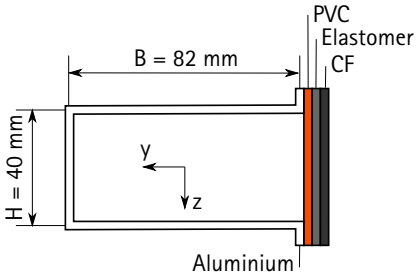

Figure 4.27: Composition and geometry of experimental wing box structure with thermomechanical web (cross section)

As presented in figure 4.27, the beam with a length of $L = 800$ mm and cross-sectional dimensions according to the figure consists of an aluminium base structure with 1 mm wall thickness, a PVC web of the same thickness constituting the adaptive component, a layer of carbon fibre (CF) fabric as ohmic heating element and an elastomer layer in between. The latter allows for heat conduction between heating layer and adaptive web but, at the same time, elastically decouples these components, so that the carbon fibre ply does not constrain the range of stiffness adaptation, and all components different from aluminium structure and polymer web can be neglected in the calculations. Since the elastomer is characterised by an inherent adhesiveness, no dedicated bonding layers are required neither between PVC and elastomer,

nor between elastomer and carbon fibre fabric. The PVC web, in contrast, is bonded to the aluminium structure by epoxy resin.

In order to minimise temperature gradients in the adaptive web due to electrical contact resistance, the carbon fibre fabric is designed to protrude in x-direction at the beam's root and at its tip, where the electrical contact is applied, by about 10% of the beam length. Moreover, the longitudinal fibres to be connected to the electrical wires have been heated using a gas torch to remove any potentially existing fibre sizing. However, compared to heating elements made of CFRP [107], the unimpregnated fabric employed here is more convenient in terms of introduction of electric currents. A controllable current source has been used to heat the CF layers and finally set the web temperature, and thermocouples have been applied to the inner surface of the PVC web at $x = 400\,\text{mm}$ and $x = 780\,\text{mm}$ for temperature monitoring. The beam is clamped at its root by means of steel plates and screw clamps, and an aluminium rib bonded to the base structure using epoxy (see figure 4.30) serves as load introduction component. According to what has been explained in chapter 3, the load introduction rib has an open shape allowing for a low warping stiffness, which is essential for a broad adaptation range. Via a cable connected to this rib, controlled transverse forces exerted by a *Zwick 1474* tensile testing machine can be applied to the beam in order to investigate its bending-twist coupling behaviour.

Figure 4.28 presents the deflection compliance recorded for different web temperatures with a pair of laser triangulation sensors at the tip of the structure, at the top surface of the upper flange (with respect to the orientation of figure 4.27). The deflection value $w_{0\,\text{tip}}$ has been determined as the mean of the values recorded by the two sensors at $y = \pm 30\,\text{mm}$. The resulting twist compliance, on the other hand, is plotted against the web temperature in figure 4.29, and both figures also show the corresponding results of analytical and FE calculations. The experimental results are presented for up to three load steps defined by different values of transverse forces between 5 N and 15 N (see [99] for a detailed documentation). They are expressed as mean values of displacement data from repeated measurements and of temperature data of both thermosensors, and error bars represent the corresponding standard deviations.

The effect of adaptive bending-twist coupling, that has already been demonstrated theoretically, is articulately reflected in the experimental results, which show changes in torsional stiffness by a factor of about 35, while the deflection stiffness is changed by a factor of less than 6. By comparison of these results with the DMA results for the pure PVC in figure 4.1, it can be

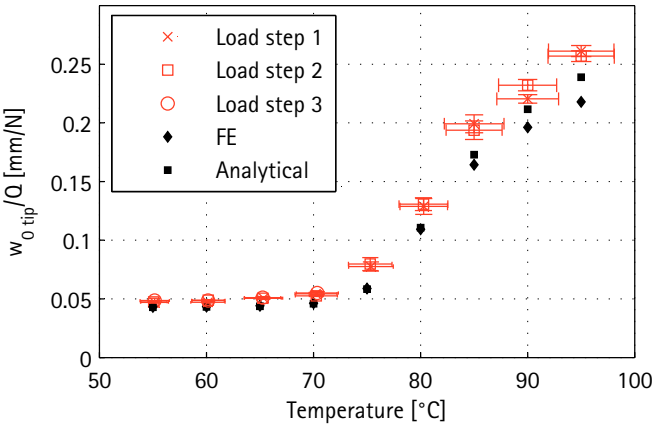

Figure 4.28: Deflection compliance at the tip of an adaptive wing box structure with thermomechanical coupling with respect to temperature. Comparison of analytical, numerical and experimental results

concluded that around half of the stiffness adaptation range of the polymer (in terms of torsional stiffness) can be preserved when integrating it in the wing box structure. Deviations of the measured displacement values from the calculated ones of up to 15% are though observed, and the scatter in the temperature data resulting from an inhomogeneous temperature distribution can already be identified in the plots as a major potential error source. Due to the thermomechanical nature of the experiment, there are however many more. The deviations are slightly higher for the twist angle, as it is expected for this derived quantity.

Despite quantitative discrepancies between calculations and experiment, the effect of adaptive twist by shear centre shift and variable torsional stiffness has been qualitatively demonstrated by the reported results, and it is well visible also in the photographs of figure 4.30 showing the adaptive wing box under load in states of low and high bending-twist coupling.

As a synthesis of the findings on the behaviour of adaptive profile beams based on glass transition, figures 4.31 and 4.32 present the changes in bending and torsional stiffness over a wide range of modulus ratios. Besides the analytical calculations relying on the theory for closed profiles introduced

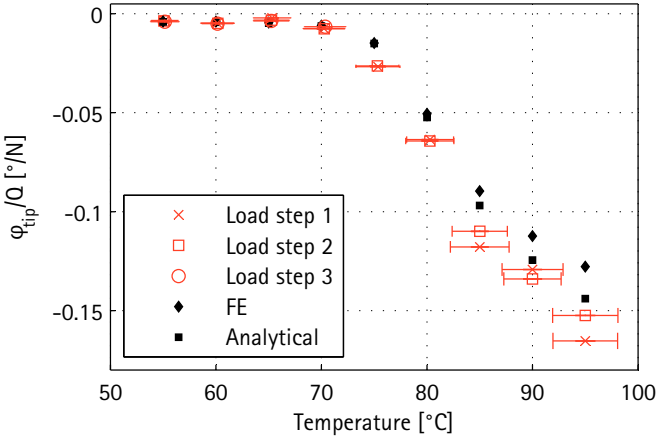

Figure 4.29: Twist compliance at the tip of an adaptive wing box structure with thermomechanical coupling with respect to temperature. Comparison of analytical, numerical and experimental results

previously, the analytical solutions of the open c-profile[10] and of the closed profile when neglecting the warping constraint are shown. In addition to the experimental results of the adaptive wing box structure introduced before, the ones of the limiting case of an aluminium c-profile[11], which has also been investigated experimentally, are shown for comparison. The results for this case are plotted close to the highest stiffness ratio shown in the diagrams, as a representation of the infinite stiffness ratio at which they would have to appear. All analytical results are based on the cross-sectional dimensions $B = 80$ mm, $H = 40$ mm which are referred to in the diagrams as "ideal geometry". The "experimental geometry", which is specified in addition, slightly differs from the ideal one only in case of the adaptive beam structure, which possesses the aforementioned dimensions. For both kinds of geometries, all wall thicknesses amount to 1 mm.

The already mentioned nature of the analytical solutions for closed sec-

[10] The analytical solution for the open c-profile is only defined for an infinite stiffness ratio but is plotted as an asymptote in figures 4.31 and 4.32 for presentation reasons.

[11] For simplicity reasons, this experimental structure is referred to as "c-profile", although it also exhibits the small aluminium flanges which are used in the adaptive beam for bonding the polymer web to the aluminium profile.

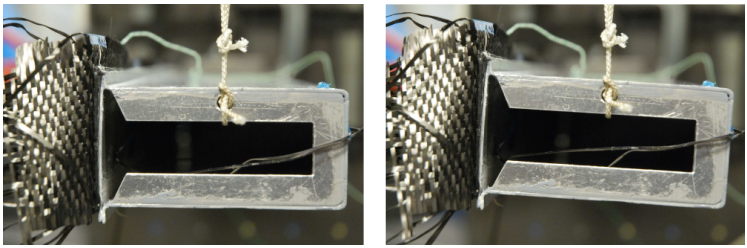

Figure 4.30: Adaptive bending-twist coupling visualised by photographs of the experimental wing box based on thermomechanical coupling loaded by $Q = 20$ N at 30°C and at 95°C

tions to overestimate the compliance at high modulus ratios is only observed for the case with neglected warping constraint in the considered range of stiffness ratios[12]. Whereas this solution virtually coincides with the one considering the warping constraint for low E_1/E_2 values, for which the twist behaviour is hardly affected by warping, the respective curves begin to substantially deviate from each other above a certain stiffness ratio, since neglecting the warping constraint is not realistic for lower web stiffness values, for which the beam's torsional characteristics are strongly influenced by warping.

A further peculiarity of the results presented in figures 4.31 and 4.32 consists in the pronounced divergence of analytical and numerical solution at low stiffness ratios. This behaviour can be explained by the fact that the design of the load introduction rib has been assumed to stay constant over the whole range of stiffness ratios, which leads to a trade-off between high warping compliance required for the states of low web modulus and high stiffness required for the rib to fulfil its load-distributing and supporting function at the other side of the modulus range. As it is reflected in the results, a design which complies better with the first requirement has been chosen, so that the cross section at the beam's tip is accordingly characterised by considerable local deformation, especially in states of high web modulus. This becomes manifest both in the deviation of the numerical solution from the analytical one, which assumes ideal load introduction, and in the separation of the numerical twist angle curve in two branches, which represent the values evaluated between $y = -35$ mm and $y = 0$ and between $y = 0$ and $y = 35$ mm, and

[12] At even higher E_1/E_2 ratios also the solution which takes the warping constraint into account has been found to predict too high compliance values.

which thus differ from each other when the cross section is deformed locally.

A comparison of the twist compliance results of the experimental wing box structure with the ones of the c-profile reveals that, with a view to the maximisation of the adaptation range, the experimental structure mainly covers the "softer" part of the modulus range that can be practically exploited for compliance changes, and slight design adjustments would allow an additional utilisation of the adjacent region of lower E_1/E_2 ratios, from which a considerable broadening of the range of achievable twist angles can be expected.

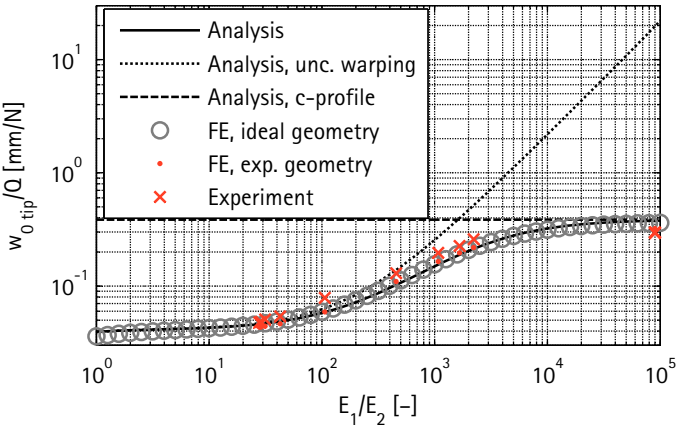

Figure 4.31: Deflection compliance of adaptive wing box based on thermomechanical coupling with respect to stiffness ratio. Comparison of analytical, numerical and experimental results

4.4 Global behaviour—the airfoil

The effectiveness of the structural concept of an adaptive-twist wing box based on shear centre shifting and variable torsional stiffness by means of thermomechanical coupling has been demonstrated by the theoretical and experimental results presented in the previous section. As the next step on the way to the implementation of the idea to realise fixed wings with adaptive twist, the concept's performance when integrated in an airfoil structure and

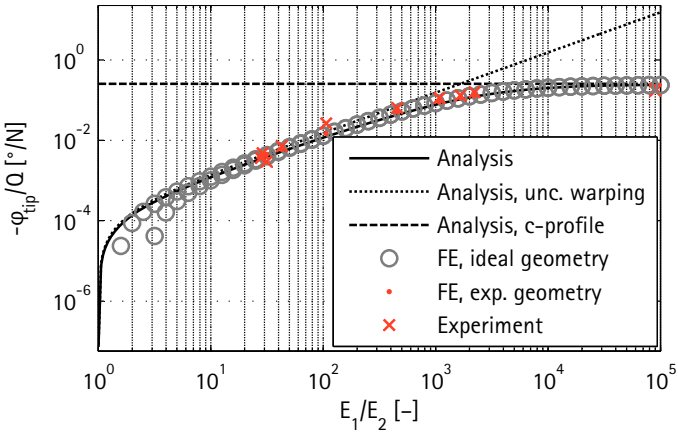

Figure 4.32: Twist compliance of adaptive wing box based on thermomechanical coupling with respect to stiffness ratio. Comparison of analytical, numerical and experimental results

the manufacturability of a wing structure with highly integrated variable-stiffness spars shall be investigated. The present section deals with these aspects, for which again an approach combining numerical and experimental work is pursued. Additionally, a numerical upscaling of the adaptive-twist airfoil to dimensions and operating conditions of a realistic fixed wing application is performed. For presentation reasons, mention of certain details is set aside also in this section, and it is referred to [99] again for these particulars.

4.4.1 Numerical investigation

Similarly to the practice applied for studying the wing box behaviour, a numerical parametric study shall first provide insight in the general trends of the adaptive airfoil's mechanical characteristics. Based on the findings of this investigation, a favourable design for an adaptive-twist airfoil shall be developed, which shall be applied for the realisation of an experimental adaptive wing structure which is discussed in 4.4.2. Like in the previous section on the adaptive wing box, another finite element model shall be employed to simulate the experimental structure. In order to account for aeroelastic effects which have to be considered for the upscaling of the airfoil, the structural

model is coupled to an aerodynamic model simulating the airflow, and iterative calculations are conducted. The numerical work is discussed in the following paragraphs.

According to the general design considerations of chapter 3, a structural layout of the adaptive-twist airfoil has been devised which is used as a baseline for all numerical models. While figure 4.33 shows the basic parameterisation of the geometry, figure 4.34 defines the numbering scheme and the particular geometrical quantities of the variable-stiffness interfaces, and figure 4.35 presents an image of the finite element model of this baseline configuration, along with the coordinate system applied in the following discussion. The design of the ribs becomes apparent from figure 4.36 which shows a cross section of the FE model.

While the skin of the airfoil and the wing box flanges are assumed to consist of symmetrical, balanced CFRP laminates composed of layers with unidirectional reinforcement, the spar plates have been chosen to be made of glass-fibre reinforced polymer (GFRP) laminates based on a bidirectional fabric, which accounts for the electric insulation requirements of these components in contact with ohmic heating layers[13]. The elastic properties of the respective constitutive plies of both types of laminates are specified in appendix A.1, and for the elastic modulus of PVC the values used for the adaptive wing box (cf. the previous section 4.3) are applied in the numerical models. The temperature dependent behaviour of the Poisson ratio of PVC has been accounted for, according to [108], by

$$\nu = \nu\big|_{T=23°\mathrm{C}} + \left(0.5 - \nu\,\big|_{T=23°\mathrm{C}}\right)\left(1 - \frac{E}{E\,\big|_{T=23°\mathrm{C}}}\right) \tag{4.4}$$

where $\nu\,\big|_{T=23°\mathrm{C}} = 0.38$ [109].

All the laminates are modelled by shell elements in the finite element simulation. The PVC parts, in contrast, are modelled by solid elements, since not only they can be expected to exhibit pronounced shear deformations in soft system states, but also at least interfaces 1 and 3 have to be represented with a three-dimensional geometry in the model to simulate the actual topology of the structure.

Parametric study The parameter study aims at a characterisation of the design space of the proposed structural concept integrated in the structure of

[13] Cf. 4.4.2 and appendix A.1.

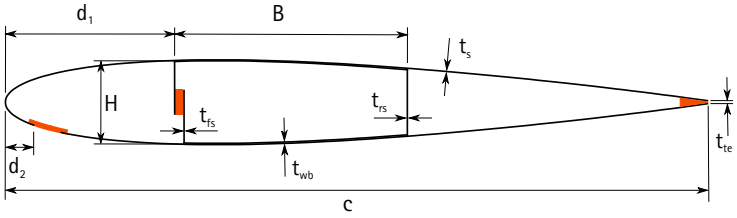

Figure 4.33: Main geometric parameters of the cross section of an adaptive airfoil based on thermomechanical coupling

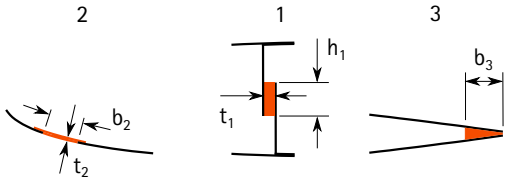

Figure 4.34: Numbering and cross-sectional geometry of thermomechanical variable-stiffness interfaces in adaptive airfoil

a fixed wing in order to gain general findings on the mechanical behaviour of adaptive-twist airfoils with variable-modulus interfaces but also to enable the design of a suitable experimental structure which shall be investigated by static mechanical testing. In contrast to the numerical upscaling discussed below, the scaling and some simplifying assumptions required under laboratory conditions have thus been adopted from the experiment for the parametric study.

This is not only reflected in the data of table 4.2, which summarises the dimensions assumed for the baseline configuration of the parameter study but also in further properties of the airfoil structure considered in the parametric study: On the one hand, the choice of a NACA 0012 shape for the parameter study corresponds to the experimental structure, and on the other hand, also the boundary conditions are inherited from the experiment: the clamping of the wing box at the root and, for practical reasons, the substitution of the distributed aerodynamic load by a concentrated force Q in z-direction acting at the wing tip, at $y = y_{\mathrm{CP}}$. According to thin-airfoil theory, the chordwise

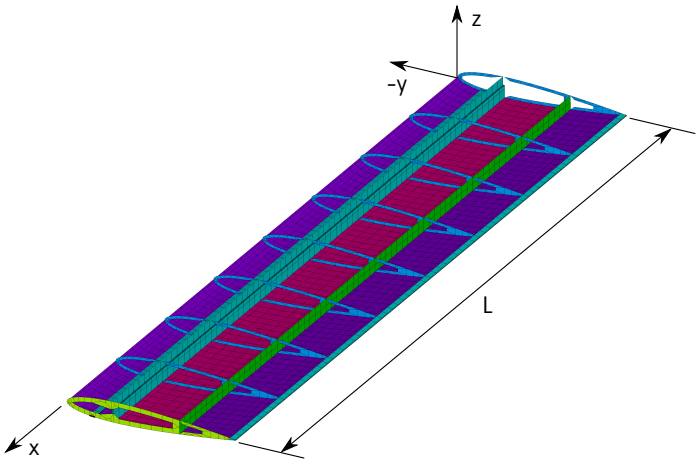

Figure 4.35: Finite element model of adaptive-twist airfoil based on thermomechanical coupling in baseline configuration (upper half of the skin is not shown) and coordinate system

distance of neutral point and centre of pressure is given by ([110])[14]

$$y_{\mathrm{NP}} - y_{\mathrm{CP}} = \frac{c_{m0}}{c_l} c \tag{4.5}$$

Since the zero-lift moment coefficient c_{m0} is zero for the symmetrical NACA 0012 airfoil, the centre of pressure coincides with the neutral point under the assumptions of linear theory. Accordingly, $y_{\mathrm{CP}} = c/4$ has been assumed for the parametric study, and the concentrated transverse force has been applied in this point, at the upper ($z > 0$) part of the airfoil's skin.

The dimensions specified in table 4.2 have not been chosen arbitrarily but are the result of a systematic sizing process which has been applied with the intention of ensuring the generation of comparable designs with realistic load-carrying capabilities for the parameter investigations. In this procedure, wall thicknesses and rib spacing of the wing structure are varied until in the most critical state, which is defined by the minimum interface modulus

[14]The zero-lift moment coefficient c_{m0} is assumed to be positive if the according moment points in the direction of increasing angles of attack.

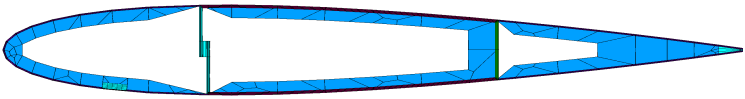

Figure 4.36: Cross section of finite element model of adaptive-twist airfoil based on thermomechanical coupling in baseline configuration

assumed as 12 MPa, the smallest buckling load equals to 90 N, the ultimate transverse force the experimental structure is supposed to be dimensioned for.

For the evaluation of the calculations of the parametric study, the *relative interface modulus* $\hat{E}$ is introduced as a dimensionless parameter specifying the state of an interface. It is defined as the ratio between an interface's elastic modulus at a certain temperature and its elastic modulus at room temperature:

$$\hat{E} = \frac{E}{E\,\big|_{23\,^\circ\mathrm{C}}} = \frac{E}{2.40\,\mathrm{GPa}} \tag{4.6}$$

Table 4.2: Geometric properties assumed for the baseline configuration of the parameter study related to the adaptive airfoil based on thermomechanical coupling

Parameter	L	c	B	d_1	d_2	b_2	b_3	t_2	t_{fs}
Value [mm]	1'300	300	120	80	40	10	10	2	1.25

Parameter	t_r	t_{rs}	t_{te}	t_s	t_{wb}
Value [mm]	1.05	1.25	0.75	0.6	1.2

Parameter	h_1/H	t_1/t_s
Value [–]	0.2	5

As a first parameter investigation, the influence of the relative importance of the different adaptive interfaces on the behaviour of the airfoil structure has been studied. Figures 4.37 and 4.38 show the results of this investigation by plotting the relative shear centre location and the normalised tip twist compliance with respect to $\hat{E}$ for different combinations of activated

interfaces. As it can be expected a priori, interface 1 (in the front spar) has the highest relative influence on the shear centre location and by that also on the twist compliance, while interface 2 (in the front cell) affects the shear centre position much less, and softening of interface 3 (at the trailing edge) even slightly moves the shear centre towards the leading edge. To which degree the airfoil's elastic behaviour is influenced by the synergetic interaction between shear centre shifting and opening of cells cannot be predicted intuitively, on the other hand. In this context it is noticeable that activating interface 2 in addition to interface 1 results in an increase in torsional compliance by a factor of about 15 (for the lowest $\hat{E}$ value), while by means of an additional activation of interface 3 a gain in compliance by another 40% can be accomplished. It should be mentioned as well that, as against the maximum increase in twist compliance by a factor of more than 40 found for the considered stiffness range, the tip deflection of the shear centre has been observed to vary only by less than 15% under these conditions, which demonstrates the capability of the suggested structural concept to provide large changes in global bending-twist coupling also when integrated in a wing structure.

Further parameter variations concern the main geometrical quantities of the adaptive-twist airfoil: the chordwise location and the width of the wing box, the height and the thickness of interface 1, as well as the chordwise placement and extension of interface 2. Chord length, skin thickness and number of ribs (nine, as evident from figure 4.35), on the other hand, are held constant for all parameter investigations. Moreover, all three interfaces are assumed to be activated and characterised by the same elastic modulus for the parametric studies and for all further analyses discussed in the following paragraphs.

The results are reported in terms of the coupling ratio at the tip of the structure $\phi_{\mathrm{tip}}/w_{\mathrm{S\,tip}}$ ($w_{\mathrm{S\,tip}}$ denoting the deflection of the shear centre at the tip) for different interface states in figures 4.39 to 4.41. They show that, first (figure 4.39), the wing box properties have a decisive influence on the airfoil structure's global behaviour. Due to its large effect on the twist in states of low torsional stiffness, the chordwise offset d_1 should be maximised, if large changes in bending-twist coupling are requested. An even higher influence on the twist/deflection ratio is observed for the wing box width B, which

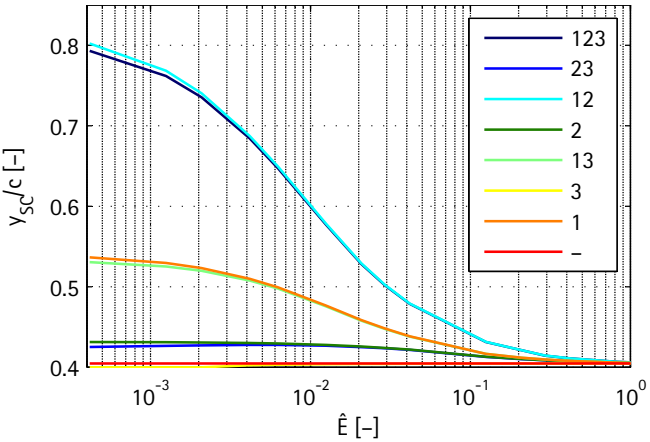

Figure 4.37: Relative shear centre location of adaptive-twist airfoil with respect to relative interface modulus for different combinations of activated adaptive interfaces (indicated by the numbers in the legend)

mainly controls the shear centre location and hence the torsional moment under quasi-open conditions.

Second (figure 4.40), the importance of the shear stiffness of interface 1 is reflected in the influence of relative height and thickness of this interface on the airfoil's bending-twist coupling: High thickness and low height of the polymer layer at the overlap raise the local shear compliance, which again affects the global behaviour mainly in the soft states, where it results in large twist angles.

Third (figure 4.41), the study on the influence of the properties of interface 2 shows that this interface should be designed to have a width of at least about 5% of the chord length (i. e. about 20% of the width of the front cell) to be able to constitute a virtual opening and thus to allow for a sufficiently low warping stiffness in states where the airfoil is requested to twist. The chordwise location of interface 2, in contrast, has only a minor influence on the global behaviour, as a result of the fact that the main function of this interface is to open the front cell, not to move the airfoil's shear centre.

Also the thickness of interface 2 (t_2) and the width of interface 3 (b_3), whose effects have been investigated in further parametric studies, turned

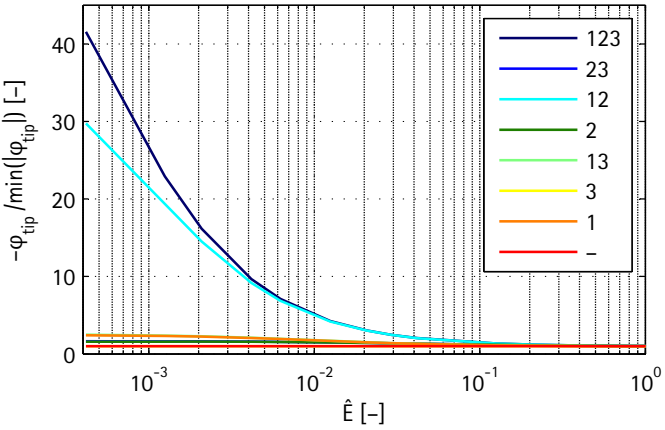

Figure 4.38: Normalised tip twist angle of adaptive-twist airfoil with respect to relative interface modulus for different combinations of activated adaptive interfaces (indicated by the numbers in the legend)

out to hardly affect the global twist of the airfoil when varied in reasonable ranges, so that the results of these calculations are not presented here.

Simulation of experimental airfoil structure As mentioned in the previous paragraph, the design of the baseline model for the parametric study has been chosen to be close to the one of the experimental airfoil structure. However, there are a number of characteristics of the experimental structure which are not implemented in the numerical models for the parameter investigations due to the more general intention of the latter but are considered in the specific simulation of the experimental airfoil structure. One of these particularities is given by the heating stripes integrated in the experimental wing to activate the variable-stiffness interfaces. As it is evident from figure 4.42, which illustrates the composition of the adaptive interfaces in the experimental structure, these 0.33 mm thick CFRP stripes are complemented by insulation layers made of aramide fibre reinforced polymer (AFRP) with a thickness of 0.51 mm. The material properties of the bidirectional laminates

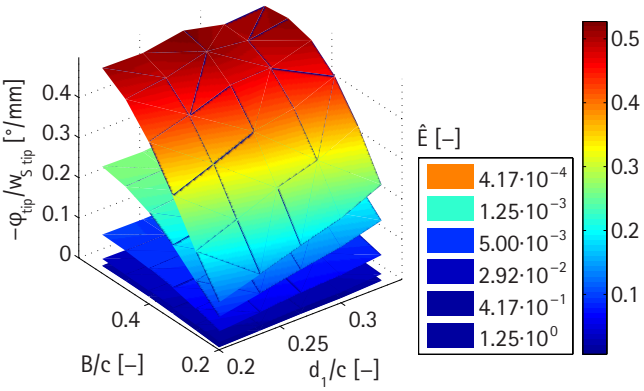

Figure 4.39: Influence of relative width and offset of wing box on the coupling ratio of an adaptive-twist airfoil for different values of relative interface modulus

employed for these heating and insulating layers are specified in appendix A.1. In case of interface 1, the presence of two heating layers on the same side of the PVC layer stands out, which can be explained by the fact that the outer CFRP layer had to be retrofitted as a replacement for the inner one which had suffered damage during the preliminary tests. Not only the wall thicknesses and overlap widths resulting from the experimental interface design, but also thicknesses at other locations which are affected by manufacturing tolerances have been measured in the experimental airfoil structure and considered in its numerical simulation. Furthermore, the detailed FE model accounts for the stepped shape of interface 2 in the real structure, for bonding layers between the spar parts and the skin and for the layer of varnish covering the skin. The respective details are reported in [99] and are also partly contained in appendix A.1. An additional difference between parameter study and experiment is constituted by the higher number of ribs of eleven in case of the latter.

The results of the finite element simulation of the realised wing structure are presented along with the experimental results in section 4.4.2.

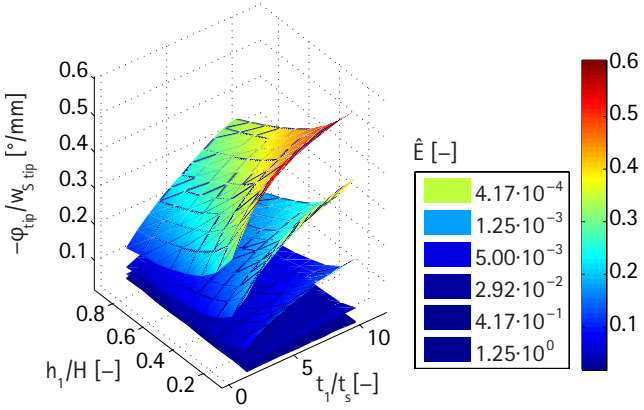

Figure 4.40: Influence of relative height and thickness of interface 1 on the coupling ratio of an adaptive-twist airfoil for different values of relative interface modulus

Upscaling In contrast to the aforementioned parametric study, which aims at an investigation of the design space of the experimental structure, and to the simulation of the experimental airfoil structure itself, the numerical upscaling pursues the objective of evaluating the effectiveness of the proposed structural concept for the characteristics and under the operating conditions of a realistic example of a fixed wing.

As such a virtual test-bench, a wing with non-swept rectangular planform of $2L = 15\,\text{m}$ span, $c = 0.6\,\text{m}$ chord length and a NACA 2412 shape is chosen. Regarding the flight conditions, an airplane mass of $m = 415\,\text{kg}$ and a stationary horizontal flight at a speed of $v = 41\,\text{m/s}$ in standard atmosphere at sea level are assumed. In terms of wing span and aspect ratio, flow velocity and wing loading these conditions are close to the ones of a typical glider plane of the 15 m competition class like the *Schleicher ASW 27* [111]. The simplifying assumptions for the wing planform used for the numerical upscaling can thus be pointed out by an illustration contrasting this planform with the one of the *ASW 27*, as shown in figure 4.43.

Table 4.3 summarises the design of the upscaled airfoil. With respect to a realistic sizing, the wing is required to exhibit a smallest buckling factor of three. This specification is met by an airfoil design in which the wall

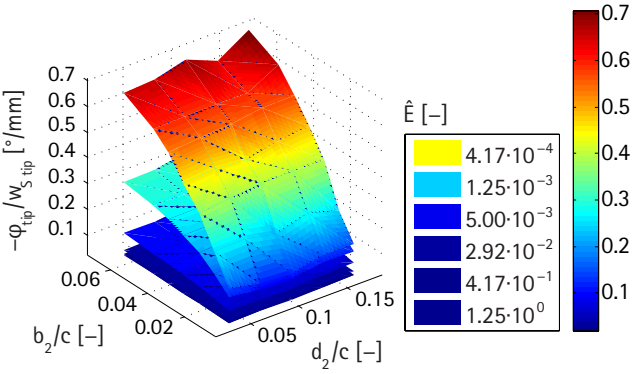

Figure 4.41: Influence of relative width and offset of interface 2 on the coupling ratio of an adaptive-twist airfoil for different values of relative interface modulus

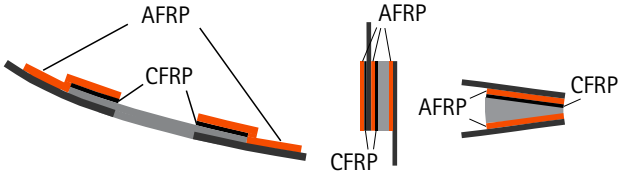

Figure 4.42: Composition of variable-stiffness interfaces in experimental adaptive-twist airfoil

thicknesses of all components are—compared to the design of the parametric study—increased by a factor of eight by uniform scaling of the thicknesses of all laminae. Owing to the wing's larger aspect ratio, a higher number of ribs, namely 24, has to be provided in the upscaled structure.

In order to assess the effectiveness of the adaptive-twist concept proposed in this dissertation under the described conditions close to the ones of a commercial glider plane, the airfoil's aeroelastic behaviour has to be included in the numerical calculations. For this purpose, not only a realistic surface loading due to aerodynamic pressure has to be implemented in the finite element simulation, but also the elastic structural model has to

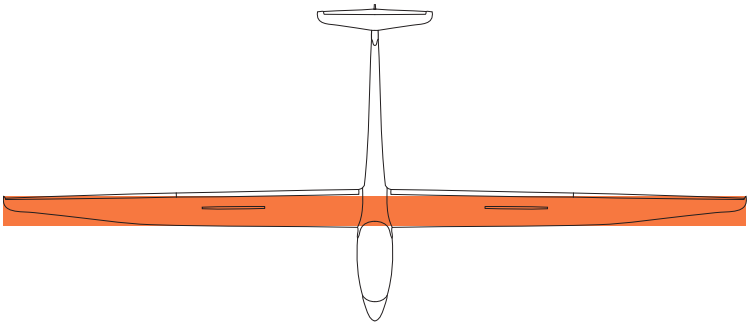

Figure 4.43: Simplified rectangular wing for numerical upscaling (shown in orange) in comparison with the wing of the Schleicher ASW 27 glider plane

Table 4.3: Geometrical parameters of upscaled adaptive-twist airfoil based on thermomechanical coupling

Parameter	L	c	B	d_1	d_2	b_2	b_3	t_2	t_{te}
Value [mm]	7'500	600	240	160	80	20	20	4	1.5

Parameter	h_1/H	t_1/t_s
Value [–]	0.2	5

be coupled to an aerodynamic model. Figure 4.44 illustrates the simulation approach, which requires iterative calculations due to the coupled nature of the aeroelastic problem. This computational procedure involves the structural analysis software *ANSYS* to implement the geometry of the structural model, to discretise the model in finite elements, to apply boundary conditions and to solve it in the elastic domain. On the aerodynamic side, the airfoil theory based software *XFOIL* is applied to calculate the pressure distribution of the two-dimensional airfoil defined by the wing's cross section assuming an incompressible and inviscid fluid, and a lifting line method [112–114] implemented by means of the computation software *MATLAB* corrects this pressure distribution for every spanwise location at which nodes are placed in the structural model. *MATLAB* is further used to run the iteration cycle and to hand over data between the different computational tools.

The static aeroelastic problem is convergent as long as increments in aero-

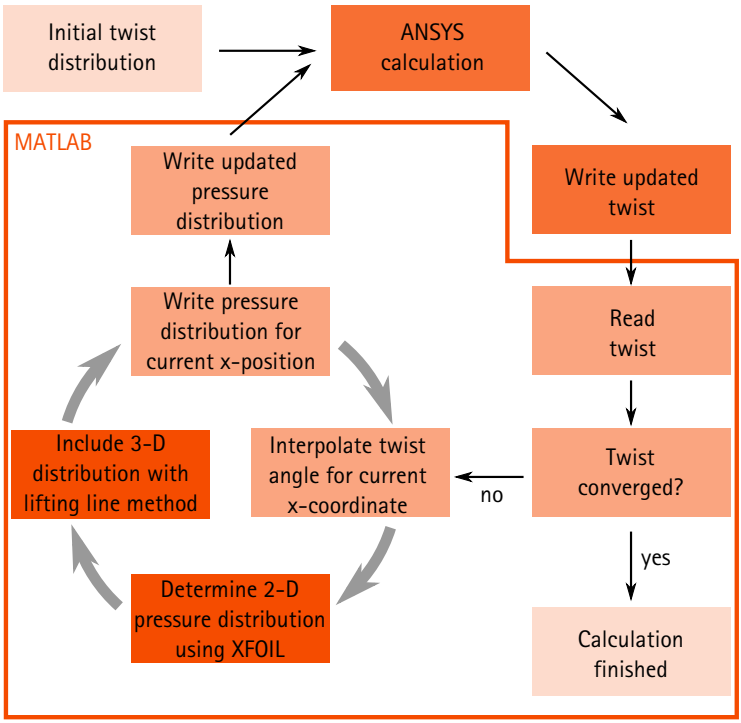

Figure 4.44: Iteration scheme for aeroelastic calculations

dynamic loads can be reacted by structural forces and moments. In this case, the iterative calculations converge to an equilibrium solution representing a statically stable aeroelastic state of the airfoil. If, in contrast, changes in aerodynamic loads cannot be compensated anymore by an elastic reaction, a static aeroelastic instability is reached, and the aforementioned iteration cycle does not converge anymore.

One of the best-known of such instabilities is the torsional divergence of an airfoil, which occurs if an increment in twisting moment cannot be reacted by the wing's torsional stiffness [115, 116]. In chapter 3, it has already been

characterised as a potential limitation for the adaptive-twist airfoil due to the aeroelastic amplification during shape adaptations relying on wash-in twist. In the computation routine described previously, this phenomenon can thus be identified in non-converging solutions, and the divergence velocity, being defined as the smallest flow velocity for which an airfoil is divergent, can be determined numerically as the smallest flow speed for which no convergent solution is found.[15] Concerning the investigation of bending-twist flutter as a dynamic aeroelastic instability, the reader is referred to the investigation of the adaptive-twist airfoil with electromechanical coupling (see 5.4.1), which is more critical in this respect.

Under the assumed flight conditions, the lift coefficient in the initial, unactivated state of the adaptive-twist airfoil has to be given by

$$c_L = \frac{mg}{\rho v^2 Lc} = 0.44 \tag{4.7}$$

assuming a gravitational acceleration of $g = 9.81\,\mathrm{m/s^2}$ and an air density of $\rho = 1.225\,\mathrm{kg/m^3}$ [110]. The upscaled adaptive wing meets this condition at an angle of attack of 2°, which has thus been assumed for all aeroelastic calculations.

The aeroelastic equilibria resulting from the numerical investigation of the adaptive-twist airfoil under conditions close to the ones of a glider wing are shown for different states of the variable-stiffness interfaces in figure 4.45. It is obvious from the plots in this figure that, due to its large impact on shear centre location and torsional stiffness, the stiffness ratio can be utilised to effectively control the wing twist, and that stable equilibria can be reached even for low relative interface moduli (down to 5‰ of the value at room temperature) at the considered flight velocity. The twist angles, which are evident from this figure in terms of their tip value and from figure 4.46 in terms of their spanwise distribution, reach maximum values of around 12° in the analysed stiffness range, so that the airfoil still provides a considerable safety margin against stall [110].

Figure 4.47 presents the corresponding values of lift coefficient as a function of $\hat{E}$, showing that changes in lift by up to more than 170% are enabled by the twist of the adaptive airfoil in the considered stiffness range.

As already mentioned, aeroelastic divergence can potentially limit the applicability of the airfoil with controllable shear centre location and torsional

[15] Strictly speaking, there are always different potential reasons for a solution not to converge. Aeroelastic divergence has thus to be verified as the actual cause of a non-converging solution by investigation of solutions obtained close to the determined critical velocity.

stiffness. However, the calculated values of divergence velocity shown in figure 4.48 demonstrate that the adaptive-twist airfoil is statically stable up to a flow speed of about 50 m/s for $\hat{E} = 5 \cdot 10^{-3}$, which represents the most critical of the considered states.

As a performance measure of the upscaled adaptive-twist airfoil in terms of its capability to change the wing loads, the roll moment coefficient

$$c_{M_{\text{roll}}} = \frac{M_{\text{roll}}}{cL^2 \rho v^2} \tag{4.8}$$

(M_{roll} denoting the airplane's roll moment) is evaluated. Although the analysed wing design is not equipped with any measure for reverse twist and the consideration of dynamic requirements for a flight control application has been set aside to date, it is however appropriate at the conceptual state of this work to demonstrate, by theoretical evaluation of such a figure of applicational interest, the concept's effectivity under the premise that technical solutions for certain issues like the aforementioned ones can be provided. In figure 4.49 the values of roll moment coefficient of the adaptive-twist airfoil with thermomechanical working principle as a function of interface stiffness are compared to the ones enabled by a conventional aileron extending over the whole span and 17% of the chord, which are plotted with respect to the aileron's deflection angle. For both morphing airfoil and discrete aileron an antimetric effect (with respect to both half wings) is assumed for this investigation. The resulting curves clearly show that the novel wing concept permits an authority over the roll moment of similar quantity as the one of conventional ailerons. This result constitutes an important theoretical finding of the upscaling of the adaptive-twist concept to realistic wing dimensions and operating conditions. It should be recalled at this point that the compliance of the proposed adaptive wing design with several further requirements that are decisive for its applicability in a commercial airfoil has already been demonstrated, for the entire stiffness range considered for the roll moment evaluation, in the previous discussion.

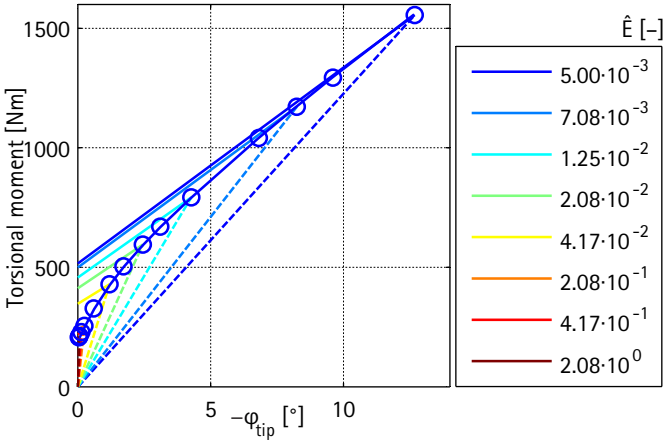

Figure 4.45: Aeroelastic equilibria of upscaled adaptive-twist airfoil based on thermomechanical coupling for different interface states

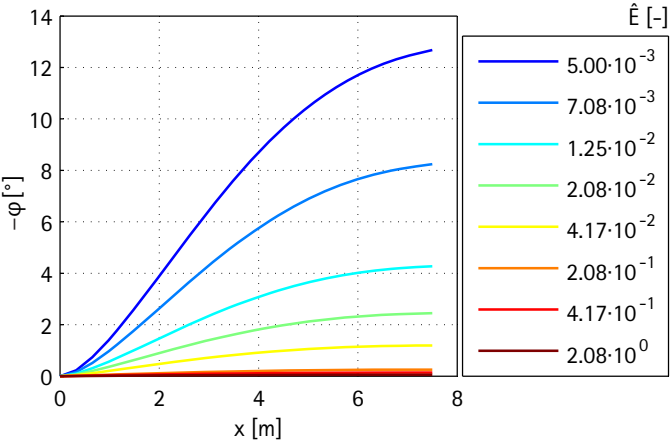

Figure 4.46: Spanwise twist angle distribution of upscaled adaptive-twist airfoil based on thermomechanical coupling for different interface states

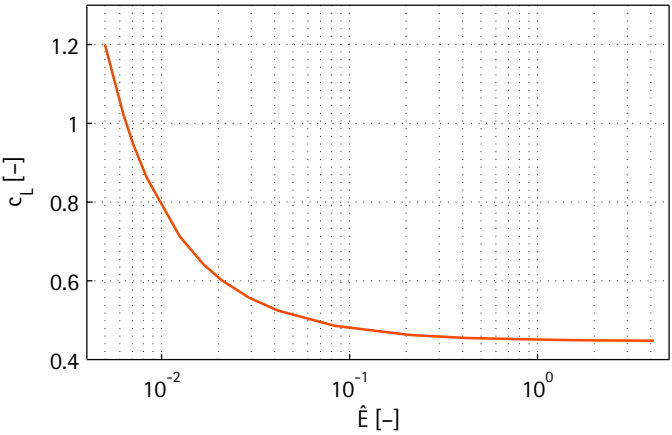

Figure 4.47: Lift coefficient of upscaled adaptive-twist airfoil based on thermomechanical coupling with respect to relative interface modulus

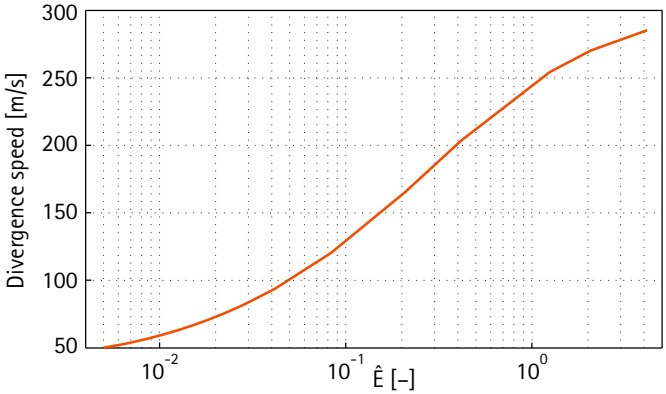

Figure 4.48: Divergence speed of upscaled adaptive-twist airfoil based on thermomechanical coupling with respect to relative interface modulus

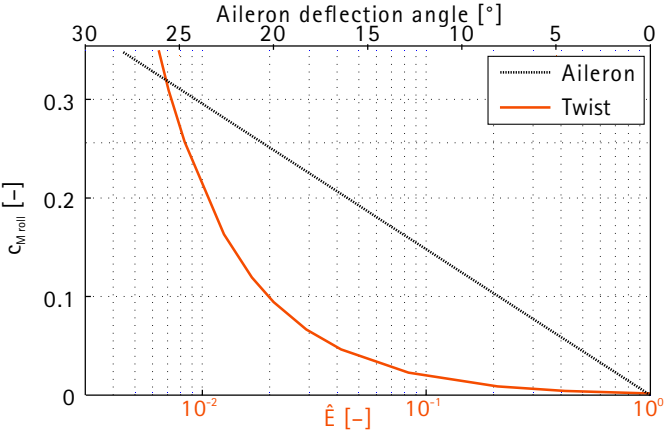

Figure 4.49: Roll moment coefficient of adaptive-twist airfoil based on thermomechanical coupling (w. r. t. relative interface modulus) and of conventional ailerons (w. r. t. aileron deflection angle)

4.4.2 Experimental investigation

In order to validate the numerical findings and to demonstrate the effectiveness of an adaptive-twist airfoil based on temperature-induced variable stiffness under laboratory conditions, such an airfoil structure has been manufactured and characterised by static mechanical testing.

The main properties of the experimental structure have already been reported in the documentation of the according numerical simulation in 4.4.1. Concerning the manufacturing, the skin has been made using the *Toho Tenax HTS40/ACG MTM 44-1* unidirectional carbon fibre/epoxy out-of-autoclave prepreg system. It has been cured under vacuum between a positive aluminium mould and—in order to obtain a smooth outer surface—a negative GFRP mould at 130°C for two hours and post-cured at 180°C for another two hours. Afterwards, the opening for the integration of interface 2 has been cut out. Wing box flanges and ribs have been manufactured using the

same material and have been bonded to the upper skin part by means of epoxy resin and, in case of the ribs, small fastening angles. Also the hand-laminated GFRP spars (with glued-in variable-stiffness interface in case of the front spar) and interface 3 have been bonded to the upper skin in this way. Figure 4.50 shows the experimental structure after the assembly of these components and attachment of 15 thermocouples along the adaptive interfaces, before closing it by bonding of the upper skin part and interface 2, which features additional seven thermosensors. The experimental airfoil structure has then been completed by glueing an aluminium block serving for the clamping into the protruding end of the wing box that is evident from figure 4.50 and by covering the outer surface by a 0.15 mm thick layer of primer and varnish.

Figure 4.50: Inner structure of experimental airfoil based on thermomechanical coupling

Figure 4.51: Completed experimental airfoil structure based on thermomechanical coupling

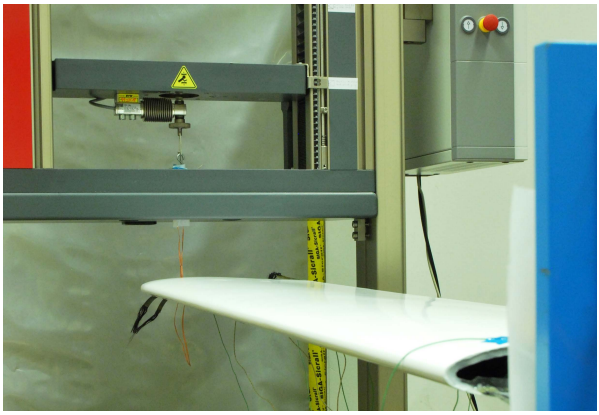

Figure 4.52: Load application to experimental airfoil structure based on thermomechanical coupling

Figure 4.51 shows a photograph of the completed airfoil, and figure 4.52 presents a photo of the set-up of the static mechanical tests, for which the structure has been placed in a *Zwick/Roell Z005* tensile testing machine equipped with a 100 N load cell in order to apply controlled transverse forces. The current sources connected to the heating layers of the variable-stiffness interfaces and the thermocouples have been integrated in a *LabVIEW* environment, such that a feedback control for the interface temperatures could be put into effect. Deflections and twist angles of the airfoil structure under transverse loads have been recorded, like in case of the adaptive wing box structure, by means of two laser triangulation sensors.

Plots of the experimental results in terms of deflection compliance in the two measuring points at the chordwise locations of the wing spars, twist compliance and coupling ratio at the airfoil's tip are provided in figures 4.53, 4.54 and 4.55, respectively, along with the according numerical findings. The data is based on measurements for which all the three interfaces are set to the same temperature and transverse forces $Q = 11$ N are applied to the structure. Error bars in the diagrams have the same significance as in the ones related to the adaptive wing box structure reported before.

Concerning the agreement of numerical and experimental results, similar observations as for the wing box structure discussed before are made: Except for the outlier value at 70°C, a good coincidence in qualitative terms is found for both deflection and twist, and there is also a good quantitative agreement for the deflection, for which the deviations between numerical and experimental values stay within 5%. For the twist angle as a derived quantity, on the other hand, the relative discrepancy amounts to up to almost 50% for certain pairs of values, due to the many uncertainties in the rather complex experimental structure with three thermomechanical interfaces and numerous components of different materials. Nonetheless, the results clearly demonstrate the effectivity of the structural concept, which permits—under the considered conditions—changes in coupling ratio by at least a factor of three[16] when integrated in a realistically sized scaled airfoil structure.

[16]It should be noted at this point that, since the coupling ratio $\phi_{\text{tip}}/w_{0\,\text{tip}}$ is not generally evaluated at the airfoil's shear centre, its deflection component is influenced by the wing's twist. For an evaluation at the shear centre, slightly higher changes in coupling ratio can be expected.

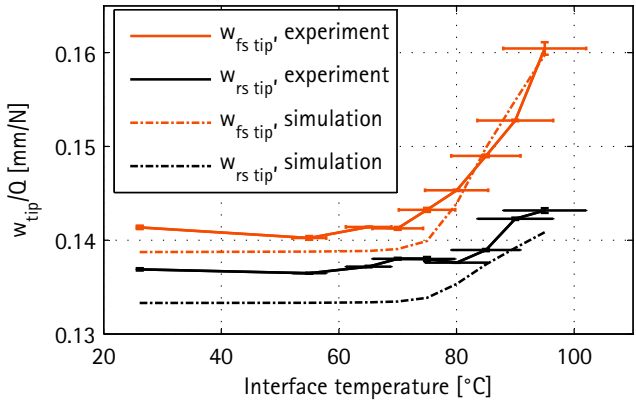

Figure 4.53: Tip deflection compliance of the experimental airfoil structure at the locations of the front wing spar (index "fs") and the rear wing spar (index "rs") w. r. t. interface temperature. Experimental vs. simulation results

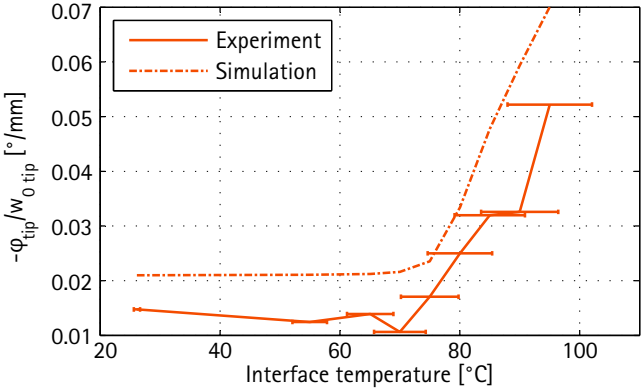

Figure 4.55: Coupling ratio $-\varphi/w_0$ at the tip of the experimental airfoil structure w. r. t. interface temperature. Experimental vs. simulation results

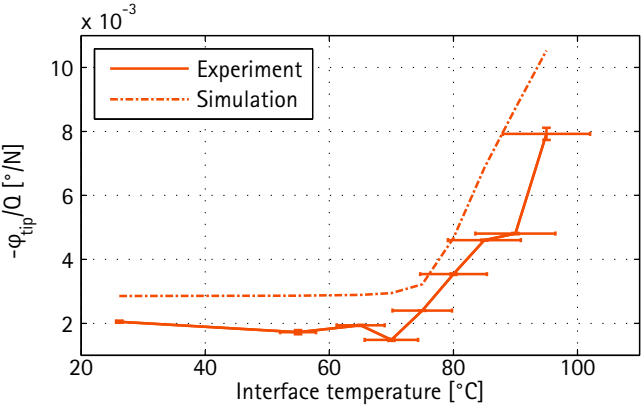

Figure 4.54: Tip twist compliance of the experimental airfoil structure w. r. t. interface temperature. Experimental vs. simulation results

5 Adaptive-twist airfoil based on electromechanical coupling

5.1 Material concept: variable adhesion by electrostatic forces

As a second smart material allowing to put the adaptive-twist concept into effect, laminates with variable shear stress transfer based on controllable electrostatic forces [68–70] have been investigated. The working principle of these *electro-bonded laminates* (EBL), which can be characterised as the electromechanical utilisation of a parallel plate capacitor, is illustrated in figure 5.1. In its most basic configuration, the EBL consists of two electrodes that are separated by a dielectric. Applying a voltage U between the electrodes causes an attraction force between them. The stress normal to the interface plane that results from the attraction is given by ([117])

$$\sigma_{\mathrm{M}} = \frac{1}{2}\varepsilon_0\varepsilon_{\mathrm{r}}\left(\frac{U}{t_{\mathrm{d}}}\right)^2 \tag{5.1}$$

It corresponds to the volumetric energy density of the EBL and is referred to as *Maxwell stress*. In equation 5.1, ε_0, ε_{r} and t_{d} denote vacuum permittivity, the dielectric's relative permittivity and its thickness, respectively. If static friction with a friction coefficient of μ occurs between electrode and dielectric, friction stresses of up to

$$\tau_{\mathrm{max}} = \mu\sigma_{\mathrm{M}} \tag{5.2}$$

are present at the contact interface. The maximum shear stress that can be transferred by the EBL can accordingly be controlled by varying the voltage between its electrodes.

In contrast to the thermomechanical material concept pursued in the previous chapter, the active principle of the electro-bonded laminate therefore does not primarily permit changes in stiffness on the material level but in strength and thus topology. As it is shown in the following sections 5.3 and 5.4, the latter can then be utilised for controllable stiffness on the structural level.

When activating the EBL interface, energy has to be spent for charging the capacitor-like system, as well as for compensation of electric losses. While the latter part is neglected at the conceptual level of the general considerations of this section, the former can be related to the Maxwell stress, which has already been introduced as the EBL's energy density. The charging energy for an EBL with interface area A can thus be expressed by

$$Q_{\mathrm{el}} = \int_{A t_{\mathrm{d}}} \sigma_{\mathrm{M}} \, \mathrm{d}V = \frac{1}{2} \varepsilon_0 \varepsilon_{\mathrm{r}} \frac{U^2 A}{t_{\mathrm{d}}} \tag{5.3}$$

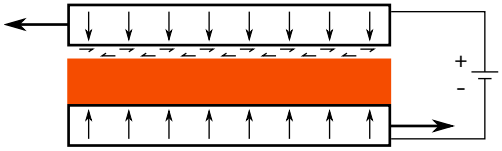

Figure 5.1: Working principle of electro-bonded laminate (EBL): Interlaminar attraction of electrodes of different electric potential separated by a dielectric (shown in orange) and friction allow shear stress to be transferred at an interlaminar interface.

The quadratic voltage dependence of the EBL's transferable shear stress, which can be deduced from equations 5.1 and 5.2, indicates that the voltage can be regarded as a powerful input quantity for the control of the topology of the electromechanical interface, which makes the integration of EBL elements a promising technology for realising stiffness changes on the structural level. This aspect is constitutive for the eligibility of EBL in the context of the structural concept proposed in this dissertation. In addition to this point, the basic relations reflected in equation 5.1 reveal further general electromechanical characteristics of the EBL and determine the order of magnitude of the involved physical quantities for the transfer of shear stress in engineering applications. Apart from the physical constant ε_0, all quantities of equation 5.1 can be adjusted to meet the specific needs of a certain application. Increasing the strength of the EBL, which can not only be assumed to be a common requirement for many technical implementations but represents at the technology's current state of maturity a necessary condition to transfer stresses of engineering relevance, thus implies increasing the dielectric constant and

the voltage while reducing the dielectric thickness. In state-of-the-art applications of EBL, voltages are hence in the kV range, dielectric thicknesses of the order of 25 μm and dielectric constants around 3.5 (referring to dielectric polymer films).

Raising the electric field intensity $|\mathrm{E}| = V/t_\mathrm{d}$ unavoidably turns electrical breakdown into the main limitation for the EBL's effectivity. Accordingly, the dielectric's breakdown strength represents another quantity of primary importance for the performance of this smart material. It has been pointed out by [118] that dielectric and insulating (i.e. breakdown-preventing) properties are naturally opposed in available materials, and multilayered dielectrics [119] have been suggested as promising candidate materials combining both qualities.

Except for the theoretical case of an application under vacuum, the presence of air gaps at the EBL's interfaces has to be taken into account. Such inclusions compromise the mechanical strength, since not only the dielectric constant of air is lower than the one of typically applied dielectrics, but—much more importantly—also the effective dielectric thickness is raised and the mechanical contact is lost at the respective locations. At least one of the electrodes—and components with possible mechanical connection—should accordingly be designed to provide a high compliance, such that it can adapt to the dielectric by way of deformation in order to close air gaps.

Up to date, the EBL's property of adjustable shear stress transfer has been applied under laboratory conditions for multilayered beams with adaptive bending stiffness [70, 120] and friction damping [59, 94] as well as for a demonstrator structure of an actively cambering morphing airfoil with variable-stiffness skin [121].

5.2 Local behaviour—the smart interface

Like in the previous chapter on the thermomechanical implementation of the adaptive-twist airfoil, the local behaviour of the smart interface shall be investigated first as a building block of the structural concept of the morphing airfoil also for the concept based on electromechanical coupling discussed in the present chapter.

In case of the thermomechanical variable-stiffness system, a linear structural analysis problem has to be solved for each temperature of interest.[1] Due to the friction-based variable-topology nature of the electro-bonded

[1] Assuming that geometric and material nonlinearities can be excluded.

laminate, the mechanical problem for structural systems with integrated EBL interfaces is generally nonlinear, in contrast. Furthermore, the importance of coupling of effects in the two physical domains is much higher for the electromechanical interface as a variable-topology system than for the thermomechanical one, which is characterised by variable stiffness: The impact that a small change in the electric field, for example, has on the mechanical performance of the EBL, which is dominated by the highly nonlinear behaviour of the contact at the interface, is substantially bigger than the one of a slight variation in temperature on the rigidity of the glass-transiting polymer. In addition, a particular research need arises from the fact that a finite element simulation of an EBL accounting for the electroelastic coupling of this problem has not been published up to date[2]. In view of the non-standard nature of such a simulation, special emphasis is placed on the modelling aspects of EBL interfaces in the present section.

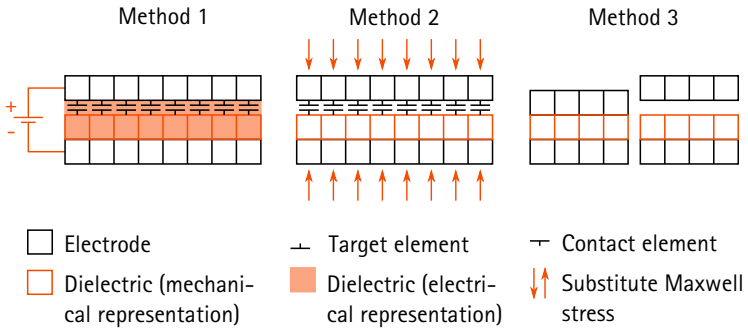

Figure 5.2: Graphical illustration of three methods of modelling an electro-bonded laminate by means of finite elements: 1. Coupled electromechanical model, 2. Purely mechanical representation with contact interface and substitute Maxwell stress, 3. Limiting interface states of ideal bonding and complete decoupling

[2]One of the simulation methods presented in the following discussion has been reported in a student thesis [122] carried out in the frame of this research project.

Table 5.1: Overview of three methods of numerical modelling of an electro-bonded laminate

	Method 1	Method 2	Method 3
Electric field	Directly modelled	Represented by substitute stress	Represented by bonded interface
Dielectric property	Directly modelled	Represented by substitute stress	Represented by bonded interface
Friction contact	Directly modelled	Directly modelled	Represented by limiting interface states
Input quantities (EBL)	U, ε_0, ε_r, t_d[a], μ	σ_M, μ	–
Output quantities (EBL)	Electric field, stress field	Substitute stress field	Stress field for limiting states
Model nature	Nonlinear	Nonlinear	Linear
Normalised computation time[b]	12	10	1

[a] As an electrical property.

[b] Considering the time for building the finite-element model and solving it (both models in case of method 3). The investigation is based on the double-lap configuration of this paragraph (see below) for a voltage of 1500 V. Concerning the mesh, hundred finite elements are placed along the length of an electrode, which defines the mesh of the dielectric in this direction. In thickness direction, the element size is $t_e/4$ for the electrodes and t_d for the dielectric. For the displacement-controlled nonlinear calculations, the onset of sliding has been determined by observation of the progress of the reaction force.

Three different strategies of numerical modelling have been studied in this dissertation: *method 1*, the fully coupled electromechanical simulation, *method 2*, for which the coupled problem is reduced to the mechanical domain by replacing the electric properties of the electromechanical model by a mechanical stress calculated according to equation 5.1, and *method 3*, which further reduces the nonlinear model of method 2 to two linear models describing the system's limiting cases of ideal bonding and complete mechanical decoupling, thus even replacing the contact effects at the interface. Figure 5.2 and table 5.1 illustrate the properties of the three ways of numerical modelling whose decreasing (in the order given) complexity and computational effort come at the cost of an increasing loss of physical foundation.

In the following paragraphs, the implementation of the three introduced simulation methods which has been performed in the frame of this dissertation using the structural analysis program *ANSYS* shall be described. This shall be done for the simplest configuration of an EBL as shown in figure 5.2, represented by a two-dimensional model. The characterised procedure can however be directly extended to the three-dimensional case.

Method 1 relies on a fully coupled electromechanical model. In addition to the mechanical representation of electrodes and dielectric by finite elements of the type *PLANE183*, their electrical properties have to be accounted for. For this purpose, the voltage applied to the EBL is defined as a boundary condition at the inner side of the elements representing the electrodes, and the dielectric characteristics are modelled by electroelastic *PLANE223* elements with very small elastic stiffness filling the space between the two electrodes. This superposed arrangement of mechanical and electrical elements simulating the dielectric allows to properly implement mechanical and electrical boundary conditions at the contact interface (the upper edge of the dielectric in figure 5.2). The mechanical contact at the interface is integrated in the numerical model by placing contact and target elements (*CONTA172* and *TARGE169*) at the edges of dielectric and electrode, respectively, constituting the interface and by defining the interface's friction coefficients[3]. This way of modelling is characterised by a complete coupling of the mechanical domain to the electrical one, being able to capture the real distribution of the electric field and of the Maxwell stress, which depends—in contrast to the simplified picture of equation 5.1—on several influences in both domains as given by boundaries, deformations and interface sliding.

The simplification of method 2 with respect to method 1 consists in the

[3]Both static and dynamic friction can be considered, while the focus of the investigations of the present doctoral thesis is on the determination of the onset point of sliding.

substitution of the electrical properties of the EBL by their simplified mechanical effect, the Maxwell stress according to equation 5.1. The electromechanical coupling considered in this way of modelling is thus one-directional and heavily simplified. Effects of deviations of the system from the ideal conditions assumed by equation 5.1 and of mechanical deformations on the electroelastic behaviour are not covered. Friction phenomena between electrode and dielectric are considered, on the other hand. Due to the remaining nonlinear nature of the substitute mechanical problem, the savings in computation time with respect to method 1 are relatively small (cf. table 5.1).

Method 3 reduces the electromechanical problem to its limiting mechanical states of perfect bonding and perfect disconnection of the interface, which approximates the behaviour at sufficiently high and zero voltage, respectively. This way, the mechanical contact at the interface is no longer represented in the simulation, and the nonlinear problem is transformed into two linear ones. Neither any kind of electromechanical coupling nor friction at the interface are included in this model, which is therefore not capable of predicting whether an EBL is in adhesion or in sliding for a certain combination of voltage and shear load. However, it can be applied to simulate the global behaviour of a structure with integrated EBL with high computational efficiency, if the conditions of one of the limiting states are known to apply. With respect to the nonlinear methods 1 and 2, reductions in computation time of about one order of magnitude can be expected, as specified in table 5.1.

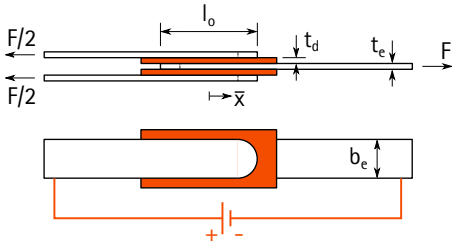

Figure 5.3: Geometry and loading of EBL in double-lap shear configuration. The electrodes' edges are rounded at the overlap to mitigate local peaks in the electric field.

In figure 5.4, the results of simulations according to methods 1 and 2

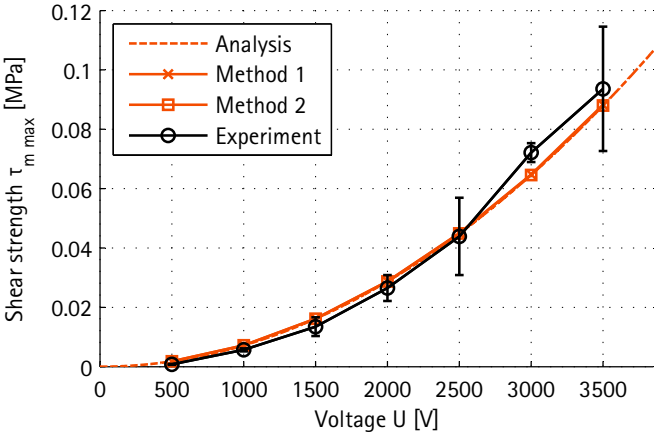

Figure 5.4: Nominal strength of EBL in double-lap shear configuration with respect to applied voltage. Comparison of analytical, numerical and experimental [123] results. $t_d = 25\,\mu m$, $t_e = 50\,\mu m$, $l_o = 20\,mm$, $b_e = 12.7\,mm$, $\varepsilon_r = 3.59$, $\mu = 0.28$

are compared to analytical and experimental results for a double-lap shear configuration of an EBL. Specifically, curves of the nominal shear strength[4] $\tau_{m\,max} = F_{max}/(2b_e l_0)$ of a double-lap joint as depicted in figure 5.3 with polyimide dielectric and copper electrodes with respect to the voltage are shown. The analytical curve represents the maximum shear stress according to relation 5.2, while the experimental plot has been extracted from [123]. For the simulations, half models have been considered, making use of the symmetry of the problem. The assumed mechanical material properties can be found in appendix A.1. This investigation shows that the abandonment of a full electromechanical coupling in the numerical model according to method 2 does not lead to a noteworthy difference in the shear strength results. Under these conditions, the application of method 2 with its about 20% lower computational effort can thus be recommended. Also the agreement of both simulations with the analytical model is found to be very good, with

[4]The subscript "m" represents the mean character of the nominal shear stress in terms of the shear stress distribution along the overlap.

a maximum deviation of less than 1%. In qualitative—and for the conceptual design scope of this chapter also in quantitative—terms, the accordance with the test results of [123] can be regarded as good, too. On the other hand, the observation that, with its strength lower than a tenth of a MPa, the electro-bonded laminate has substantially worse load carrying capabilities than most engineering materials in general and than the polymers coming into consideration for the thermomechanical material concept discussed in the previous chapter in particular. Therefore it can already be concluded that special attention has to be paid to this limitation during the design of adaptive-twist airfoils based on integrated EBLs.

The shear stress distribution at the interface which is observed in the finite element results obtained by methods 1 and 2 is depicted in an idealised way in figure 5.5.[5] While for low tension forces F the shear stress curve follows the analytical solution quoted in 4.2, the interface's shear strength limit τ_{max} is reached at the locations of the stress peaks for higher loading. If the force is further increased, these regions of exceeded strength expand towards the centre until they cover the interface completely at the load level corresponding to the EBL's nominal shear strength $\tau_{m\,max} = \tau_{max}$.

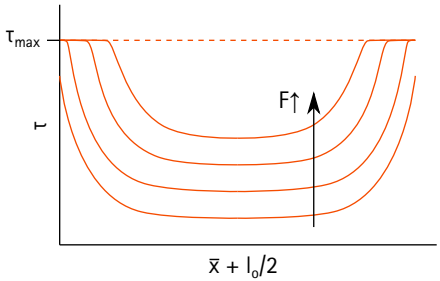

Figure 5.5: Idealised qualitative shear stress distribution of EBL lap joint with respect to load level as determined by finite element modelling (symmetrical case). The dashed line represents the distribution at the nominal EBL shear strength $\tau_{m\,max} = \tau_{max}$.

[5] In order to obtain a symmetric illustration, the results have been transferred to a configuration with an inner electrode of twice the thickness of each of the outer ones.

5.3 Meso behaviour—the wing box

In the previous chapter, the adaptive wing box has been investigated as the constitutive element of the variable-twist airfoil based on polymeric glass transition. This analysis shall also be performed for the case of an electromechanical implementation. In this context, the present section aims at the demonstration of, first, the transferability of the general findings of chapter 2 and section 4.3 to a design based on the EBL material concept and, second, the realisability of an experimental wing box structure with electromechanical coupling.

5.3.1 Numerical investigation

A cantilever beam structure which is—except for its variable-topology layout—similar in its basic design to the one of the previous chapter has been considered for simulations and experiments. Due to the higher demand of the electro-bonded laminate on the shape accuracy of the web to which it is applied, the beam's aluminium base structure could however not be manufactured by bending as in the case of the beams with thermal activation, so that a standard profile had to be used. Figure 5.6 illustrates the geometry of the cross section of the considered beam, which is prismatic and has a length of L, and table 5.2 reports the according numerical values.

In correspondance with the conditions of the experimental wing box structure treated in section 5.3.2, the electrode is assumed to be made of steel, while the multilayered polymer film *3M CM500* [124] is applied for the dielectric. As motivated before, not only the dielectric thickness is chosen to be as small as possible in order to maximise the Maxwell stress, but also a very thin electrode is selected, which allows for a good adaptation to the dielectric under electrostatic forces. Further aspects of the simulation like the mechanical boundary conditions are adopted from the thermomechanical implementation.

The wing box considered in this section is a generic example for which no detailed sizing according to specific requirements is performed. The present investigation rather aims at a demonstration of the structural concept introduced in the previous chapter under the conditions given by the electro-bonded laminate. Due to the conceptual nature of the simulations, the wing box is thus modelled using method 3, which requires the least numerical effort and thus permits to efficiently design the corresponding experimental structure discussed in 5.3.2.

In terms of its structural layout, the wing box based on electro-bonded laminates is similar to the thermally activated one. For this reason, no additional parametric study needs to be performed to identify general trends of the global elastic behaviour of wing box structures equipped with EBL. In fact, as the thickness of the electrode is usually much smaller than the one of the non-adaptive base structure for the reason stated in section 5.1, the limiting cases of a closed symmetrical section and an open c-profile with additional flanges can be used to approach the behaviour of the considered wing box with EBL web in the states of sufficiently high electrostatic attraction and zero attraction, respectively.

The results of the numerical simulations of the wing box structure based on electromechanical coupling are presented together with the corresponding analytical and experimental findings in the following section 5.3.2.

Table 5.2: Geometric properties of experimental wing box structure with EBL web

Parameter	L	B	H	d_g	t_1	t_e	t_d
Value [mm]	650	42	22	3	1.5	0.05	0.025

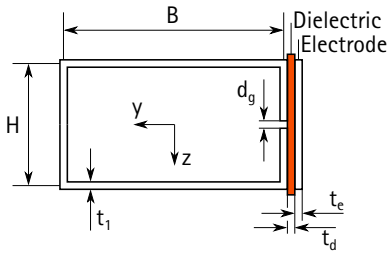

Figure 5.6: Composition and geometry of experimental wing box structure with EBL web (cross section)

5.3.2 Experimental investigation

A photograph of the experimental adaptive-twist beam with EBL web is shown in figure 5.7.[6] The way of load application by means of weights, a rope and a wheel is as well evident from this image as the *Stanford Research Systems PS350* high voltage source used to control the EBL and the laser pointer attached to the tip of the beam to visualise deformations by projection on a screen. This photograph of the experimental setup is completed by the one of figure 5.8 presenting the deflection measurement in two points at the beam's tip by two *Micro-Epsilon ILD 1700-10* laser triangulation sensors. Since the smallest distance of the measuring points for a pair of such measuring heads is larger than the width of the wing box structure, the extension bar visible in the photograph had to be attached to the beam, such that the deflections at two points—and thus the twist—of the wing box structure can be recorded while its elastic behaviour is influenced as little as possible. Concerning the distance of the measurement points on this bar, a value of 100 mm has been selected.

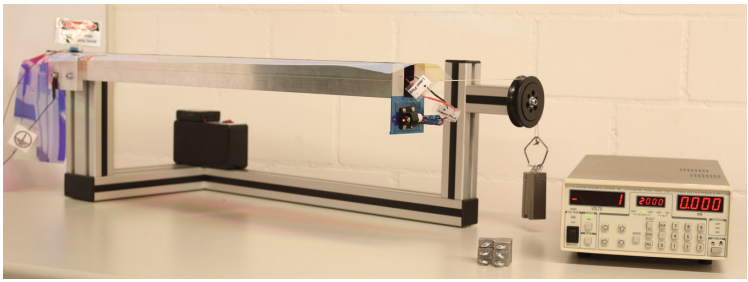

Figure 5.7: Experimental setup of wing box structure based on electromechanical coupling

[6] In the presented configuration, dielectric and electrode are just laid on top of the base structure, so that they stay attached to the latter also at zero voltage due to gravity. If the whole beam has to be rotated about the x-axis, they can be clamped at the beam's root. The considerations of 5.4 show however that this point has no relevance for the parallel interface design developed for the airfoil structure.

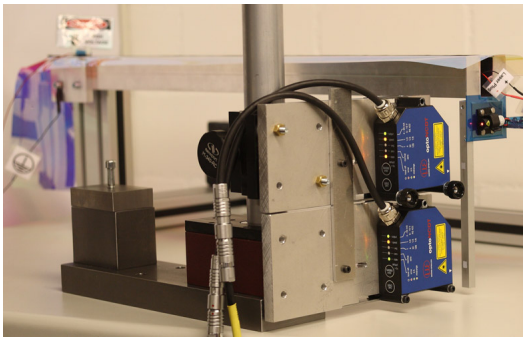

Figure 5.8: Deflection measurement at experimental wing box structure based on electromechanical coupling

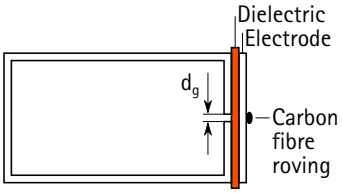

Figure 5.9: Cross-sectional illustration of the experimental wing box based on electromechanical coupling including the carbon fibre roving applied for local reinforcement of the electrode

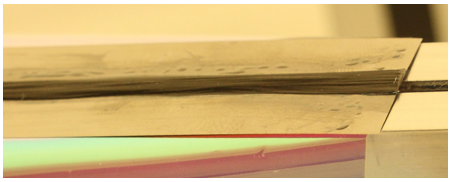

Figure 5.10: Local reinforcement of the electrode of the experimental wing box structure by carbon fibre roving

In order to compensate for the local reduction in stiffness caused by the gap in the web of the base structure while maintaining the electrode's global compliance, a carbon fibre roving slightly wider than d_g was laminated on the outer surface of the electrode along the entire beam length, at the location of the gap. This detail is illustrated in figure 5.9 and also obvious from the close-up image of figure 5.10.

Figure 5.11 presents the results of the investigation of the wing box structure with electrostatically controlled adaptive mechanical topology in terms of twist compliance for EBL states of 0 V [7] and 5000 V. It contrasts the values measured for the experimental structure loaded with $Q = 4$ N with the results of the finite element simulation mentioned in 5.3.1 as well as with the analytical solutions according to the theory introduced in chapter 2. Concerning the latter, an open c-profile with two additional flanges, each of height $(H - d_g)/2$, and a closed profile with symmetrical, rectangular cross section have been considered. The elastic contributions of dielectric and electrode are thus modelled exclusively in terms of their ability to close the gap.

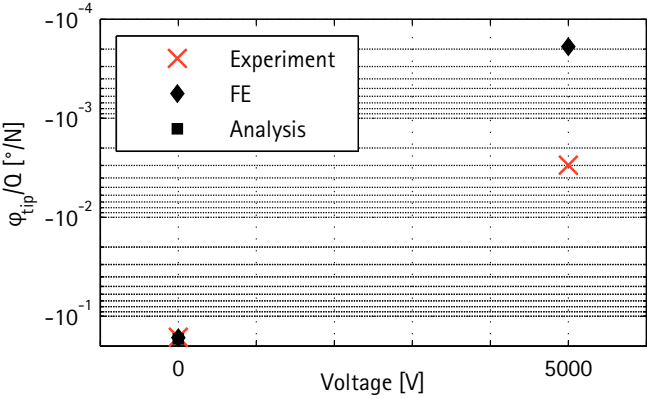

Figure 5.11: Twist compliance at the tip of an adaptive wing box structure with electromechanical coupling with respect to EBL state. Comparison of analytical, numerical and experimental results

[7] Before any voltage is applied.

The pronounced change in bending-twist coupling obtained by way of activation of the smart web, which is characteristic of the structural concept proposed in this dissertation, is articulately reflected also in these results: A variation in twist compliance by more than fifty times is observed between the two considered interface voltages of zero and 5000 V. As it can be expected, a maximum absolute value of twist compliance of similar magnitude as the one of the thermally activated beam is found. The qualitative agreement between experimental, numerical and analytical results is good, and so is the quantitative one for the non-activated state, for which the relative deviation stays below 5%. At 5000 V, however, the experimental wing box structure stays more than one order of magnitude below the stiffness predicted by the simulation (not to mention the zero twist of the analytical model). It can be concluded from this observation that in reality the EBL does not close as well as assumed ideally. Due to the safety margin of the experiment with respect to electrical breakdown, providing higher voltage can be considered as a viable way to increase the stiffness of the wing box structure in the quasi-closed state but would require a voltage supply different from the applied one specified above. Nevertheless, the demonstration of the effectiveness of the suggested structural concept in an electromechanical implementation has been achieved by this experimental study, in spite of the mentioned imperfection of the employed smart material.

Concerning the second critical failure mode of the electro-bonded laminate, its mechanical strength, the stress coming along with the loading by a shear force of $Q = 4\,\mathrm{N}$ turned out to be already close to the strength limit of the interface. This observation gives reason to the recommendation of at least two interfaces in parallel arrangement for a wing dimensioned for similar conditions as the one of section 4.4.

At this point, the remanent strength of the electro-bonded laminate after setting an applied voltage to zero should be mentioned. A residual polarisation of the dielectric, explained for EBL specimens by charge injection into the polymer [123], leads to a remaining torsional stiffness of the beam which has the same order of magnitude as the one in the state of applied voltage. Voltage signals of reverse polarity (after switching off the original voltage) have been found to suppress this effect, but a systematic investigation of this electric phenomenon goes beyond the scope of the present doctoral thesis, which is rather focused on the structural concept of adaptive twist than on the smart material behaviour of a particular implementation.

5.4 Global behaviour—the airfoil

The combination of the experience of the thermomechanical adaptive-twist airfoil with the findings on the electrostatic variable-stiffness approach on the interface and the wing box level paves the way for the development of an adaptive-twist airfoil relying on electro-bonded laminates. Generally, the modus operandi in terms of design, simulation, manufacturing and testing of the wing of this chapter is similar to the one followed in the previous chapter. However, the two airfoils exhibit—in addition to their different types of smart material—two important differences that should be highlighted from the beginning, since they have implications on several decisions taken during the development process of the adaptive-twist wing discussed in the present chapter. First, reversibility to its original state after shape adaptation under constant flight conditions is formulated as a requirement for the airfoil based on electromechanical coupling, in contrast to the design described in the previous chapter to which no specification related to reverse twist has been assigned. Second, the suitability of the EBL-based airfoil for future wind-tunnel tests has to be ensured, such that aeroelastic experiments can be carried out after minor modifications.[8] This capability of substantial influence on the demands on the wing in terms of, for example, shape accuracy and surface quality has not been required for the thermally activated airfoil either.

For practical reasons, some definitions on the system states of the adaptive-twist airfoil with electrostatic active principle that will be referred to in the following discussion shall be made here. The definition system is based on the figures *0* and *1*, which are used to denote EBL spar interfaces that are deactivated and activated, respectively. The sequence of specified interfaces follows the chord, starting from the leading edge. The airfoil state *10*, for example, indicates a situation in which voltage is applied to the electrostatic interface in the front spar while the one in the rear spar is at zero voltage. Accordingly, the notations *00*, *01* and *11* will be used to describe the respective operating states of the airfoil.

5.4.1 Numerical investigation

The geometric parameterisation of the adaptive-twist airfoil with electromechanical coupling is shown for a cross section of the prismatic NACA 0012 wing in figure 5.12, while figure 5.13 presents a detailed illustration of the

[8] The wind tunnel tests themselves are not part of this dissertation project.

spars equipped with EBL interfaces. The wing's spanwise geometry, on the other hand, is evident from the screenshot of the numerical model contained in figure 5.14.

The design of the wing exhibits the general characteristics of adaptive-twist airfoils introduced at the end of chapter 3: The narrow wing box is placed far forward, ensuring small twist angles for a symmetrical EBL state. Gaps in the skin allow for low warping stiffness in the states in which one of the smart interfaces is open. A configuration with additional EBL interfaces in place of these openings would provide enhanced adaptivity but is avoided for its higher complexity. In case of a practical application, the gaps have to be filled by components which are stiff enough to maintain the airfoil's aerodynamic shape but, at the same time, soft enough not to compromise the twist compliance too much. Finally, frame-like, segmented ribs allow for a low warping stiffness.

With a view to ensuring the suitability of the wing design for the integration of electro-bonded laminates, the thicknesses of dielectric layers, electrodes and outer spar plates at each interface are chosen as small as possible, following the same rationale as explained for the material, local and meso level of the electromechanical concept in the preceding sections.

A particularity of the wing design is given by the dovetail-shaped linear bearings for the spars, as evident from the figures, which are explained in the context of the experimental airfoil in section 5.4.2. Like in previous parts, the report of some minor details of the numerical model is set aside in this section for editorial reasons. It is referred to [125] instead for a more complete documentation.

Due to the knowledge on the structural concept of semi-passive wing twist gained with the thermally activated airfoil structure, an extensive parametric study investigating the global elastic behaviour of the adaptive-twist wing can be dispensed with in the present chapter. After reporting on the finite element simulation of the experimental airfoil structure, the discussion of this section turns towards the aeroelastic modelling and the preliminary design of an upscaled EBL-based adaptive-twist airfoil, which have been performed under similar conditions as the respective investigation of the previous chapter. The upscaled airfoil is then subjected to a less comprehensive parametric study analysing the sensitivity of its performance to the variation of certain design parameters.

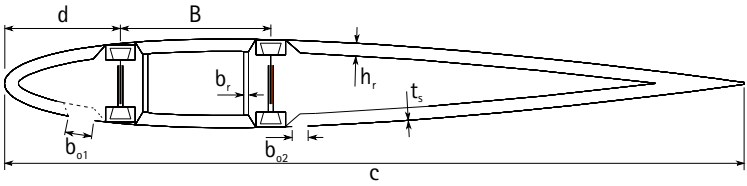

Figure 5.12: Geometry of adaptive-twist airfoil based on electromechanical coupling (cross section)

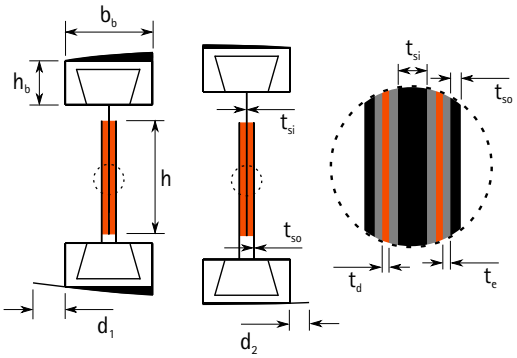

Figure 5.13: Geometry of wing spars of adaptive-twist airfoil based on electromechanical coupling. Close-up of EBL interfaces (spar plates shown in black, electrodes in grey and dielectrics in orange)

Simulation of experimental airfoil structure Table 5.3 presents the values of the geometric parameters selected for the experimental adaptive-twist airfoil, showing that a half wing with the same chord length as the thermally activated airfoil but smaller span has been realised. Half span L and protrusion l_p of the linear bearings are defined in figure 5.14. Concerning the ribs, a thickness of $t_r = 0.45$ mm has been assigned, and again the load introduction rib at the tip is reinforced, exhibiting a thickness of $2t_r$.

It should be mentioned that, like for the glass transition–based wing, the

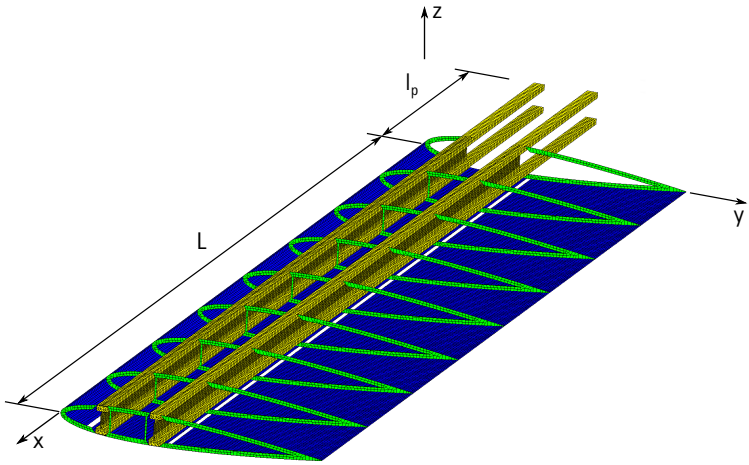

Figure 5.14: Finite element model of adaptive-twist airfoil based on electromechanical coupling (experimental configuration). The upper skin shell is hidden.

dimensions of the experimental airfoil based on electromechanical coupling are not chosen in an arbitrary way but rather result from a sizing process accounting for the most critical requirements of the demonstrator structure, such that the functionality of the proposed design is demonstrated in a realistic environment. The airfoil shall be sized for future wind tunnel tests under a flow speed of $v = 35$ m/s and a lift coefficient of $c_L = 0.4$, which yields a lift force resultant of about 100 N. Similar to the one of the previous chapter, the experimental airfoil has been dimensioned for a concentrated force $Q = 100$ N acting at the tip, in the centre of pressure. This is a conservative simplification for all relevant sizing criteria. In light of the critical shear strength of the electro-bonded laminates, the adhesion of the spar interfaces is ensured by simulations based on method 2, assuming a friction coefficient of $\mu = 0.3$[9]. Furthermore, safety against buckling has to be provided by appropriate selection of wall thicknesses. The sized experimental airfoil exhibits a smallest buckling factor of 3.1 even in the most critical situation of system state *00,* in which both spar interfaces are open, which is not intended as a regular state

[9] Friction coefficient values of about 0.3 have been determined experimentally for similar interfaces [123].

Table 5.3: Geometric properties of experimental adaptive-twist airfoil based on electromechanical coupling

Parameter	L	l_p	c	B	d	t_s	h_r	b_r
Value [mm]	1'000	200	300	61	47	0.85	5	2

Parameter	b_{o1}	b_{o2}	h	d_1	d_2	b_b	h_b
Value [mm]	6	6	12.7	7	2.5	12	6

Parameter	t_{si}	t_{so}	t_e	t_d
Value [mm]	1	0.1	0.05	0.025

of operation of the airfoil. Finally, in order to operate properly during wind tunnel tests, the experimental airfoil has to fulfil aeroelastic stability requirements. Whereas the divergence velocity has been determined in the same way as for the thermally activated airfoil to be around $v_{\text{div}} = 45$ m/s, also dynamic aeroelastic calculations of approximate character have been performed to demonstrate the safety of the EBL-based airfoil design against flutter. These calculations are discussed further below in the present section.

While in terms of the material employed for the skin the EBL-based experimental airfoil agrees with the thermally activated one, the ribs and the spar plates of the former are made of GFRP. Electrode and dielectric materials correspond to the ones of the experimental wing box structure discussed in 5.3, and aluminium is employed for the linear bearings. The respective material and laminate properties can be found in appendix A.1.[10]

In the experimental structure, only every second rib bridges the gap in the airfoil's front cell, as indicated by the dashed line in figure 5.12, which allows to lower the warping stiffness. This measure has a minor influence on the wing's global load-carrying qualities, since the local bending and shear stiffnesses of the skin at the leading edge are comparably high due to the high curvature in this area.

The boundary conditions which are imposed in the numerical simulation can be directly derived from the report on the fixation of the different com-

[10] During the realisation of the experimental airfoil based on electromechanical coupling new material tests have been performed. Some of the obtained properties, which are used for the calculations of the present chapter, slightly differ from the ones determined in the frame of the thermomechanical implementation.

ponents of the experimental airfoil given in 5.4.2, clampings being modelled by a constraint of all degree of freedoms of the respective nodes.[11]

Except for the linear bearings, for the simulation of which solid elements are used, all components of the airfoil structure are discretised into shell elements. The average characteristic length of the elements, which mostly have an approximately square (respectively cubic) geometry, is around 4 mm.

The results of the simulation of the demonstrator airfoil are reported together with the experimental ones in section 5.4.2.

Dynamic aeroelastic calculations Several characteristics of the novel airfoil design proposed in this doctoral thesis give rise to the assumption that wings based on the structural concept of adaptive twist are more prone to bending-twist flutter [126, 127] than conventionally designed ones: On the one hand, the reductions in torsional and, secondarily, bending stiffness, which are utilised for shape adaptations, can be expected to generally lower the flutter speed. On the other hand, the shear centre shifts that are equally intrinsic to the concept can lead to configurations in which the shear centre is located more forward (chordwise) than in conventional wing designs. As the positions of centre of gravity and centre of pressure do not considerably differ from the ones of common airfoils, this property also indicates flutter proneness.

For the stated reasons, flutter has to be considered as one of the critical requirements for the sizing of adaptive-twist airfoils in general and for the experimental airfoil of this chapter in particular. A comprehensive analysis of the dynamic aeroelastic behaviour of adaptive-twist airfoils based on the proposed structural concept goes, however, beyond the scope of the dissertation on hand. The aim of the present dynamic aeroelastic investigation is rather to obtain a rough approximation of the flutter velocity in order to ensure a design for the experimental airfoil which is uncritical in terms of flutter under the conditions assumed for the sizing of this structure. At the same time, the flutter calculations shall make use of the aeroelastic simulation environment that is already available from the numerical upscaling investigations discussed below.

The differential equations of motion describing the bending-twist flutter problem for a discretised model of an airfoil can be written as [116, 128]

$$\mathbf{M}\frac{\mathrm{d}^2\mathbf{a}}{\mathrm{d}t^2} + \mathbf{K}\mathbf{a} = \mathbf{A}_\mathrm{K}\mathbf{a} + \mathbf{A}_\mathrm{D}\frac{\mathrm{d}\mathbf{a}}{\mathrm{d}t} + \mathbf{A}_\mathrm{M}\frac{\mathrm{d}^2\mathbf{a}}{\mathrm{d}t^2} \tag{5.4}$$

[11] Rigid-body motions of the parts of the linear bearings are completely constrained in all simulations.

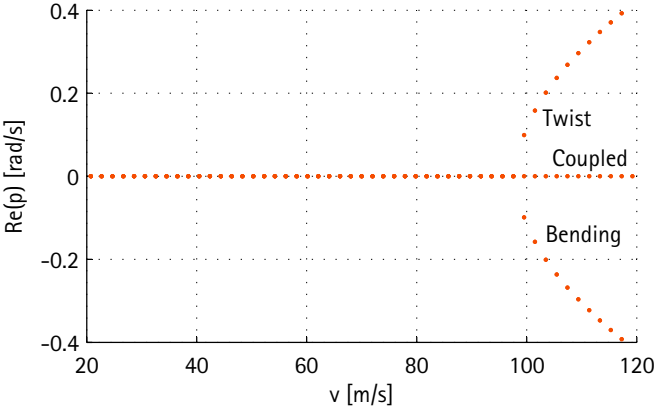

Figure 5.15: Real parts of eigenvalues with respect to flow velocity as a result of the flutter analysis of the experimental airfoil based on electromechanical coupling in system state 10

In this equation, the $n \times n$ matrices $\mathbf{M}$, $\mathbf{K}$, $\mathbf{A_K}$, $\mathbf{A_D}$ and $\mathbf{A_M}$ represent the structure's mass and stiffness matrix and the airflow's contributions in terms of stiffness, damping and inertia, respectively. Moreover, the $n \times 1$ vector $\mathbf{a}$ contains the system's degrees of freedom.

For reasons of simplicity, instationary aerodynamic effects are neglected here, which is justified in view of the mentioned approximate and design-oriented scope of the flutter investigation of this chapter. The choice of such a steady-state aerodynamic operator allows to discard the last two terms of equation 5.4, and the flutter equation for this case reads

$$\mathbf{M}\frac{\mathrm{d}^2\mathbf{a}}{\mathrm{d}t^2} + \mathbf{K}\mathbf{a} = \mathbf{A_K}\mathbf{a} \tag{5.5}$$

In usual numerical models, like in the structural finite element model used for the calculations of the present chapter, the number of nodes and thus the number of degrees of freedom n is big, so that the solution of a flutter equation of the form of equations 5.4 and 5.5 would imply a large numerical effort. In order to reduce the number of degrees of freedom, the problem is transferred to the modal domain. If the $n \times k$ matrix $\mathbf{B}$ contains a

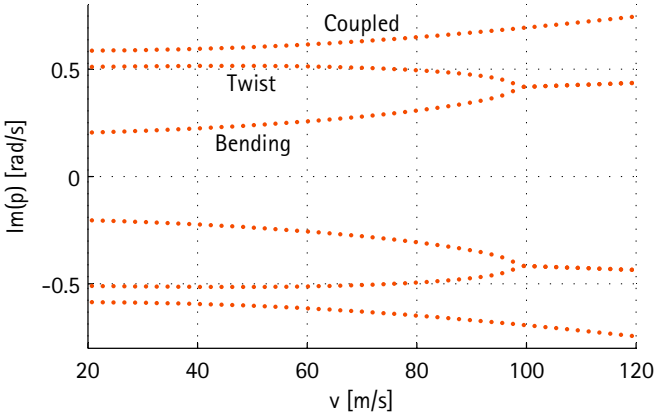

Figure 5.16: Imaginary parts of eigenvalues with respect to flow velocity as a result of the flutter analysis of the experimental airfoil based on electromechanical coupling in system state 10

selection of k eigenvectors of the system, the operations

$$\widehat{\mathrm{M}} = \mathrm{B}^{\mathrm{T}}\mathrm{M}\mathrm{B},\ \widehat{\mathrm{K}} = \mathrm{B}^{\mathrm{T}}\mathrm{K}\mathrm{B},\ \widehat{\mathrm{A}_{\mathrm{K}}} = \mathrm{B}^{\mathrm{T}}\mathrm{A}_{\mathrm{K}}\mathrm{B} \tag{5.6}$$

can be performed, which allow to express equation 5.5 in the modal domain:

$$\widehat{\mathrm{M}}\frac{\mathrm{d}^2\widehat{\mathbf{a}}}{\mathrm{d}t^2} + \widehat{\mathrm{K}}\,\widehat{\mathbf{a}} = \widehat{\mathrm{A}_{\mathrm{K}}}\widehat{\mathbf{a}} \tag{5.7}$$

where the $k \times 1$ vector $\widehat{\mathbf{a}}$ denotes the generalised modal displacements.

Also if only a small number of eigenmodes is considered ($k \ll n$), the flutter problem can be expressed with sufficient accuracy for the stated scope, while problem size and computational effort are drastically reduced by the modal transformation.

A p-method is chosen to solve the modal flutter equation 5.7. An exponential ansatz of the form

$$\widehat{\mathbf{a}} = \widehat{\mathbf{a}}_0 \mathrm{e}^{pt} \tag{5.8}$$

for the generalised modal displacement fulfils equation 5.7 if p is a solution

of the characteristic equation

$$\det\left(\widehat{\mathrm{M}}p^2 + \widehat{\mathrm{K}} - \widehat{\mathrm{A}_\mathrm{K}}\right) = 0 \tag{5.9}$$

Modal mass matrix $\widehat{\mathrm{M}}$ and modal stiffness matrix $\widehat{\mathrm{K}}$ can be determined by modal transformation of the respective matrices extracted from the structural finite element model, where the eigenvectors result from a modal analysis of this model. The modal aerodynamic stiffness matrix $\widehat{\mathrm{A}_\mathrm{K}}$, on the other hand, can be calculated by modal transformation of the elastic response of the structural model under aerodynamic load for the considered eigenmodes. The flutter velocity v_{flut} can then be determined by repeated solution of equation 5.9 for different flow speeds as the minimum velocity for which a real part of an eigenvalue p changes its sign from negative to positive, i. e. the state of oscillation changes from damped to intensifying.

For the flutter calculations of this chapter, the first $k = 3$ eigenmodes of the structural model are selected: a torsional, a flexural and a mixed mode. Concerning the mass distribution, the density values specified in the appendix are used. In figures 5.15 and 5.16, real part and imaginary part of the system's eigenvalues are plotted with respect to flow velocity as a result of the flutter analysis of the experimental adaptive-twist airfoil introduced before. The plots are based on the most flutter-critical state of operation given by system state *10*. With a resulting flutter speed of $v_{\mathrm{flut}} \approx 99$ m/s, bending-twist flutter can be excluded to occur for the experimental airfoil under the operating conditions assumed for the sizing. It has to be stated, however, that the simplification coming along with the steady-state aerodynamic operator used in the flutter calculations does not generally lead to conservative results. Nevertheless, the conclusion drawn for the design of the experimental airfoil remains valid due to the large safety margin between intended operating speed and flutter velocity.

Upscaling Similar to the one of the adaptive-twist airfoil based on thermomechanical coupling discussed in the previous chapter, a numerical upscaling to realistic dimensions and flight conditions of a glider wing application is performed for the electromechanical implementation of the proposed adaptive-twist concept.

While the planform of the wing in which the EBL-based smart structure is applied is exactly the same as the one of chapter 4, the upscaled airfoil of the present chapter differs slightly from the previous one in terms of its

symmetrical NACA 0012 shape and the assumptions made for flight velocity ($v = 40$ m/s) and airplane mass ($m = 300$ kg). These conditions, which are no less representative of the virtually envisaged glider plane application [129] than the ones of chapter 4, correspond to an equilibrium lift coefficient of $c_L = 0.33$, which is reached by the adaptive-twist airfoil in its symmetrical configuration at an angle of attack of $\alpha = 3.5°$.

The calculations related to the upscaling investigation of the present chapter are performed in a very similar simulation environment as the ones of the previous chapter, so that no additional discussion of the calculation procedure is required at this point.

With respect to the sizing of the upscaled wing structure, not only strength and stability requirements are imposed, but also the upscaled airfoil's capability of returning to its neutral state after performance of a (wash-in) twist manoeuvre in state *01* by subsequent activation of state *10* is evaluated. Furthermore, static aeroelastic stability is ensured for all the designs reported in the frame of the upscaling analysis. On the other hand, due to the large numerical effort, flutter calculations have not been performed for upscaled wing configurations. On grounds of the close tie of the sizing conditions of the experimental airfoil to the ones of the upscaled wing and of the former's considerable safety against bending-twist flutter, it can however be supposed that the design of adaptive-twist airfoils with sufficient flutter velocity is possible under the conditions assumed for the numerical upscaling.

Table 5.4 reports the values of the design parameters of the baseline configuration of the upscaled adaptive-twist airfoil with electromechanical coupling that ensue from the sizing according to the mentioned conditions.[12] The upscaled structure contains 31 ribs with thickness $t_r = 1.4$ mm along its (half) span, which are assumed to be made—in contrast to the GFRP ones of the experimental design—of CFRP.

In order to investigate the sensitivity of the upscaled adaptive-twist airfoil to changes in the main design quantities, a parametric study has been performed. As a result of this analysis, tip twist angle and lift coefficient are plotted in figures 5.17 to 5.24 for different values of wing aspect ratio L/c and relative wing box offset d/c, for the two system states *01* and *10*. The simulation assumes that state *10* is set subsequently to an operation of the

[12] The skin thickness of the upscaled structure varies locally to account for additional degrees of freedom in the design, which is especially helpful in light of the buckling criterion. Lower and upper skin shell have different thicknesses of t_{sl} and t_{su}, respectively. Between the wing spars, the skin is thicker, exhibiting a thickness of t_{sb}. In table 5.4, the first of the respective values refers to the design based on the lower EBL shear strength assumption, and, accordingly, the second one denotes the implementation assuming a higher EBL strength (see below).

Table 5.4: Geometric properties of upscaled adaptive-twist airfoil based on electromechanical coupling in baseline configuration

Parameter	L	c	B	d	t_{sl}	t_{su}	t_{sb}
Value [mm]	7'500	600	120	90	1.2/0.85	2.2/2.6	3.5/4.3

Parameter	h_r	b_r	h	t_{si}	t_{so}
Value [mm]	10	5	30	6	0.5

airfoil in state *01*. For the parametric study, the EBL interfaces are modelled using a variation of method 2: Instead of defining normal stress and friction coefficient for the interface, a shear strength value τ_{max} is assigned to the contact elements. The two different shear strength values $\tau_{max} = 0.15$ MPa and $\tau_{max} = 0.3$ MPa are considered for the upscaling calculations. Whereas the former is of the order of the nominal shear strength observed experimentally in double-lap shear tests as described in 5.2[13], the latter accounts for a potential improvement of the interfaces' load carrying capability, either by further development of the EBL technology or by arrangement of more than one double-lap interface in parallel in the wing spars.

The results obtained under the assumption of a smaller EBL shear strength are presented in figures 5.17 to 5.20. The curves show that, as expected, raising the slenderness of the wing planform generally comes along with higher twist compliance and thus increased lift coefficients. The nonlinear nature of the EBL interfaces, which slide locally at higher loads, leads to the phenomenon that the pronounced asymmetry in shear stiffness of the wing box cannot be maintained at elevated aspect ratios, resulting in the recorded behaviour of the lift adaptation range.

It should be recalled at this point that no specific application utilising the airfoil's adaptive properties has been envisaged up to now. In general, the requirements for the lift adaptation strongly depend on the type of application: While, for example, changes in lift of different sign have to be provided in case of an implementation for flight control purposes, a high-lift application requires only (reversible) increments in lift with respect to the equilibrium

[13] The results reported in 5.2 for polyimide dielectrics show a nominal shear strength of less than 0.1 MPa. For the multilayer material applied in the experimental adaptive-twist airfoil values around 0.15 MPa have been determined in double-lap shear tests. However, it has to be mentioned that the strength values can not be directly transferred from the conditions of the sample tests to the more complex and less ideal airfoil structure.

point. As a general performance measure which allows to evaluate the concept's adaptive capability independently from the requirements of a specific application, variations in lift coefficient around the equilibrium value can be considered. Referring to the results mentioned above, such reversible changes in lift around the equilibrium lift coefficient are only possible in case of designs with an intermediate aspect ratio under the considered conditions.

Also increases in the chordwise offset of the wing box lead to a more pronounced wash-in tendency, which is reflected in the numerical results. Again, the EBL interfaces slide locally for certain configurations of the parameter analysis, leading to twist curves that do not strictly increase with the offset. However, the wing box offset appears as a design parameter which can be used to shift the centre of the adaptation range (in terms of the lift coefficient). In the context of an evaluation of the airfoil's lift adaptation capabilities as mentioned above, the demonstration of the possibility to adjust this centre point to a relatively wide range of lift coefficients by variation of this parameter constitutes an important result.

The curves based on the assumption of a higher shear strength of the electro-bonded laminates, which are shown in figures 5.21 to 5.24, reflect the high dependence of the performance of the structural concept on the load-carrying capability of the smart interfaces. They demonstrate that a higher EBL shear strength allows for considerable increases in the adaptation amplitude over a wide range of parameter values. In this case, maximum changes in lift coefficient of the order of 20% are observed between the two states.

However, it is noticeable that the (absolute) values of maximum tip twist angle and lift coefficient of all considered configurations, also of the ones based on a higher τ_{max}, stay far below the values obtained for the thermomechanical adaptive-twist airfoil in states of low interface modulus. Reasons for the much more narrow adaptation range of the electromechanical implementation are given, first, by the comparably low shear strength of the electro-bonded laminates, which compromises the achievable changes in coupling ratio at the order of aerodynamic loads for which the airfoil structure is designed, and, second, by the specification of twist reversibility which has been considered for the design of the electromechanical airfoil, in contrast to the thermally activated one. The relation between the requirements of high wash-in twist and reversibility to the neutral state, which can be intuitively identified as conflicting aims, will be further elaborated on in the following chapter 6.

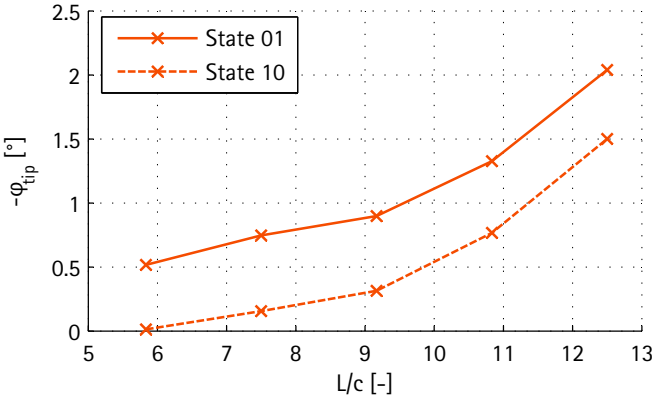

Figure 5.17: Tip twist angle of upscaled adaptive-twist airfoil based on electromechanical coupling with respect to wing aspect ratio for system states 01 and 10. d/c = 0.15, τ_{max} = 0.15 MPa

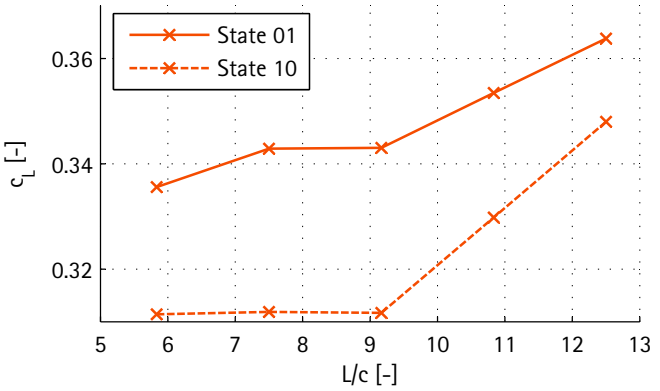

Figure 5.18: Lift coefficient of upscaled adaptive-twist airfoil based on electromechanical coupling with respect to wing aspect ratio for system states 01 and 10. d/c = 0.15, τ_{max} = 0.15 MPa

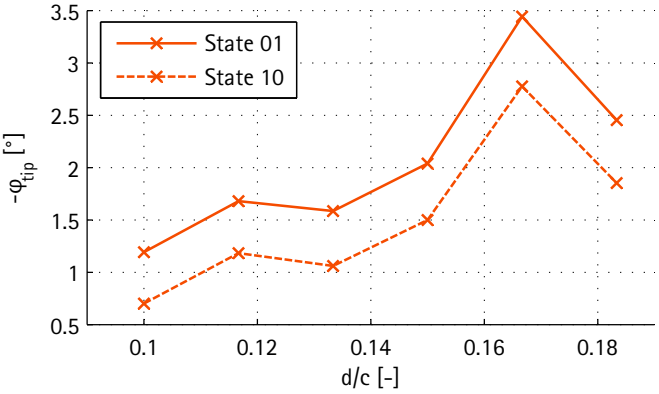

Figure 5.19: Tip twist angle of upscaled adaptive-twist airfoil based on electromechanical coupling with respect to relative wing box offset for system states 01 and 10. L/c = 12.5, τ_{max} = 0.15 MPa

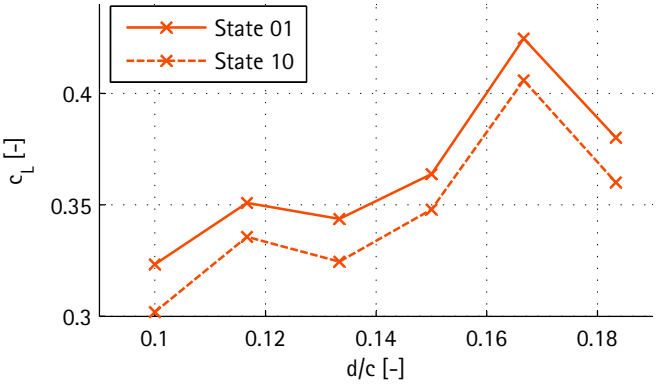

Figure 5.20: Lift coefficient of upscaled adaptive-twist airfoil based on electromechanical coupling with respect to relative wing box offset for system states 01 and 10. L/c = 12.5, τ_{max} = 0.15 MPa

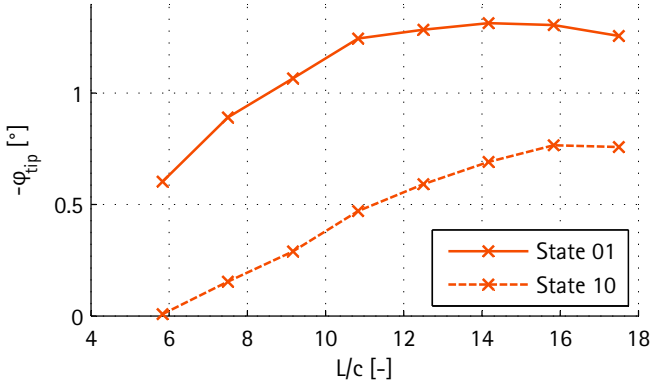

Figure 5.21: Tip twist angle of upscaled adaptive-twist airfoil based on electromechanical coupling with respect to wing aspect ratio for system states 01 and 10. $d/c = 0.15$, $\tau_{max} = 0.3$ MPa

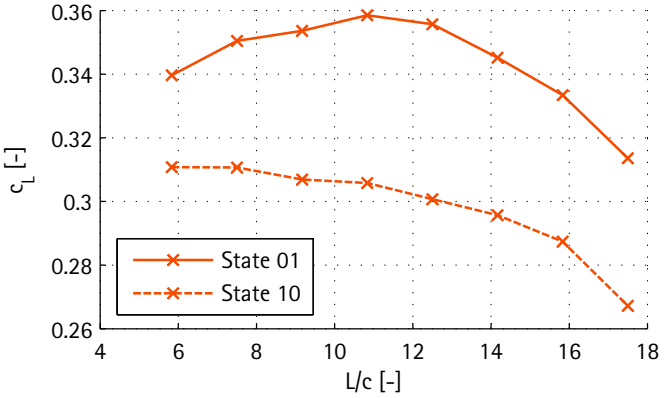

Figure 5.22: Lift coefficient of upscaled adaptive-twist airfoil based on electromechanical coupling with respect to wing aspect ratio for system states 01 and 10. $d/c = 0.15$, $\tau_{max} = 0.3$ MPa

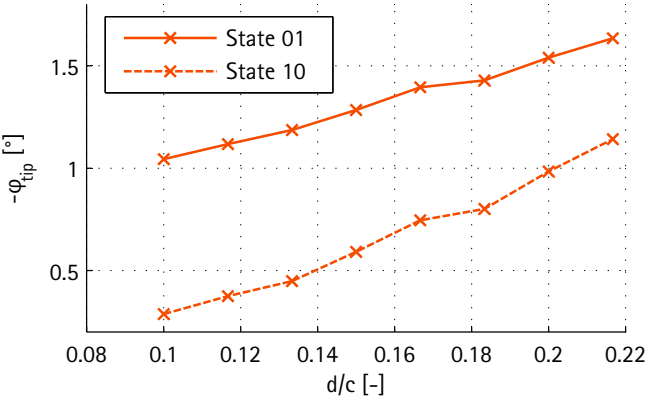

Figure 5.23: Tip twist angle of upscaled adaptive-twist airfoil based on electromechanical coupling with respect to relative wing box offset for system states 01 and 10. L/c = 12.5, τ_{max} = 0.3 MPa

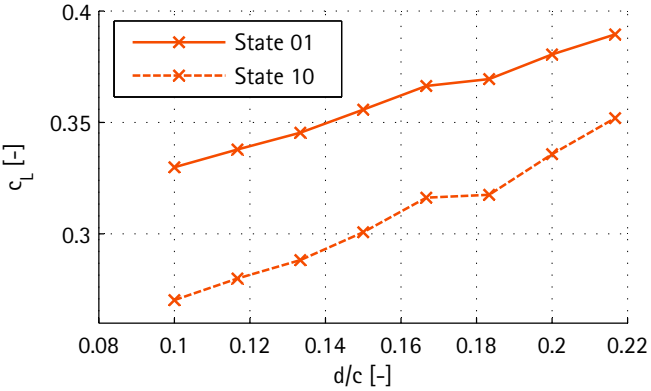

Figure 5.24: Lift coefficient of upscaled adaptive-twist airfoil based on electromechanical coupling with respect to relative wing box offset for system states 01 and 10. L/c = 12.5, τ_{max} = 0.3 MPa

5.4.2 Experimental investigation

In order to demonstrate the structural concept's effectivity under laboratory conditions also for the case of an electromechanical implementation, an EBL-based experimental airfoil as introduced already in the context of its numerical simulation in 5.4.1 has been manufactured and tested.

In principle, the procedure followed for the experimental part related to the electromechanical airfoil is similar to the one of the thermomechanical demonstrator. However, it has been mentioned before that the electromechanical airfoil has—in contrast to the thermomechanical one—to fulfil the requirements of reversibility in terms of twist and of wind tunnel suitability, which has consequences on its structural design and its manufacturing.

The reversibility specification calls for the integration of smart interfaces in both wing spars. In order to avoid the complexity of additional electro-bonded laminates, openings are provided in the airfoil skin instead of smart interfaces.

On the other hand, the requirement of suitability for future wind tunnel tests poses high demands not only on the wing's surface quality but also on its shape accuracy. For this reason, the two gaps in the airfoil skin were realised by bonding of three separately manufactured skin parts instead of cutting of a cured skin shell which would suffer from a spring-back effect due to release of residual stresses.

Another particularity of the experimental adaptive-twist airfoil based on electromechanical coupling results from the properties of the electro-bonded laminates employed for the spar interfaces. Due to the fact that under laboratory conditions the likelihood of electrical breakdown through the dielectric can be limited to a very low value only by very high efforts related to inspection and installation, the structure has to provide for the possibility to exchange the dielectric films. Otherwise a breakdown would result in the need to replace the whole airfoil or seriously damage it to replace the defective component. Besides electrical breakdown, wear can also affect the performance of the dielectric layers, so that for a medium-term operation of the experimental airfoil a convenient way of dielectric replacement is suggested in any case. In addition, the results which have already been presented in relation to electro-bonded laminates indicate a relatively low maturity level of this technology. Under these conditions, it has been decided to ensure the replaceability of the entire wing spars, so that damaged dielectrics can be replaced and the experimental airfoil can be upgraded in the future if an implementation of an electro-bonded laminate with higher performance

becomes available.

The wing spars are thus designed to be replaceable by means of dovetail-shaped linear bearings extending along the whole span and protruding at the root for clamping purposes. At the tip of the airfoil, the linear motion can be constrained after mounting of the spars by screwing an aluminium plate on the tip of every bearing.

It should be emphasised here that the construction based on the linear bearings has been developed only due to the particular conditions and requirements of the experimental airfoil. It is not by any means intended as a more general suggestion for the wing design of adaptive-twist airfoils, which are distinguished by the very absence of conventional mechanisms and which would not require such components in a technically more mature implementation.

Figure 5.25 contains a photograph of the experimental airfoil before closure by bonding of the remaining skin shells, and figure 5.26 shows a photo of the tip of the completed wing with mounted tip plates.

A 40 mm wide[14] steel block centred with respect to the wing box centroid serves as a clamping for the airfoil, as evident in figure 5.27. It is inserted 90 mm deep into the structure and bonded to the skin by means of epoxy.

Load application and deformation measurement are performed in a similar way as for the experiments related to the thermomechanical airfoil, except for the measurement points, which are located at $x = L/2$ in order not to exceed the limit of the metering range of the laser sensors[15] in case of the more compliant EBL-based airfoil. These points, which are located at the chordwise positions of the wing spars[16], will be referred to as "point 1" and "point 2" in the following discussion, where "point 1" denotes the measurement point located at the front spar. Referring to the application of shear forces to the airfoil structure, the M5 load introduction screw, which is connected to the tip rib and the skin by means of a bonded aluminium block, is evident from the photograph of figure 5.26.

Concerning the way of voltage application, two *Stanford Research Systems PS350* high voltage sources have been used.

In theory, the capacitance of each of the double-lap EBL interfaces in the

[14] In chord direction.

[15] The same laser sensors as used for the electromechanical wing box are applied.

[16] The exact placement of the measuring points corresponds to the definition of the distance B representing the wing box width.

spars in system state *00* is given by

$$C_{el} = \varepsilon_0 \varepsilon_r \frac{2hL}{t_d} = 32.1\,\text{nF} \tag{5.10}$$

Capacity measurements at low voltage have shown values of 9.3 nF for the front interface and 17.4 nF for the rear one, in contrast. The main cause for the deviation of the electric properties of the experimental interfaces from the ones under ideal conditions can be assumed to consist in the presence of air gaps between electrodes and dielectrics. Although it has been particularly taken care of maintaining strict geometric tolerances during the manufacturing of the experimental airfoil, air inclusions can never be completely avoided, especially in a handmade structure. The substitute electric properties of the simulation have been corrected by the knockdown factors observed between ideal and real capacity, assuming that the effect of trapped air can be modelled by a dielectric layer with unchanged thickness but lower relative permittivity. This correction, however, concerns only the electric properties of the interface, while the loss in mechanical contact coming along with each air inclusion is not accounted for. For such local effects, no similar correction approach is available. The importance that has to be attached to the decreased area of mechanical contact can be concluded from the fact that the relative reduction in contact area caused by air inclusions has to be bigger than the respective relative reduction in electric capacity, due to the fact that air gaps still contribute to the capacity while completely cancelling the mechanical contact.

The EBL interfaces are structurally designed to close at higher voltages and thus force out trapped air. This capability is however not reflected distinctly in terms of a large beneficial influence in the experimental results.

The results of the structural tests carried out with the experimental airfoil based on electromechanical coupling are presented in figures 5.28 to 5.30, contrasted with the respective numerical findings. Figures 5.28 and 5.29 report the deflection compliance for the interface states *01* and *10*, respectively, and both of them contain also state *00*, which is found as the limiting case at $U = 0\,\text{V}$. The deflection results are reported for both measurement points ("point 1" and "point 2") as defined previously.

All the deflection curves confirm the expectation that applying voltage to one of the spar interfaces has a stiffening effect on the global elastic behaviour of the airfoil. However, the simulation predicts a much higher influ-

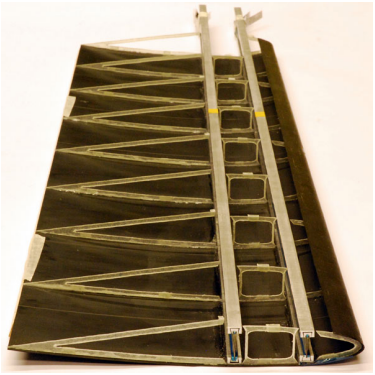

Figure 5.25: Inner structure of experimental airfoil based on electromechanical coupling

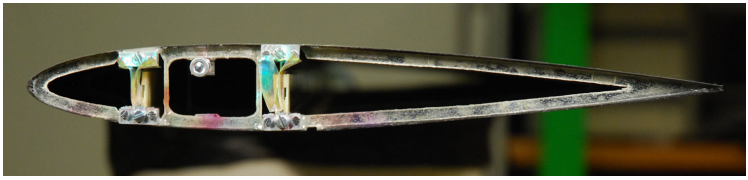

Figure 5.26: Tip of experimental airfoil based on electromechanical coupling

ence of the interface voltage than it is observed in the experiment: Whereas for $U = 0\,\mathrm{V}$ (state *00*) experimental and finite element results agree to about 12%, the calculated deflection compliances decrease much more with the voltage than the measured ones, leading to very high deviations at the maximum voltage of $U = 3000\,\mathrm{V}$. The phenomenon that the EBL interfaces exhibit mechanical properties at higher voltages that are not only far from the ones of a closed interface but also stay substantially below the theoretical expectations in terms of shear strength is, in light of their reduced electrical performance demonstrated before, not surprising and explains the behaviour observed for the airfoil structure.

In spite of the quantitative discrepancies between numerical prediction and experimental reality in terms of deflection compliance, all the results share a characteristic: The deflection curves of both measurement points

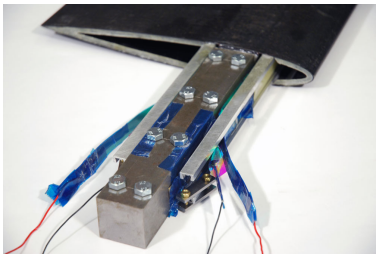

Figure 5.27: Root of experimental airfoil based on electromechanical coupling

gradually diverge from each other as the voltage is increased, in opposite ways in the two system states. In this behaviour, twist angles of opposite sign, depending on the system state, are manifested, which are plotted (in terms of twist compliance) in figure 5.30 with respect to the voltage.

It is surprising that the relative deviations of numerical and experimental results are smaller for the twist angle than for the deflections from which it is derived, not only at zero Volts but also at higher voltages at which these discrepancies are very high for the deflection. Apparently, the twist behaviour is less sensitive to the influence/-s that cause/-s the deviations of numerical and experimental deflection values. This suggests that sliding of the EBL interfaces is not the only effect which is present in the experimental structure but not considered by the simulation. It is likely that an additional influence of this kind consists in a sliding of the linear bearings. A play of these components in the direction of their (imperfectly) constrained degree of freedom is potentially at the bottom of the observed decoupling of the deviations related to deflection and twist.

Due to the dimensions of the experimental structure and the fact that the linear bearings are hardly accessible inside the airfoil, attempts to further restrain the linear bearings from sliding hold little prospect of success at reasonable expense.

No definite explanation has been found for the decreasing absolute values of twist deflection for both system states in the simulation results. The fact that they cannot be reproduced at different spanwise locations and for different loads indicates that their relevance for the application of the structural concept in general is however low. The phenomenon might be explained by a numerical error, whose likelihood is increased at higher voltages due to the small deflection values.

Like in case of the wing box equipped with EBL spar, remanent charges of the electrostatic interfaces of the experimental airfoil have been observed after switching off the voltage.

In spite of the reduced performance of the smart material and a possible overlay of the desired effects by sliding—both reflections of the nature of experimental work—, the investigated airfoil structure based on electromechanical coupling permits changes in twist of the order of 300% in both directions, which can be considered as a success in light of the scope of the present chapter. It should be added at this point that the concentrated tip load applied in the experiments is presumed to constitute an especially unfavourable boundary condition with respect to the strength of the EBL. The EBL-based adaptive-twist airfoil can thus be expected to perform considerably better under distributed loading as given by the aerodynamic pressure in a real application.

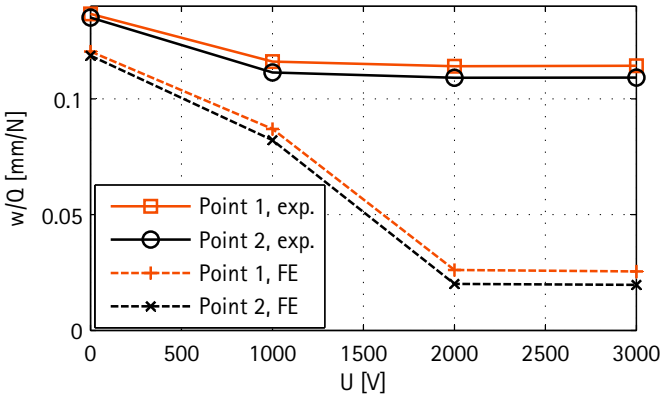

Figure 5.28: Deflection compliance of the experimental airfoil structure at the two measurement points in state 01 with respect to interface voltage. Experimental vs. simulation results. Q = 10 N

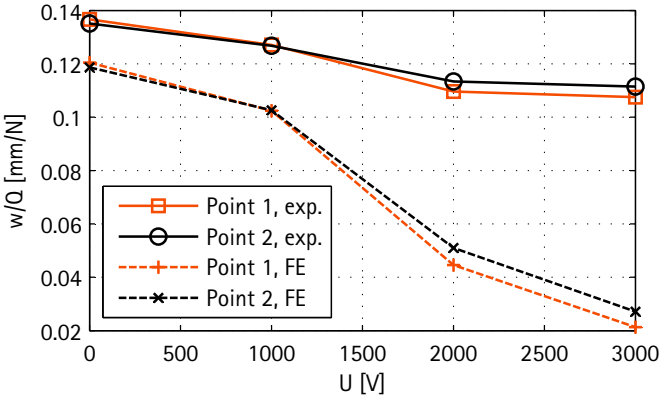

Figure 5.29: Deflection compliance of the experimental airfoil structure at the two measurement points in state 10 with respect to interface voltage. Experimental vs. simulation results. Q = 10 N

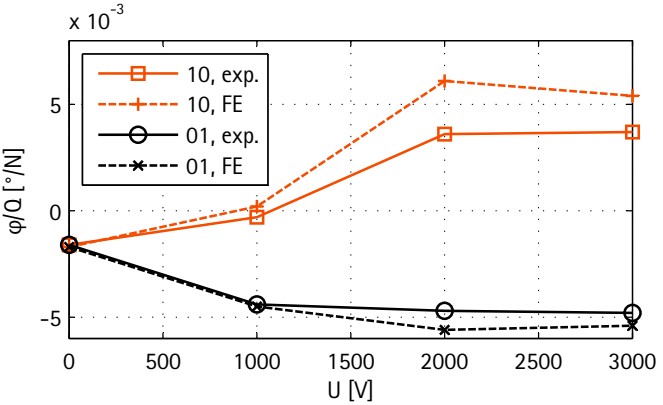

Figure 5.30: Twist compliance of the experimental airfoil structure in states 01 and 10 with respect to interface voltage. Experimental vs. simulation results. Q = 10 N

6 Applicability of adaptive-twist airfoils

Starting from an analytical derivation of the proposed operating principle of adaptive twist (chapter 2), on which a general strategy for the implementation of the idea under the aeroelastic conditions of a fixed wing has been founded (chapter 3), this doctoral thesis moved on to the elaboration of structural designs based on this concept (chapters 4 and 5). For both smart material approaches that have been investigated, the design-related parts are characterised by their development from the investigation of local and intermediate phenomena on the levels of material, smart interface and wing box to a concretion towards realistic structural designs of an airfoil. On the one hand, the set-up of the entire thesis is thus directed towards the development of implementations of application-oriented adaptive-twist airfoils. On the other hand, with a view to the generality of the results, investigations had to be carried out as independently from particular conditions of certain applications as possible. The present chapter attempts to close parts of the gap ensuing from this setting by a discussion of the transferability of the achieved results to the conditions of a commercial application. In particular, it is the objective of this chapter to discuss, based on the presented findings, the applicability of the adaptive-twist concept in designs of fixed wings as they emerge under the requirements of commercial flight and the conditions of an industrial environment. In the frame of these considerations, special emphasis will be placed on the comparison of the two smart materials with thermo- and electromechanical active principle. In a similar way as the results of chapters 4 and 5 verify the predictions on the adaptive capabilities of the novel structural concept that have been made in chapter 2, the discussion of the present chapter can thus be understood as an examination of the theses that have been formulated for the applicability of this concept in airfoils in chapter 3.

It has not only been demonstrated by the presented findings that the suggested structural concept is generally effective and in principle applicable under flight conditions but also a-priori perceptions that certain theoretical limitations inhere in the concept which hamper its practical relevance or at least strongly confine its design space could be allayed. Especially concerning

aeroelastic instabilities, seemingly heavy limitations of the idea, the possibility to shift the occurrence of divergence and flutter to sufficiently high flight velocities by an appropriate structural design has been shown.[1] The fulfilment of elastic stability requirements has further been demonstrated for the adaptive-twist airfoil as well as its capability to provide changes in lift that are comparable to the ones of conventional wing attachments in one of the investigated implementations.

At the same time, the adaptive-twist concept holds the potential of advances in various technical respects. Due to its semi-passive nature, it is especially promising in terms of energy efficiency. The absence of actuators and conventional mechanisms bears a high potential with respect to the degree of structural integration achievable by designs of adaptive-twist airfoils. Furthermore, the lack of such machinery decreases the system complexity and allows to exclude the aforementioned characteristic problems related to rigid-body mechanisms, namely high weight, wear, play, noise, particle release, error proneness as well as need for lubrication and additional maintenance.[2] The latter points, as well as potential reductions in assembly costs, constitute direct economic benefits of the more integral design of the adaptive-twist airfoil. In comparison with active morphing wing concepts with smart actuation and compliant kinematics, with which it shares some of the mentioned general advantages, the adaptive-twist approach stands out not only by smaller limitations caused by the requirement conflict introduced in chapter 1, which it avoids by its variable-stiffness nature but also by a potential energetic benefit due to the utilisation of aeroelastic coupling and by the absence of complications related to the selection, integration and placement of actuators. Moreover, already by its conception based on the wing box as the constitutive element, the proposed idea can be identified as well compatible with the structural layout of conventional wings[3] and thus be distinguished from many morphing concepts that suggest more exotic structural designs and can hence be assumed to be accordingly difficult to implement under industrial conditions.

[1] This has been demonstrated only for a certain airfoil design. However, the results strongly suggest that the conclusion is transferable to other implementations.

[2] Admittedly, the potential advantage of the adaptive-twist airfoil in these respects depends on its implementation. The variable-topology spar, for example, is ultimately based on rigid-body motion as well, since its interfaces are intended to slide in their open state. The relative motions can however be expected to be relatively small.

[3] As a potential exception to the good general integrability, pressurised fuel tanks in airplane wings should be mentioned, which would presumably compromise the effectiveness of the novel concept by their contribution to the torsional stiffness.

In the face of the numerous quoted distinct advantages of the adaptive-twist airfoil, the question of its downsides arises. The answer to this question is mainly found in the semi-passive nature of the concept, which defines both its most outstanding benefits and its major limitations. Lacking active components, the adaptive-twist airfoil stays behind its competitors that feature actuators in terms of adaptation authority and flexibility, as a matter of nature. The amplitude of the adaptation range for semi-passive twist based on the proposed idea is in fact comparably high due to the synergetic interplay of variations in shear centre location and torsional stiffness and due to the small influence of the requirement conflict. The weak point of the adaptive-twist airfoil is rather given by its restrictions in terms of reversibility. It has already been shown in chapter 3 that twist adaptations based on the suggested semi-passive approach cannot be repeated under steady-state conditions without reducing the attainable twist amplitude and raising the deflection. For a large number of alternate activations of back and front spar, the twist converges to zero and the deflection converges to a maximum finite value. The rate of this decay certainly depends on numerous parameters, but the observations based on the example of chapter 3 show that, with a reduction in twist by a factor of two already for the second cycle, it is not at all a matter of a fatigue effect but rather of an influence which can be expected to compromise any repeated operation of the adaptive-twist airfoil.

A parameter of primary influence on the crucial revertive behaviour is constituted by the chordwise wing box offset, which has received detailed consideration in the context of both investigated implementations of adaptive-twist airfoils. As it has been demonstrated, raising the offset of the wing box, and by that moving the shear centre to the trailing edge, leads to a shift of all aeroelastic equilibria towards more negative twist angles und thus to a general wash-in tendency of the airfoil. For high values of wing box offset, high twist amplitudes in nose-up direction can be achieved due to the large difference in torsional stiffness between (quasi-)open and (quasi-)closed state of the wing box. On the other hand, the airfoil is not able to twist back autonomously to a state of neutral or even wash-out behaviour after the lift-increasing shape adaptation in such a case.

As a second parameter which considerably affects the airfoil's capability of reverse twist, the cross-sectional aspect ratio of the wing box shall be discussed at this point. This quantity has been investigated in the previous chapters in terms of its influence on the elastic behaviour of the adaptive

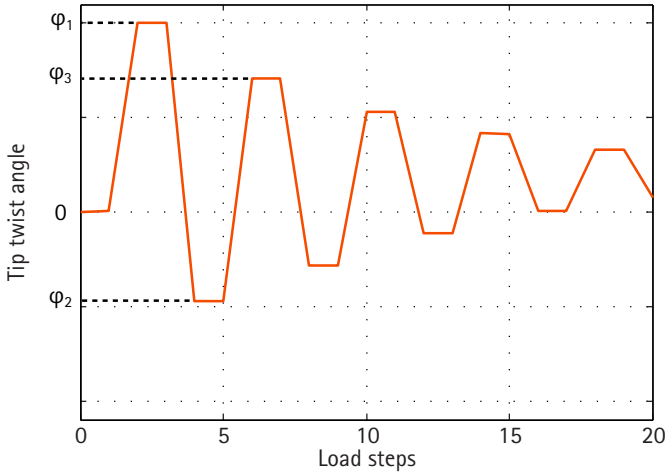

Figure 6.1: Definition of characteristic tip twist angles for the evaluation of the revertive behaviour of the adaptive-twist airfoil by means of an example of a cyclic twist curve. Wash-in twist angles are positive.

wing box structures, but its effect on the concept's reversibility has not been addressed yet. In order to quantify the airfoil's revertive properties, a representative adaptation sequence shall be defined. For this purpose, the system states *01*, *10* and *11* are employed, referring to the definitions of chapter 5. In the more general considerations of the present chapter, however, "0" denotes a spar interface that is either open or soft, depending on its implementation as a variable-topology or variable-stiffness interface, and "1" accordingly represents a closed or stiff spar.[4] Like in chapter 3, the presumed adaptation sequence is constituted by repeated manoeuvres of (wash-in) twist and reverse twist, namely by a repetition of the series of system states *11*, *01*, *11*, *10*. The equilibrium tip twist angles in the first *01* state, the first *10* state and the second *01* state are further termed ϕ_1, ϕ_2 and ϕ_3, respectively, as

[4]For stylistic reasons, "opening" and "closing" are applied sometimes in the following discussion as generic terms for both types of interfaces which include the meanings of "softening" and "stiffening", respectively.

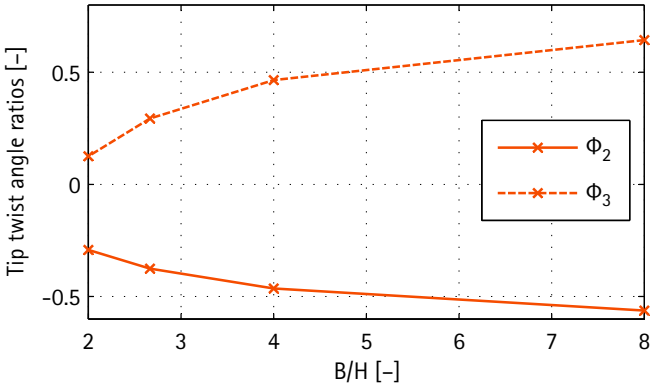

Figure 6.2: Influence of the cross-sectional aspect ratio of the wing box on dimensionless figures for reversibility evaluation

illustrated in figure 6.1.[5] Based on these assumptions, the following dimensionless ratios are defined: $\Phi_2 = \phi_2/\phi_1$ and $\Phi_3 = \phi_3/\phi_1$. While the first of these quotients quantifies the relative amount of twist which is available for a reverse manoeuvre, the second one provides information about the relative potential of twist adaptivity that is maintained by the airfoil after the first adaptation cycle. Figure 6.2 presents the results of a cyclic investigation in terms of the effect of the cross-sectional aspect ratio of the wing box on the two dimensionless ratios. Since such an analysis based on the aeroelastic calculation environment applied for the simulations of chapters 4 and 5 would result in a large numerical effort, the simplified aeroelastic model of chapter 3 has been used again. The results clearly reflect the beneficial influence of a relatively wide wing box design on the airfoil's capabilities with respect to reversible and repeatable shape adaptations. Not only the amplitude of reverse twist achievable by the first *10* system state, but also the wash-in adaptation potential that is preserved over one morphing cycle increases considerably with the cross-sectional aspect ratio of the wing box. These findings point out the importance of utilising the degrees of freedom related to the spar positions for the structural design or optimisation in case of an application

[5] For these considerations, twist angles are not expressed in the coordinate system used for the structural investigations of previous chapters. Twist angles in wash-in direction are rather assumed to be positive here.

where the cyclic characteristics play a role. Since common airfoil shapes place rather narrow boundaries here due to the location of their centre of pressure close to the quarter-chord point[6], aerodynamic profiles with particularly high chordwise offset of the centre of pressure are sought-after if the wing box shall be designed as wide as possible.

In this context also the usually beneficial influence of lift-induced shifting of the centre of pressure should be mentioned, which has not been considered up to now in this work. As it is evident from equation 4.5, the centre of pressure of aerodynamic profiles with negative zero-lift moment coefficient c_{m0}—as characteristic of (positively) cambered profiles—moves towards the leading edge when the lift is increased. This leads to a twisting moment in the same direction as the one that is created by the shear centre shift of the adaptive-twist airfoil when the lift shall be increased. An accordingly favourable addition of the torsional moments related to both effects in the opposite direction is observed for shape adaptations which decrease the lift.

It has to be recalled that the reversibility considerations made up to now assume an iterative operation based on aeroelastic equilibria. In a real application, shape changes would however be controlled, such that, for example, smart interfaces can be closed before an equilibrium state is reached, or a state of zero lift can be set during reverse twisting, allowing in principle to restore the airfoil's initial adaptive potential by activation of state *00*. The additional degrees of freedom in terms of system states accessible in a controlled operation can thus be expected to widen the design space of the adaptive-twist airfoil under reversibility requirements.

Independently of the various possibilities of adjusting its revertive characteristics by structural design measures and control strategies, the semi-passive adaptive-twist concept is, due to its general limitations in this respect, less suited for applications that require iterative adaptations than an active approach to morphing. The highest potential of application of semi-passive twist is therefore found in airfoil functions that have to be activated only very few times between two states of lift alleviation.

Speaking in the categories of an airplane wing, the concept is much more applicable for high-lift than for flight control functions. Depending on the mission, the latter require changes in lift with frequencies of the order of 0.3–10 Hz [96] during longer flight phases and thus with a very high number of repetitions. The former, in contrast, have to be activated—assuming the

[6]This consideration holds at least under the assumption of coincidence of centre of pressure and shear centre in state *11*, which can be considered as appropriate for many applications, especially the ones requiring reverse twist capability.

mission of an ordinary transport airplane as an example—for take-off in a state of zero lift, deactivated after take-off and activated again for landing under flight loads and finally deactivated again on the ground. For such an application the wing would have to be twisted in positive direction (following the sign convention of the present chapter) before take-off under the effect of its weight, either by purely passive structural tailoring or by a designated activation of state *10* of the adaptive-twist system. During take-off, the increasing lift force could be exploited for a negative twist towards the neutral configuration required for the subsequent cruise flight. This wash-out twist adaptation would be carried out, depending on the design, in state *11* or *10*, terminated by an activation of state *11*.[7] Before landing, the adaptive-twist airfoil would have to be set to state *01* to increase the lift coefficient by a positive twist and to be "frozen" in the wash-in configuration by activation of state *11*. After landing, the wing can be reset to its original configuration by opening the interfaces that have been closed with respect to the initial state. In view of the low number of twist operations that are required for the characterised high-lift function—also when considering a safety margin that accounts for potential aborted landing attempts—the use of the adaptive-twist airfoil for such an application seems generally feasible. Discrete high-lift devices like flaps, slats and droop noses could be replaced by such an application of the morphing system, while a different approach has to be chosen for substituting flight control surfaces.

The idea of lift alleviation manoeuvres to reset the adaptive-twist airfoil during flight and thus renew its potential of shape adaptations has already been presented. While such strategies based on zero-lift flight or even inverted flight appear unsuitable in the practical terms of commercial flight under usual conditions, they cannot be generally excluded in this scientific thesis for example as potential measures of emergency or further exception in specific applications.

It has to be mentioned again that it cannot be in the scope of this dissertation to provide ready technical solutions for a certain use of the novel airfoil concept in a particular application. The considerations on its applicability under the conditions of a transport airplane made above with a special emphasis on the crucial point of reproducibility of shape adaptations shall rather motivate its general eligibility for an implementation in aeroelastic systems developed and realised in an industrial environment.

[7] The original philosophy of the adaptive-twist concept, which bases on the utilisation of states of low torsional stiffness for shape adaptations, suggests the latter approach. The former might however be more suited for certain applications.

A topic that connects to the issue of repeatability of shape adaptations during a single flight is the one of long-term durability. The points in which the adaptive-twist concept differs from conventional solutions in this respect are given by pronounced strain and temperature changes in softened variable-stiffness elements and by frictional wear at opened variable-topology interfaces. Concerning these matters, it can be referred to previous findings in the field of material science and engineering.

Concerning the variable-stiffness approach, the maximum strain values observed in the softened interface of the wing box of the adaptive airfoil structure of chapter 4 were of the order of magnitude of 1%[8]. If highly deformable polymer materials are applied for the variable-stiffness interfaces—as for example elastomers[9] that withstand maximum strains of up to several thousand percents [130]—, no general endurance issues due to the strain in glass-transiting variable-stiffness interfaces are thus identified. In this context, dielectric elastomer actuators [131, 132] can be mentioned, which share their strain-based nature with the discussed concept and for which promising endurance properties have been reported [133]. Particular demands are posed on the glass-transiting polymer interfaces, in contrast, by the temperature changes tied to the airfoil's twist adaptations. Such *thermal cycling* is known to cause microscopic cracks in polymer materials, which lower the strength [134–137][10]. Also this general limitation of the variable-stiffness concept suggests applications for which only a low adaptation frequency and a low total number of cycles is required.

As to the variable-topology approach, influence of wear of the dielectric due to friction at the dielectric-electrode interface can potentially affect the friction coefficient and the polymer film's dielectric and insulating properties. While concerning the tribology of the polymer-metal contact it can be referred to the literature [138–141], no systematic study on potential degrading influences of friction on the electrical properties of electro-bonded laminates, on the other hand, is known to the author, so that this topic has to be mentioned in the same breath as the points addressed in the outlook section of the following chapter. However, the results of the test of electro-bonded laminates in a friction-based damping system for several million load cycles reported in [59], in which only "marginal signs of deterioration" [59] were observed, give rise to the assumption that interface degradation due to friction does not represent a strong limitation of the electromechanical

[8] In terms of the maximum shear stress component.
[9] Referring to the soft state of the interfaces.
[10] These references relate to investigations based on polymer composites.

approach.

A point of high relevance with respect to potential applications, which is also characterised by larges differences between the two strategies based on variable (local) stiffness and on variable topology, is given by the energy consumption of the adaptive-twist airfoil. The fundamental relations which determine the energy requirements for both implementations of morphing wings have already been introduced by equations 4.2 and 5.3. Both of these basic energy laws neglect losses that occur in reality, in case of the thermomechanical system given by heat flows to the environment, in case of the electromechanical one by leakage currents. Nevertheless, they allow for a first approximation of the energy expense that is related to the operation of the adaptive-twist concept in both cases and for a demonstration of the fundamental difference of the two working principles in terms of energy consumption.

In order to compare both types of smart materials in this respect, the amounts of energy required for the adaptation of the upscaled adaptive-twist airfoils of chapters 4 and 5 have been estimated based on equations 4.2 and 5.3. Due to their different nature as variable-stiffness and variable-topology approaches, both concepts are not directly comparable. Under the assumptions made for the investigations of chapter 4, a direct relation between the thermal energy required for heating of the glass-transiting polymer interfaces and the resulting twist compliance of the airfoil can be determined. The calculated thermal energy is thus plotted with respect to the wing's tip twist angle in figure 6.3. Since it is only accounted for lossless heating of the PVC layers here (using the heat capacity values reported in [99]), the results represent a lower bound for the energy that has to be supplied in reality. The energy required for the activation of the EBL-based adaptive-twist airfoil, in contrast, does not directly depend on the resulting wing twist, as the variable-topology system can only adopt the two discrete system states of activation and deactivation. However, depending on the airfoil's state, different voltages are required to effectively operate the electromechanical system. The calculated charging energy is therefore presented as a function of the applied voltage in figure 6.4.[11] The comparison of both plots reveals the fundamental difference of both material concepts in terms of energy requirement. Even at the highest voltage shown in figure 6.4, the estimated energy consumption of one state change of the electromechanical system is

[11] For the electromechanical interfaces, the plotted energy accounts for charging of the electrobonded laminates of ***both*** spars. Like this, a more fair comparison with the thermally activated airfoil, which possesses additional skin interfaces, is ensured.

lower by more than four orders of magnitude than the one of activating the thermomechanical system. Concerning the energy which has to be additionally spent for the compensation of losses in a real application, the demand related to heat flows to the environment can be expected to be higher than the one caused by electric leakage currents under usual conditions, which even amplifies the difference between both smart materials. Furthermore, it should be considered that the energy extracted from a charged EBL during discharging is not entirely lost but can in principle be partly recycled by charging and discharging a second capacitor. Varying specific conditions related to the structural and material design of the thermomechanical system, as for example concerning the amount of employed smart material or the polymer's specific heat capacity as a function of temperature, can certainly lower the heating energy but cannot considerably change the assessment of the two concepts in terms of their energy efficiency, which is based on a difference by orders of magnitude.

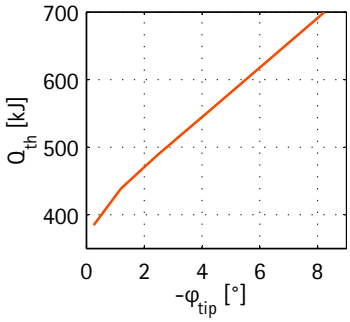

Figure 6.3: Energy requirement of upscaled airfoil based on thermomechanical coupling with respect to tip twist angle

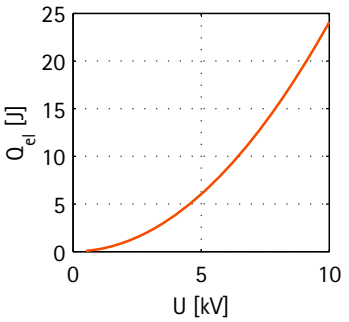

Figure 6.4: Energy requirement of upscaled airfoil based on electromechanical coupling with respect to interface voltage

One aspect that is theoretically in favour of the thermomechanical concept in an application-oriented energy comparison should nevertheless be highlighted: the difference of the two smart materials in terms of the system states that require energy to be supplied. If a thermally activated interface is designed to have its glass transition temperature above its operating temperature (e. g. during flight), energy has to be provided only for heating in

order to lower the stiffness (and possibly cooling to accelerate returning to the state of high stiffness). An EBL interface, on the other hand, has to be continuously kept charged in all states in which it has to transfer shear stress, which implies the permanent supply of energy to compensate for losses due to leakage currents in these states. Assuming the aforementioned mission of a transport airplane consisting of a take-off in high-lift configuration, a cruise flight at a lower lift coefficient and a landing in high-lift configuration, the duration of the cruise flight phase for which the continuous leakage currents eat up the energy savings of the EBL-based airfoil related to the activation of interfaces in comparison with the thermally activated one, such that the energy demand for the entire mission is the same for both concepts, would theoretically be 46'000 hours.[12] This calculation clearly shows that the electromechanical concept maintains its clear energetic superiority also under consideration of the continuous energy consumption of closed interfaces.

The nature of electro-bonded laminates to require permanent voltage application in load-carrying states does not only affect the energy demand of the electromechanical adaptive-twist airfoil in the described way but has also an important impact on the airfoil's operational safety. A malfunction of the high voltage supply of an EBL interface or an electrical breakdown through a dielectric during the operation of the airfoil would lead to an unintentional increase in twist and deflection compliance. This can, depending on the structural design and on the flight conditions, potentially endanger the airfoil's integrity in terms of strength and structural, aeroelastic and flight stability, and ultimately cause a catastrophic system failure. The design of an adaptive-twist airfoil, especially for an application where a failure can be critical for the safety of human beings, has to provide for extremely reliable measures ensuring the failure tolerance of the entire system in case of such or any other potentially hazardous events. Again, no definite solutions shall be proposed here but mechanical guides and stops limiting the sliding of the interfaces, redundant voltage supplies, (post-breakdown) self-healing dielectrics and, most likely, a combination of several structural and electrical means, shall be mentioned as preliminary ideas for provisions in this respect. The fail-safe properties of the thermomechanical airfoil design are, in comparison, generally much less critical, at least in an implementation based on passive cooling. Redundant heating systems have to be however installed also in this case, if, for example, a safe landing requires a shape adaptation.

[12] In addition to the aforementioned assumptions, the volume resistivity value of $2.3 \cdot 10^{14}$ Ωm reported for polyimide [142] and a simple resistive circuit have been presumed for this rough estimation.

In the context of the design of adaptive-twist airfoils for operational safety, the main difference of the considered smart materials in terms of strength has to be mentioned. The highest shear stress transferable by a thermomechanical interface is limited by the shear strength of the temperature-variable polymer in the stiff state,[13] for which typical test results of tens of MPa are reported [143–147], depending on the material and the experimental conditions. As to the electro-bonded laminate in its state-of-the-art implementation, in contrast, it has been pointed to the substantially lower shear strength limit of around 0.15 MPa in chapter 5, which places tight constraints on the design space of the EBL-based adaptive twist airfoil accessible to the structural engineer. The possibility to arrange several electro-bonded laminates in parallel to enhance the transferable shear load has been mentioned, too. Concerning the other side of the adaptation range, the electrostatic approach, as a variable-topology system, is favourable in terms of the lower boundary for the shear stress transfer. However, the investigation of the adaptive-twist airfoil based on thermomechanical coupling presented in chapter 4 has shown that thermally activated interfaces in principle provide sufficient compliance to the wing structure in their soft states, so that the EBL's drawback in terms of strength clearly outweighs its less relevant advantage related to higher maximum compliance when comparing both approaches for such an application.

The different stress transfer characteristics of the two considered smart material systems result from their different nature in terms of the type of bonding that is established at the interface: While the thermally activated interface is based on a material bonding, the electro-bonded laminate relies on a friction-based one. This fact naturally implies a higher material demand of the thermomechanical concept with respect to the electromechanical one. The general advantage of the latter in terms of lightweight efficiency that can be deduced from this difference is further amplified by the smaller possible thickness of electrodes compared to heating layers[14] and by the lower mass related to the required infrastructure: Although depending on many conditions, generally lighter implementations can be expected for the voltage supplies and electric connections of an EBL system that are designed for low electric currents, in contrast to the heating systems of a thermally activated concept which are—at least in the considered case of ohmic heating—based

[13] Assuming a strong bonding between the interface and the structure in which it is integrated.

[14] The relevance of this point depends on the degree of structural integration of these layers. If, for example, the heating layers can be integrated as load-carrying components, no general mass penalty is related to them.

on the very supply of electric currents, so that conductive material has to be dedicated to that purpose.

Not only the energetic and lightweight qualities of the adaptive-twist airfoil, but also the dynamics of its shape adaptations are decisively influenced by the properties of the applied smart material system in terms of involved amounts of material and transport of stimulus energy. Theoretically, its capacitive characteristics give the electro-bonded laminate a large benefit in activation speed with respect to the thermomechanical approach that is based on heat conduction. In practice, this advantage has been verified only for activating the interfaces. After short circuiting the electrodes, on the other hand, the electrostatic interfaces investigated in the frame of this dissertation are, for the considered electric fields applied before, characterised by pronounced remanent charges—presumably due to charge injection into the dielectric—, such that they cannot be switched off instantaneously.

Under certain conditions, the thermally-controlled smart material system can be designed to work with passive cooling, which beneficially affects the airfoil's failure tolerance due to the autonomous return of the system to states of high stiffness, as highlighted above. This potential advantage is linked at the same time to one of the biggest challenges in the development of an adaptive-twist airfoil based on thermomechanical coupling, the reconciliation of the characteristic temperatures of the variable-stiffness polymer with the operating temperatures of the application. The mentioned approach of cooling by means of passive heat transfer to the environment requires the glass transition temperature of the heatable polymer to be sufficiently above the highest temperature this environment is exposed to during operating states in which a stiffness adaptation has to be performed.[15] On the other hand, the glass transition temperature should be chosen as little above the lowest operating temperature[16] of the polymer as possible in order to minimise the heating energy.

Referring again to the application of a commercial flight vehicle, the skin of a subsonic jet airplane experiences operating temperatures between around –60°C and 80°C [148] as caused by the ambient temperature at cruising altitude and solar radiation in a hot environment on ground, respectively. This temperature range can be employed as a first approximation for the wing structure in which the adaptive interfaces have to be integrated. It might not be required to activate the variable-stiffness system at the higher lim-

[15]Which temperatures are considered "sufficiently above" in this context depends on the specification concerning the dynamics of the cooling process.

[16]Again considering only operating states in which adaptations are performed.

iting temperature under usual conditions, since the airfoil can be designed to be in a twisted state due to gravity loading before take-off, but, certainly, it has to be able to operate at temperatures substantially above the lower one, accounting for example for the need of an emergency landing shortly after take-off, when the structure has not been substantially cooled yet. It stands to reason that the varying operating temperatures of applications like this one strongly confine the thermomechanical design space of the glass transition–based variable-stiffness approach, which finally further exacerbates this concept's general problem of high energy demand. In order to put the considered exemplary application into perspective, it shall be mentioned that for supersonic flight even higher maximum skin temperatures of 100°C [149]–230°C [150] have to be accounted for, while the range of operating temperatures between –20°C and 50°C [151] commonly specified for wind turbine blades as another potential application of the concept would slightly facilitate the design problem.

An EBL-based adaptive twist airfoil would not be affected that much by operation temperatures, but electric discharges ("lightning strikes") [152] have to be considered as unusual operating condition which can potentially affect the operation of the electrostatic system. In an application the need for shielding of EBL interfaces by a Faraday cage would therefore have to be investigated in order to preclude any detrimental influence of the ambient electric field.[17]

Many more points and questions would arise during the development of an adaptive-twist airfoil for a specific application which cannot be covered here. Like it is the case for every novel design concept, openness to unconventional technical detail solutions would be required during this process.

[17] For EBL interfaces integrated in the wing skin, the shielding is more complicated. Either they would have to be designed not to be safety critical, or special protection measures would have to be taken.

7 Conclusions and outlook

Shape-adaptable airfoils based on compliant kinematics and smart materials promise advances in system performance and efficiency. In contrast to active approaches to shape morphing, which are often strongly affected by the requirement conflict characteristic of the design problem of shape-adaptable airfoils, a semi-passive structural concept with adaptive stiffness has been proposed in this dissertation. Utilising aeroelastic coupling instead of actuators, this approach holds the potentials of high energy efficiency and low system mass. The concept has been investigated and demonstrated in wing box and airfoil implementations based on two different smart material systems. Building upon the analytical, numerical and experimental findings of this study, application-related aspects of the approach were discussed in the previous chapter. In the present chapter, the main results obtained over the course of the work presented in this doctoral thesis shall be summarised and critically analysed with respect to their significance and implications as well as to points that have to be left to future research.

7.1 Concluding summary of the main findings

The structural concept for adaptive twist pursued in this work is based on the idea that well-directed reductions in the shear stiffness of a thin-walled profile can be utilised for considerable semi-passive twist deformations of a structure under shear load due to the synergetic combination of the effects of shear centre shifting and decreasing torsional stiffness.

An extensive parametric study relying on analytical and finite element calculations has provided insight in the elastic behaviour of cantilever wing box structures with adaptive bending-twist coupling based on this working principle. Not only the effectiveness of the structural concept, which enables large changes in the coupling behaviour, but also the possibility to adjust the mechanical properties of an adaptive wing box in a wide range by variation of design parameters has been demonstrated. The largest changes in torsional compliance have been observed for (in relative terms) wide cross sections due to their large shear centre shifts and their distance from a configuration that is,

in terms of cross-sectional shear stress distribution, symmetric. Furthermore, designs with high web thickness ratio and high slenderness have been found to enable large changes in twist, but the highest coupling ratios have been recorded for lower parameter values in both cases.

The important characteristic of the structural concept to allow for large changes in torsional stiffness while having only a small effect on the flexural rigidity is well reflected in the results of the parametric study.

In this context, also the possibility of utilising elastic couplings of anisotropic laminates to enhance the adaptive coupling behaviour of the beam structures has been examined, showing that the comparably high warping stiffness of laminate layups that exhibit such couplings overweighs the twist compliance enabled by these laminates, such that no benefit has been observed under the considered conditions.

The parameter study has revealed the lack of an analytical model which describes appropriately the elastic properties of the adaptive beams in the transition range between closed and open configuration. However, it could be pointed out that the analytical solution accounting for the warping constraint of the clamping yields suitable approximate results up to high stiffness ratios.

In order to apply the adaptive-twist concept in a fixed wing, where the transverse shear component of the lift force can be exploited for twist deformations and thus changes in lift, a suitable structural layout for a wing with semi-passive adaptive twist has been devised. A configuration with two smart wing spars, whose alternate activation permits a reversible twist behaviour under aeroelastic conditions, has been proposed for this purpose. At the same time it has been shown that the revertive capability of the semi-passive concept under constant flow conditions is limited to a low number of cycles. The requirement for the wing design to provide a low warping rigidity in the airfoil's states of high torsional compliance has as well been emphasised in this context.

As a first implementation, the realisation of adaptive-twist airfoils has been approached based on a smart material concept with thermomechanical coupling: Polymer elements with adjustable temperature have been integrated in the structure in order to put—by way of glass-transition—the desired changes in elastic modulus into effect. Two configurations of variable-stiffness elements have been compared, showing that a monolithic design requires a low thickness of the temperature-variable polymer layer, whereas the opposite is true for a lap arrangement. Moreover, the buckling stability of monolithic adaptive webs, which is low in soft system states and which conflicts with the interface's shear compliance, has been pointed out as critical

for an application of monolithic spars in a wing box.

A scaled experimental wing box structure with PVC web and elastically decoupled carbon fibre heating element has demonstrated the effectivity of the adaptive-twist concept under laboratory conditions, allowing for changes in tip twist up to a factor of about 35.

Parametric investigations on the elastic behaviour of adaptive-twist airfoils with a variable-stiffness interface in the front spar have shown the benefit in adaptation amplitude that can be achieved by integrating additional smart interfaces in the skin, especially in the front cell. Moreover, they have demonstrated the positive effects of high width and large chordwise offset of the wing box on the magnitude of achievable twist, as well as the ones of low height and large thickness of the spar interface.

Building upon the findings of the parametric study, a suitable wing design could be elaborated, based on which a scaled experimental airfoil structure has been manufactured. Under structural testing, this realistically sized demonstrator airfoil has allowed for maximum changes in tip twist by a factor of about four, showing that the adaptive-twist approach is effective also when integrated in a wing structure.

The scalability of the structural concept to the dimensions and flight conditions of the wing of a glider plane has been demonstrated by means of aeroelastic calculations. In such an implementation, the adaptive-twist concept has been found to enable changes in lift coefficient of similar quantity as the ones of conventional wing attachments while ensuring divergence stability up to flight velocities of at least 50 m/s.

As a second material system for the smart interfaces of the adaptive-twist concept electro-bonded laminates have been investigated. Besides a fully coupled electroelastic simulation of such variable-topology elements relying on controllable electrostatic attraction forces and frictional shear stress transfer, a simplified simulation approach based on the substitution of electrical properties by a mechanical stress has been proposed, whose results are in good agreement with the experimental findings of double-lap shear tests.

Similarly to the thermomechanical implementation, a wing box structure with EBL web has been subjected to experiments. The adaptive behaviour has also been verified in this configuration, which puts changes in twist of the order of fifty times into effect. On the other hand, the experimental results have pointed out the non-ideal behaviour of the electro-bonded laminate at its current stage of development: Not only the mechanical strength of the electrostatic bonding has stayed below the theoretical expectations (and below the one of the thermomechanical solution), but also the torsional stiff-

ness in the more rigid state has been, under small shear loads, substantially lower than predicted by the simulation.

Also the electromechanical implementation of the adaptive-twist wing box has been applied to an airfoil structure. By its structural layout in general and its two EBL spars in particular, the scaled experimental wing structure realised for this purpose is capable of reverse twist. Structural tests of this airfoil have confirmed again, qualitatively, the expected adaptive behaviour but have once more revealed the limited performance of the smart material leading to large differences between measured and simulated deflection values at higher voltages. Air inclusions have been supposed to constitute the main cause for the deviation of the real behaviour of the smart material from the ideal one. However, the experimental airfoil has allowed for changes in tip twist by a factor of around three.

Due to the low shear strength of the electro-bonded laminate in its state-of-the-art implementation, not only the performance of the experimental airfoil has stayed below the expectations, but also the numerical upscaling of the wing based on electromechanical coupling has yielded substantially lower changes in lift coefficient than for the thermomechanical airfoil. Nevertheless, a realistic structural design for a glider wing could be found also for the EBL-based solution. Moreover, dynamic aeroelastic calculations have demonstrated the feasibility of designing adaptive-twist airfoils with sufficient safety against bending-twist flutter.

Based upon the analytical, numerical and experimental results, the general eligibility of the adaptive-twist concept for varying the lift force of a fixed wing could be concluded. It has been emphasised that the only major general limitation of the structural concept itself is given by the limited reversibility of adaptations, so that it can be fully recommended only for applications which require only few adaptations under continuous loading.

The extent to which the potential of the structural concept can be exploited as well as the applicability of the concept under specific conditions depend on the smart material employed, and the different properties of the two material systems investigated in the frame of this dissertation have been pointed out in this context: Glass-transiting polymers offer a continuous variation of the elastic modulus as well as sufficient strength and stiffness at temperatures below the glass transition but suffer from slow adaptation dynamics, high energy demand and restrictions given by time-varying operating temperatures. The respective characteristics of electro-bonded laminates are contrary: They are characterised by high activation speed, low energy demand and independence from operating temperatures but do not provide

control over the interface stiffness, and the maximum strength and rigidity achievable at the present state of the technology are low, resulting in a more confined design space and in worse fail-safe qualities of the adaptive-twist airfoil. No general recommendation can thus be made for one of the two material concepts, but rather can particular requirements be expected to decide on the better suitability of one or the other for a certain application.

7.2 Significance and implications of the results

Novelty of the structural concept It has been shown in this dissertation for the first time that well-directed stiffness or topology changes induced in the load-carrying structure of an airfoil by means of smart materials can be utilised for semi-passive twist deformations in order to change the aerodynamic loads on the airfoil.

The proof of concept achieved by the results obtained from the analytical, numerical and experimental investigations conducted in the frame of this thesis lays the foundation for the application of airfoils based on this unconventional working principle and structural design. Speculations about specific implementations in which the adaptive-twist-airfoil is most likely to be applied shall be set aside here, but it can be supposed that the results of this dissertation have revealed the potential that the concept holds, due to its distinct characteristics discussed in chapter 6, for certain niche applications.

In contrast to other approaches to semi-passive airfoil twist by way of variation of the elastic properties of an airfoil structure, which remain with rigid-body mechanisms and conventional actuators [30–44,75,76], the design philosophy of morphing has been pursued consequently in the present work, and the significance of kinematics and effectuators as diagnostic criteria in this context has been emphasised in chapter 1.

Furthermore, the concept stands out from most of the proposed solutions (except only for one [36–39,44]) by its capability to reversibly open the airfoil structure, which allows for a substantially higher torsional compliance.

Advances in the proof of concept for semi-passive twist It should also be mentioned at this point that the modus operandi followed for the investigation and demonstration of the presented structural concept is distinguished from other approaches by its systematic way of addressing issues arising from the characteristics of the novel wing design or the smart materials employed, which might be identified as particular obstacles—of insurmountable nature

in an extreme case—for a practical application of the concept beyond the academic environment already at an early development stage. This is manifested in the special consideration of potentially critical points like divergence, flutter and reversibility in the scalability demonstrations of the present work. In particular, with respect to the approach chosen for the—in some measure—related wing box concept in [36–39, 44], the present one takes important steps forward, addressing not only for the first time the integration of an adaptive-twist wing box in an airfoil structure but also the concept's applicability and scalability based on simulations accounting for aeroelastic coupling.

Pointing to the limits of the theory of thin-walled structures Concerning the analytical investigations of chapters 2 and 4, the consideration of the cross-sectional stiffness distribution as a variable in the treatment of the elastic problem for a wide range of stiffness ratios can be mentioned as an individual contribution of the present work as well. Particularly, the calculations shed light on the behaviour of the closed-form solutions of the theory of thin-walled profiles for both cases of constrained and unconstrained warping in the transition region between open and closed cross sections.

Contributions to simulation and testing of smart materials For both kinds of investigated smart material systems, the respective experimental airfoil structure realised in this research project represents the first shape morphing application of the material technology developed and sized under application-oriented conditions.

For the case of the electro-bonded laminate it should be highlighted that also the fully-coupled electroelastic simulation of this smart material system, as well as the according substitute simulation in the mechanical domain, are—as far as known to the author—original contributions of this dissertation which lay the grounds for a further numerical investigation of this technology.

The results of this research project point out the promising potential of the adaptive-twist airfoil concept and, at the same time, the need for smart materials that permit to exploit this potential as fully as possible. New ideas for smart effectuators which put large changes in stiffness into effect while offering high energy efficiency and fast adaptation are very much sought-after in this sense and can hopefully be stimulated by the findings of the present work.

Stimulation of related research During the course of the present project, the activities related to the investigation and development of adaptive-twist airfoils have brought up ideas that promoted research in related areas. Such stimulating implications have become manifest, for instance, in the preliminary investigations related to variable cross-sectional properties by way of compliant mechanisms [50] and to stiffness variation by elastic instabilities [153] as alternative working principles of semi-passive shape adaptation as well as to novel designs of active morphing airfoils with controllable camber based on a variable-stiffness skin that allows to mitigate the effects of the characteristic requirement conflict [121, 122, 154].

A new design philosophy The introductory considerations of chapter 1 have highlighted the significance of variable stiffness–based structural concepts like the one of this dissertation as representatives of a novel design philosophy. In contrast to classical lightweight design, which has always been driven by maximisation of stiffness, this alternative conception is based on the awareness of the limitation of highly-rigid designs for shape-adaptable lightweight structures and, consequently, on the utilisation of intentional time-variable stiffness reductions. In this sense, the design philosophy represented by variable-stiffness approaches like the one proposed in this thesis implies no less than a paradigm shift in the culture of structural engineering.

7.3 Outlook

While this research project has accomplished the invention and demonstration of the concept of smart and compliant adaptive-twist airfoils, many points remain open at the present stage. Concerning the gap between the state of the art defined by the presented results and an industrial application, the main problems requiring technical solutions have been discussed in chapter 6, while more will arise that cannot be covered in this thesis. The present section shall, in contrast, focus on matters that can be addressed by follow-up research in direct connection to the findings of this project in order to bring the concept forward to higher maturity.

In the frame of this dissertation static mechanical tests have been conducted for an experimental proof of concept of the adaptive-twist airfoil. Wind tunnel experiments are however required to prove the airfoil's effectiveness under aeroelastic conditions. In order to perform a complete morphing cycle including a reverse twist adaptation in such tests, some extensions have

to be provided with respect to the current state of the technology for both kinds of implementations. Concerning the thermomechanical system, active cooling devices should be added to the smart interfaces, such that state changes can be accomplished reasonably fast. As to the electromechanical spar interfaces, the issue of remanent charges should be investigated in a systematic way in order to be able to provide countermeasures against charge injection into the dielectric that enable a rapid discharge of the electro-bonded laminate.

Higher adaptation amplitudes of experimental adaptive-twist airfoils would be most welcome in future tests. On the side of the structural system itself, which could be brought to a relatively high level of technical maturity, a structural optimisation can be recommended to raise the performance of the airfoil for a particular set of conditions and requirements. On the side of the smart materials, the adaptation range of the thermomechanical implementation can be widened by directed tailoring of the glass-transiting polymer to the specifications of the experimental structure, based on material selection and/or design. Concerning the electro-bonded laminate, on the other hand, much more fundamental research is required. A systematic investigation of the failure mechanisms of EBL is as well essential to the further development for this material technology to be eligible for adaptive-twist airfoils (like for most other structural applications) as continuing the development of dielectric materials that offer both high dielectric constant and high breakdown strength and the elaboration of manufacturing strategies for integrated EBL interfaces which allow for a reduction of air inclusions.

Only quasi-static applications of the adaptive-twist airfoil have been considered in this work. An interesting field of future research could however consist in the dynamic utilisation of this and similar structural concepts. Variable-stiffness structures like the proposed one promise a high authority for adjustments of the dynamic behaviour, since not only the structure's elastic properties, but also their damping characteristics are affected by the state of the adaptive system. While the thermomechanical approach would permit to control the polymer's loss factor by varying its temperature, the electromechanical one would offer voltage-dependent friction damping. In an aeroelastic environment, different ways of coupling between aerodynamic and structural effects can additionally be exploited to adapt a system's dynamic behaviour. Considering the limitations of the state-of-the-art implementations of the adaptive-twist concept in terms of reversibility and—in case of the EBL-based airfoil—strength, the condition of cyclic loading with relatively small amplitudes that can be presumed for dynamic applications should

be advantageous.

Such an implementation would certainly require the development of a control system for the dynamic activation of the smart interfaces. However, due to the pronounced aeroelastic coupling that is inherent to the adaptive-twist airfoil, dynamic simulations of the system's revertive behaviour and according control strategies should be elaborated on also for applications requiring shape adaptations between quasi-static system states. The additional degrees of freedom coming along with an operation of the adaptive-twist airfoil beyond its equilibrium states can be expected to contribute substantially to the prospects for a better utilisation of the potential of the structural concept.

Bibliography

[1] L. F. Campanile. Smart shape control: using compliant and active materials to adapt structural geometry. Challenges and good reasons. In *14th International Conference on Adaptive Structures and Technologies (ICAST)*, Seoul, 2003.

[2] J. C. Maxwell. On reciprocal figures, frames, and diagrams of forces. *Transactions of the Royal Society of Edinburgh*, 1869.

[3] A. G. M. Michell. The Limits of Economy of Material in Frame-structures. *Philosophical Magazine*, 8:589–597, 1904.

[4] J. Wiedemann. *Leichtbau. Elemente und Konstruktion*. Springer, Berlin, 3rd edition, 2007.

[5] T. Hubel. *Untersuchungen zur instationären Aerodynamik an einem vogelähnlichen Flügelschlagmodell*. PhD thesis, Technische Hochschule Darmstadt, 2006.

[6] http://worldofaircraftdesignandaviation.blogspot.ch.

[7] O. Lilienthal. *Der Vogelflug als Grundlage der Fliegekunst. Ein Beitrag zur Systematik der Flugtechnik*. R. Gaertners Verlagsbuchhandlung, Berlin, 1889.

[8] D. Lentink, U. K. Müller, E. J. Stamhuis, R. de Kat, W. van Gestel, L. L. M. Veldhuis, P. Henningsson, A. Hedenström, J. J. Videler, and J. L. van Leeuwen. How swifts control their glide performance with morphing wings. *Nature*, 446:1082–1085, 2007.

[9] J. Valasek, editor. *Morphing Aerospace Vehicles and Structures*. John Wiley & Sons, Chichester, 2012.

[10] A. Stevenson, editor. *Oxford Dictionary of English*. Oxford University Press, Oxford, 2010.

[11] G. Reich and B. Sanders. Introduction to Morphing Aircraft Research. *Journal of Aircraft*, 44(4):1059, 2007.

[12] J. B. Cole. Variable camber airfoil. US patent No. 4053124, 1977.

[13] C. Hoffman. The Shape of Wings to Come. *Popular Science*, 263(4), 2003.

[14] A. K. Jha and J. N. Kudva. Morphing aircraft concepts, classifications, and challenges. In *Smart Structures and Materials 2004: Industrial and Commercial Applications of Smart Structures Technologies*, San Diego, 2004.

[15] T. A. Weisshaar. Morphing Aircraft Technology – New Shapes for Aircraft Design. In *Multifunctional Structures/Integration of Sensors and Antennas. Meeting Proceedings RTO-MP-AVT-141*, Neuilly-sur-Seine, 2006.

[16] Z. Min, V. K. Kien, and L. J. Richard. Aircraft morphing wing concepts with radical geometry change. *The IES Journal Part A: Civil & Structural Engineering*, 3(3):188–195, 2010.

[17] A. Y. N. Sofla, S. A. Meguid, K. T. Tan, and W. K. Yeo. Shape morphing of aircraft wing: Status and challenges. *Materials and Design*, 31:1284–1292, 2010.

[18] H. Baier and L. Datashvili. Active and Morphing Aerospace Structures – A Synthesis between Advanced Materials, Structures and Mechanisms. *International Journal of Aeronautical and Space Sciences*, 12(3):225–240, 2011.

[19] S. Barbarino, O. Bilgen, R. M. Ajaj, M. I. Friswell, and D. J. Inman. A Review of Morphing Aircraft. *Journal of Intelligent Material Systems and Structures*, 22(9):823–877, 2011.

[20] R. De Breuker, M. M. Abdalla, and Z. Gürdal. A Generic Morphing Wing Analysis and Design Framework. *Journal of Intelligent Material Systems and Structures*, 22(10):1025–1039, 2011.

[21] X. Lachenal, S. Daynes, and P. M. Weaver. Review of morphing concepts and materials for wind turbine blade applications. *Wind Energy*, 16(2):283–307, 2013.

[22] W. Raither. *Adaptive Materials for Structural Applications*, chapter Shape Control: Shape-Adaptable Airfoils. Lecture Notes, ETH Zurich, 2012.

[23] B. K. Wada, J. L. Fanson, and E. F. Crawley. Adaptive Structures. *Journal of Intelligent Material Systems and Structures*, 1:157–174, 1990.

[24] D. Müller and D. Reiners. Formvariable Strukturen auf bewegten Klappensystemen – Das Hornkonzept zur Strömungsbeeinflussung an der Hinterkante. In *DGLR-Jahrestagung*, pages 793–802, Munich, 1997.

[25] D. Müller. *Das Hornkonzept. Realisierung eines formvariablen Tragflügelprofils zur aerodynamischen Leistungsoptimierung zukünftiger Verkehrsflugzeuge*. PhD thesis, Universität Stuttgart, 2000.

[26] J. N. Kudva. Overview of the DARPA Smart Wing Project. *Journal of Intelligent Material Systems and Structures*, 15:261–267, 2004.

[27] W. B. Spillman Jr, J. S. Sirkis, and P. T. Gardiner. Smart materials and structures: what are they? *Smart Materials and Structures*, 5(3):247–254, 1996.

[28] T. K. Barlas and G. A. M. van Kuik. State of the art and prospectives of smart rotor control for wind turbines. *Journal of Physics: Conference Series*, 75(1):012080, 2007.

[29] L. F. Campanile. Lightweight Shape-Adaptable Airfoils: A New Challenge for an Old Dream. In D. Wagg, I. Bond, P. Weaver, and M. Friswell, editors, *Adaptive Structures: Engineering Applications*, pages 89–135. John Wiley & Sons, Chichester, 2007.

[30] P. C. Chen, D. Sarhaddi, R. Jha, D. D. Liu, K. Griffin, and R. Yurkovich. Variable Stiffness Spar Approach for Aircraft Maneuver Enhancement Using ASTROS. *Journal of Aircraft*, 37(5):865–871, 2000.

[31] M. Amprikidis, J. E. Cooper, and O. Sensburg. Development of An Adaptive Stiffness All-Moving Vertical Tail. In *45th AIAA/ASME/ASCE/AHS/ASC Structures, Structural Dynamics & Materials Conference*, Palm Springs, 2004.

[32] M. Amprikidis and J. E. Cooper. Experimental Validation of Wing Twist Control using Adaptive Internal Structures. In *45th AIAA/ASME/ASCE/AHS/ASC Structures, Structural Dynamics & Materials Conference*, Palm Springs, 2004.

[33] J. E. Cooper. Adaptive Stiffness Structures for Air Vehicle Drag Reduction. In *Multifunctional Structures/Integration of Sensors and Antennas. Meeting Proceedings RTO-MP-AVT-141*, Neuilly-sur-Seine, 2006.

[34] V. Hodigere-Siddaramaiah and J. E. Cooper. On the Use of Adaptive Internal Structures to Optimise Wing Aerodynamic Distribution. In *47th AIAA/ASME/ASCE/AHS/ASC Structures, Structural Dynamics, and Materials Conference*, Newport, 2006.

[35] J. E. Cooper. Adaptive Aeroelastic Structures. In D. Wagg, I. Bond, P. Weaver, and M. Friswell, editors, *Adaptive Structures: Engineering Applications*, pages 137–162. John Wiley & Sons, Chichester, 2007.

[36] J.-B. Runge, D. Osmont, and R. Ohayon. Twist control of airfoils using a "reactive" method. In *Proc. SPIE 7643, Active and Passive Smart Structures and Integrated Systems 2010*, 2010.

[37] J.-B. Runge, D. Osmont, and R. Ohayon. Twist Control of Aerodynamic Profiles by a "Reactive" Method (Experimental Results). In *ASME 2010 Conference on Smart Materials, Adaptive Structures and Intelligent Systems*, 2010.

[38] J.-B. Runge, D. Osmont, and R. Ohayon. Twist Control of Aerodynamic Profiles by a "Reactive" Method: Experimental and Simulation Results. In *21st International Conference on Adaptive Structures and Technologies (ICAST)*, 2010.

[39] J.-B. Runge. *Maîtrise du vrillage de profils aérodynamiques par contrôle «réactif»*. PhD thesis, Conservatoire National des Arts et Métiers, Paris, 2010.

[40] R. M. Ajaj, M. I. Friswell, W. G. Dettmer, G. Allegri, and A. T. Isikveren. Conceptual Modeling of an Adaptive Torsion Wing Structure. In *52nd AIAA/ASME/ASCE/AHS/ASC Structures, Structural Dynamics and Materials Conference*, Denver, 2011.

[41] R. M. Ajaj, M. I. Friswell, W. G. Dettmer, G. Allegri, and A. T. Isikveren. Dynamic modelling and actuation of the adaptive torsion wing. *Journal of Intelligent Material Systems and Structures*, 2012.

[42] R. M. Ajaj, M. I. Friswell, W. G. Dettmer, G. Allegri, and A. T. Isikveren. Performance and control optimisations using the adaptive torsion wing. *The Aeronautical Journal*, 116(1184):1061–1077, 2012.

[43] R. M. Ajaj, M. I. Friswell, W. G. Dettmer, A. T. Isikveren, and G. Allegri. Roll control of a MALE UAV using the adaptive torsion wing. *The Aeronautical Journal*, 117(1189):299–314, 2013.

[44] J.-B. Runge, D. Osmont, and R. Ohayon. Twist control of aerodynamic profiles by a reactive method (experimental results). *Journal of Intelligent Material Systems and Structures*, 24(8):908–923, 2013.

[45] F. Austin, M. J. Rossi, W. Van Nostrand, and G. Knowles. Static Shape Control for Adaptive Wings. *AIAA Journal*, 32(9):1895–1901, 1994.

[46] L. F. Campanile and D. Sachau. The Belt-Rib Concept: A Structronic Approach to Variable Camber. *Journal of Intelligent Material Systems and Structures*, 11(3):215–224, 2000.

[47] F. Gandhi and P. Anusonti-Inthra. Skin design studies for variable camber morphing airfoils. *Smart Materials and Structures*, 17(1):015025, 2008.

[48] J. Manzo and E. Garcia. Demonstration of an in situ morphing hyperelliptical cambered span wing mechanism. *Smart Materials and Structures*, 19(2):025012, 2010.

[49] M. H. Shirk, T. J. Hertz, and T. A. Weisshaar. Aeroelastic Tailoring – Theory, Practice, and Promise. *Journal of Aircraft*, 23(1):6–18, 1986.

[50] U. Stebler. Morphing structures with adaptive cross-sectional properties based on compliance and variable stiffness. Bachelor's thesis, ETH Zurich, 2012.

[51] O. Bilgen, K. B. Kochersberger, D. J. Inman, and O. J. Ohanian. Novel, Bidirectional, Variable-Camber Airfoil via Macro-Fiber Composite Actuators. *Journal of Aircraft*, 47(1):303–314, 2010.

[52] G. A. Lesieutre, J. A. Browne, and M. I. Frecker. Scaling of Performance, Weight, and Actuation of a 2-D Compliant Cellular Frame Structure for a Morphing Wing. *Journal of Intelligent Material Systems and Structures*, 22(10):979–986, 2011.

[53] A. Suleman and P. Moniz. Active Aeroelastic Aircraft Structures. In C. Motasoares, J. Martins, H. Rodrigues, J. Ambrósio, C. Pina, C. Motasoares, E. Pereira, and J. Folgado, editors, *III European Conference on Computational Mechanics*, page 5. Springer Netherlands, 2006.

[54] G. Y. M. Thwapiah. *Shape Adaptation of Active Material Systems Using Aeroelastic Coupling Effects*. PhD thesis, ETH Zurich, 2011.

[55] G. D. Miller. Active Flexible Wing (AFW) Technology. Technical report, Air Force Wright Aeronautical Laboratories, Wright-Patterson Air Force Base, 1988.

[56] J. Onoda, T. Endo, T. Hidehiko, and N. Watanabe. Vibration Suppression by Variable-Stiffness Members. *AIAA Journal*, 29(6):977–983, 1991.

[57] T. Kobori, M. Takahashi, T. Nasu, N. Niwa, and K. Ogasawara. Seismic response controlled structure with active variable stiffness system. *Earthquake Engineering and Structural Dynamics*, 22:925–941, 1993.

[58] I. J. Busch-Vishniac. *Electromechanical Sensors and Actuators*. Springer, New York, 1999.

[59] A. Bergamini. *Electrostatic Modification of the Bending Stiffness of Adaptive Structures*. PhD thesis, ETH Zurich, 2009.

[60] I. K. Kuder, A. F. Arrieta, W. E. Raither, and P. Ermanni. Variable Stiffness Material and Structural Concepts for Morphing Applications. *Progress in Aerospace Sciences*, in press.

[61] http://www.atomicsnow.com.

[62] M. Philen, Y. Shan, C. E. Bakis, K. W. Wang, and C. D. Rahn. Variable Stiffness Adaptive Structures utilizing Hydraulically Pressurized Flexible Matrix Composites with Valve Control. In *47th AIAA/ASME/ASCE/AHS/ASC Structures, Structural Dynamics, and Materials Conference*, Newport, 2006.

[63] Y. Shan, M. Philen, A. Lotfi, S. Li, C. E. Bakis, C. D. Rahn, and K. Wang. Variable Stiffness Structures Utilizing Fluidic Flexible Matrix Composites. *Journal of Intelligent Material Systems and Structures*, 20(4):443–456, 2009.

[64] R. Vos. *Mechanics and Applications of Pressure Adaptive Honeycomb*. PhD thesis, University of Kansas, 2009.

[65] R. Vos and R. Barrett. Mechanics of pressure-adaptive honeycomb and its application to wing morphing. *Smart Materials and Structures*, 20(9):094010, 2011.

[66] O. Mierheim, S. Löser, C. Gregor, and W. Raither. Einsatz instabiler Strukturen zur Formadaption bei Tragflügeln. In *German Aerospace Congress*, pages 755–764, Darmstadt, 2008.

[67] S. Daynes, P. M. Weaver, and K. D. Potter. Aeroelastic Study of Bistable Composite Airfoils. *Journal of Aircraft*, 46(6):2169–2173, 2009.

[68] O. Tabata, S. Konishi, P. Cusin, Y. Ito, F. Kawai, S. Hirai, and S. Kawamura. Micro fabricated tunable bending stiffness devices. *Sensors and Actuators A*, 89:119–123, 2001.

[69] A. Bergamini, R. Christen, and M. Motavalli. Electrostatic tuning of the bending stiffness of simple, slender multi-layer composite structures. In *Proceedings of SPIE 5760, Smart Structures and Materials 2005: Damping and Isolation*, pages 152–163, 2005.

[70] A. Bergamini, R. Christen, B. Maag, and M. Motavalli. A sandwich beam with electrostatically tunable bending stiffness. *Smart Materials and Structures*, 15:678–686, 2006.

[71] F. Gandhi and S.-G. Kang. Beams with controllable flexural stiffness. *Smart Materials and Structures*, 16:1179–1184, 2007.

[72] B. O. Gordon and W. W. Clark. Morphing Structures by way of Stiffness Variations. In *The 48th AIAA/ASME/ASCE/AHS/ASC Structures, Structural Dynamics, and Materials Conference*, Honolulu, USA, 2007.

[73] W. Raither, A. Bergamini, F. Gandhi, and P. Ermanni. Adaptive bending-twist coupling in laminated composite plates by controllable shear stress transfer. *Composites Part A: Applied Science and Manufacturing*, 43(10):1709–1716, 2012.

[74] K. E. Griffin and M. A. Hopkins. Smart Stiffness for Improved Roll Control. In *AIAA 36th Structures, Structural Dynamics and Materials Conference*, New Orleans, 1995.

[75] S. Kuzmina, G. Amiryants, J. Schweiger, J. Cooper, M. Amprikidis, and O. Sensburg. Review and Outlook on Active and Passive Aeroelastic Design Concept for Future Aircraft. In *ICAS 2002*, Toronto, 2002.

[76] J. Cooper, M. Amprikidis, S. Ameduri, A. Concilio, J. S. Millán, and M. Castañón. Adaptive Stiffness Systems for an Active All-Moving Vertical Tail. In *European Conference for Aerospace Sciences*, Moscow, 2005.

[77] M. Dugas. *Ein Beitrag zur Auslegung von Faserverbundtragflügeln im Vorentwurf*. PhD thesis, University of Stuttgart, 2003.

[78] A. Dodworth. Stiffer is better: lessons learned in composites design of lightweight automotive structures. Lecture, Automotive Composites Conference and Exhibition, Troy, 2011.

[79] W. Raither, A. Bergamini, and P. Ermanni. Profile beams with adaptive bending-twist coupling by adjustable shear center location. *Journal of Intelligent Material Systems and Structures*, 24(3):334–346, 2013.

[80] R. Bredt. Kritische Bemerkungen zur Drehungselastizität. *Zeitschrift des Vereines deutscher Ingenieure*, 40(29):813–817, 1896.

[81] A. Föppl. Der Drillungswiderstand von Walzeisenträgern. *Zeitschrift des Vereines deutscher Ingenieure*, 61(33):694–695, 1917.

[82] L. Euler. *Methodus inveniendi lineas curvas maximi minimive proprietate gaudentes, sive solutio problematis isoperimetrici latissimo sensu accepti*. Bousquet, Lausanne/Geneva, 1744.

[83] C. L. M. H. Navier. *Résumé des leçons données à l'Ecole des ponts et chaussées sur l'application de la mécanique à l'établissement des constructions et des machines*. Firmin Didot, Paris, 1826.

[84] S. P. Timoshenko. On the correction for shear of the differential equation for transverse vibrations of prismatic bars. *Philosophical Magazine Series 6*, 41(245):744–746, 1921.

[85] H. Wagner and W. Pretschner. Verdrehung und Knickung von offenen Profilen. *Luftfahrtforschung*, 11:174–180, 1934.

[86] F. W. Bornscheuer. Systematische Darstellung des Biege- und Verdrehvorganges unter besonderer Berücksichtigung der Wölbkrafttorsion. *Der Stahlbau*, 21:1–9, 1952.

[87] C. Kaiser. *Elastische Kopplungen in aktiven und passiven Laminaten sowie dünnwandigen Faserverbundbalken*. PhD thesis, Technische Universität München, 1999.

[88] W. M. Kutta. Habilitation treatise, unpublished, 1902.

[89] N. Joukowsky. Über die Konturen der Tragflächen der Drachenflieger. *Zeitschrift für Flugtechnik und Motorluftschiffahrt*, 1(22):281–284, 1910.

[90] W. M. Kutta. Auftriebskräfte in strömenden Flüssigkeiten. *Illustrierte aeronautische Mitteilungen*, 6:133–135, 1902.

[91] N. Joukowsky. Über die zugeteilten Wirbel. *Arbeiten der Physikalischen Sektion der Kaiserlichen Gesellschaft der Freunde der Naturkunde und Ethnologie*, 13(2), 1906.

[92] W. Kutta. Über eine mit den Grundlagen des Flugproblems in Beziehung stehende zweidimensionale Strömung. *Sitzungsberichte der Königlich Bayerischen Akademie der Wissenschaften. Mathematisch-physikalische Klasse*, 2:3–58, 1910.

[93] D. W. Lobitz and P. S. Veers. Load Mitigation with Bending/Twist-coupled Blades on Rotors Using Modern Control Strategies. *Wind Energy*, 6:105–117, 2003.

[94] A. Bergamini, R. Christen, M. Motavalli, and P. Ermanni. Distributed damping of large structures. In *19th International Conference on Adaptive Structures and Technologies (ICAST)*, Ascona, 2008.

[95] R. Ginés, A. Bergamini, R. Christen, M. Motavalli, and P. Ermanni. Frictional behaviour of polymer films under mechanical and electrostatic loads. *Smart Materials and Structures*, 22:075023, 2013.

[96] J. N. Kudva, K. Appa, A. P. Jardine, C. A. Martin, and B. F. Carpenter. Overview of recent progress on the DARPA/USAF Wright Laboratory Smart Materials and Structures Development–Smart Wing program. In *Proc. SPIE 3044, Smart Structures and Materials 1997: Industrial and Commercial Applications of Smart Structures Technologies*, pages 24–32, 1997.

[97] R. L. Wegel and H. Walther. Internal dissipation in solids for small cyclic strains. *Physics*, 6(4):141–157, 1935.

[98] L. H. Sperling. *Introduction to Physical Polymer Science*, chapter Glass-rubber transition behavior, pages 349–425. John Wiley & Sons, Hoboken, 4th edition, 2006.

[99] W. Raither, M. Heymanns, A. Bergamini, and P. Ermanni. Morphing wing structure with controllable twist based on adaptive bending-twist coupling. *Smart Materials and Structures*, 22(6):065017, 2013.

[100] L. E. Nielsen and R. F. Landel. *Mechanical Properties of Polymers and Composites*. Marcel Dekker, New York, 2nd edition, 1994.

[101] J. Duncan. *Principles and Applications of Thermal Analysis*, chapter Principles and Applications of Mechanical Thermal Analysis, pages 119–163. Blackwell Publishing, Oxford, 2008.

[102] S. Alford and M. Dole. Specific Heat of Synthetic High Polymers. VI. A Study of the Glass Transition in Polyvinyl Chloride. *Journal of the American Chemical Society*, 77(18):4774–4777, 1955.

[103] I. S. Elashmawi, N. A. Hakeem, L. K. Marei, and F. F. Hanna. Structure and performance of ZnO/PVC nanocomposites. *Physica B: Condensed Matter*, 405(19):4163 – 4169, 2010.

[104] R. M. Christensen. *Theory of Viscoelasticity*. Academic Press, New York, 2nd edition, 1982.

[105] W. Hovgaard. The stress distribution in welded overlapped joints. *Proceedings of the National Academy of Science of the United States of America*, 16(11):673–678, 1930.

[106] O. Volkersen. Die Nietkraftverteilung in zugbeanspruchten Nietverbindungen mit konstanten Laschenquerschnitten. *Luftfahrtforschung*, 15:41–47, 1938.

[107] M. Arias. *Experimentelle Untersuchung des kontinuierlichen und gepulsten Widerstandsschweissen als Fügeverfahren zur Herstellung von Faserverbundbauteilen mit thermoplastischer Matrix*. PhD thesis, ETH Zurich, 1998.

[108] E. Baur, S. Brinkmann, T. Osswald, and E. Schmachtenberg. *Saechtling Kunststoff-Taschenbuch*. Carl Hanser Verlag, München, 2007.

[109] G. Becker and D. Braun. *Kunststoff-Handbuch. Polyvinylchlorid*. Carl Hanser Verlag, München, 1986.

[110] H. Schlichting and E. Truckenbrodt. *Aerodynamik des Flugzeuges. Erster Band*. Springer, Berlin, 3rd edition, 2001.

[111] *Type-Certificate. Data Sheet. ASW 27*. EASA, 2008.

[112] F. W. Lanchester. *Aerodynamics: Constituting the First Volume of a Complete Work on Aerial Flight*. A. Constable & Co., London, 1907.

[113] L. Prandtl and A. Betz. Vier Abhandlungen zur Hydrodynamik und Aerodynamik. *Selbstverlag des Kaiser Wilhelm-Instituts für Strömungsforschung*, 1927.

[114] J. D. Anderson. *Fundamentals of Aerodynamics*. McGraw-Hill, New York, 2001.

[115] H. Reissner. Neuere Probleme aus der Flugzeugstatik. *Zeitschrift für Flugtechnik und Motorluftschiffahrt*, 17(18):137–146, 1926.

[116] R. L. Bisplinghoff and H. Ashley. *Principles of Aeroelasticity*. John Wiley & Sons, New York, 1962.

[117] J. C. Maxwell. *A Treatise on Electricity and Magnetism*, volume 1. Clarendon Press, Oxford, 1873.

[118] L. Di Lillo. *Dielectrics for Variable Stiffness Elements*. PhD thesis, ETH Zurich, 2013.

[119] L. Di Lillo, A. Bergamini, D. A. Carnelli, and P. Ermanni. Frequency-dependent dielectric response model for polyimide poly(vinilydenefluoride) multilayered dielectrics. *Applied Physics Letters*, 101(1):012906, 2012.

[120] A. Bergamini, R. Christen, and M. Motavalli. Electrostatically tunable bending stiffness in a GFRP CFRP composite beam. *Smart Materials and Structures*, 16(3):575–582, 2007.

[121] W. Raither, E. Furger, M. Zündel, A. Bergamini, and P. Ermanni. Variable-stiffness skin concept for camber-morphing airfoils. 24th International Conference on Adaptive Structures Technologies (ICAST), 2013.

[122] M. Zündel. Experimental investigation of morphing airfoils with variable-stiffness skin. Semester project, ETH Zurich, 2013.

[123] L. Di Lillo, W. Raither, A. Bergamini, M. Zündel, and P. Ermanni. Tuning the mechanical behaviour of structural elements by electric fields. *Applied Physics Letters*, 102(22):224106, 2013.

[124] Radiant Light Film CM500. Technical Data. 3M Industrial Adhesives and Tapes Division, 2006.

[125] W. Raither, L. De Simoni, L. Di Lillo, A. Bergamini, and P. Ermanni. Adaptive-Twist Airfoil Based on Electrostatic Stiffness Variation. In *22nd AIAA/ASME/AHS Adaptive Structures Conference*, National Harbor, 2014.

[126] F. W. Lanchester. Torsional vibrations of the tail of an aeroplane. *Reports and Memoranda of the Aeronautical Research Council*, 276:458–460, 1916.

[127] L. Bairstow and A. Fage. Oscillations of the tail plane and body of an aeroplane. *Reports and Memoranda of the Aeronautical Research Council*, 276, 1916.

[128] D. H. Hodges and G. A. Pierce. *Introduction to Structural Dynamics and Aeroelasticity*. Cambridge University Press, Cambridge, 2002.

[129] ASW 27 B. Alexander Schleicher GmbH & Co., 2003.

[130] G. Heinrich, editor. *Advanced Rubber Composites*. Springer, Berlin, 2011.

[131] W. C. Roentgen. Ueber die durch Electricität bewirkten Form- und Volumenänderung von dielektrischen Körpern. *Annalen der Physik und Chemie*, 11:771–786, 1880.

[132] R. Pelrine, R. Kornbluh, Q. Pei, and J. Joseph. High-Speed Electrically Actuated Elastomers with Strain Greater Than 100%. *Science*, 287(5454):836–839, 2000.

[133] R. Pelrine, P. Sommer-Larsen, R. D. Kornbluh, R. Heydt, G. Kofod, Q. Pei, and P. Gravesen. Applications of dielectric elastomer actuators. In *Smart Structures and Materials 2001: Electroactive Polymer Actuators and Devices*, volume 4329, pages 335–349, 2001.

[134] D. S. Adams, D. E. Bowles, and C. T. Herakovich. Thermally Induced Transverse Cracking in Graphite-Epoxy Cross-Ply Laminates. *Journal of Reinforced Plastics and Composites*, 5(3):152–169, 1986.

[135] G. A. Owens and S. E. Schofield. Thermal Cycling and Mechanical Property Assessment of Carbon Fiber (Fabric) Reinforced PMR-15 Polyimide Laminates. *Composites Science and Technology*, 33:177–190, 1988.

[136] K. Ahlborn. Durability of carbon fibre reinforced plastics with thermoplastic matrices under cyclic mechanical and cyclic thermal loads at cryogenic temperatures. *Cryogenics*, 31(4):257–260, 1991.

[137] S. Kobayashi, K. Terada, and N. Takeda. Evaluation of long-term durability in high temperature resistant CFRP laminates under thermal fatigue loading. *Composites Part B: Engineering*, 34(8):753–759, 2003.

[138] M. Kar and S. Bahadur. Micromechanism of wear at polymer-metal sliding interface. *Wear*, 46(1):189–202, 1978.

[139] J. Mens and A. de Gee. Friction and wear behaviour of 18 polymers in contact with steel in environments of air and water. *Wear*, 149(1–2):255–268, 1991.

[140] N. Maeda, N. Chen, M. Tirrell, and J. N. Israelachvili. Adhesion and friction mechanisms of polymer-on-polymer surfaces. *Science*, 297(5580):379–382, 2002.

[141] N. Myshkin, M. Petrokovets, and A. Kovalev. Tribology of polymers: Adhesion, friction, wear, and mass-transfer. *Tribology International*, 38:910–921, 2006.

[142] High Performance Films. Kapton polyimide film. DuPont Films.

[143] B. J. Briscoe, B. Scruton, and F. R. Willis. The shear strength of thin lubricant films. *Proceedings of the Royal Society of London. A. Mathematical and Physical Sciences*, 333(1592):99–114, 1973.

[144] J. K. A. Amuzu, B. J. Briscoe, and D. Tabor. Friction and shear strength of polymers. *ASLE Transactions*, 20(4):354–358, 1977.

[145] K. Liu and M. Piggott. Shear strength of polymers and fibre composites: 1. thermoplastic and thermoset polymers. *Composites*, 26(12):829–840, 1995.

[146] K. C. Shin, J. J. Lee, and D. G. Lee. A study on the lap shear strength of a co-cured single lap joint. *Journal of Adhesion Science and Technology*, 14(1):123–139, 2000.

[147] L. F. M. da Silva, T. N. S. S. Rodrigues, M. A. V. Figueiredo, M. F. S. F. de Moura, and J. A. G. Chousal. Effect of adhesive type and thickness on the lap shear strength. *The Journal of Adhesion*, 82(11):1091–1115, 2006.

[148] R. Aniversario, S. Harvey, J. McCarty, J. Parsons, and D. Peterson. Design, Ancillary Testing, Analysis, and Fabrication Data for the Advanced Composite Stabilizer for Boeing 737 Aircraft. Volume 1. Technical Summary. Technical report, DTIC Document, 1983.

[149] *Accelerated Aging of Materials and Structures: The Effects of Long-Term Elevated-Temperature Exposure*. Committee on Evaluation of Long-Term Aging of Materials and Structures Using Accelerated Test Methods. National Materials Advisory Board. Commission on Engineering and Technical Systems. National Research Council. National Academy Press, 1996.

[150] J. Jenkins, R. Field, and W. Sefic. Elevated-temperature effects on strain gages on the YF-12A wing. *Experimental Mechanics*, 19(3):81–86, 1979.

[151] E. Hau. *Wind Turbines. Fundamentals, Technologies, Application, Economics*. Springer, Berlin, 2006.

[152] M. Uman and V. Rakov. The interaction of lightning with airborne vehicles. *Progress in Aerospace Sciences*, 39(1):61–81, 2003.

[153] D. Carbonaro. Compliant buckling mechanism for aeroelastic passive morphing of a wing structure. Semester project, ETH Zurich, 2013.

[154] E. Furger. Variable-camber morphing airfoils with adaptive stiffness. Semester project, ETH Zurich, 2012.

A Appendix

A.1 Supplementary data

Material properties

Table A.1: Elastic properties [99] applied in calculations of chapter 4

	E_{11} [GPa]	E_{22} [GPa]	G_{12} [GPa]	ν_{12} [–]
Aluminium	60.6	$= E_{11}$	$= \frac{E_{11}}{2\left(1+n_{12}\right)}$	0.3
CFRP (unidirectional ply)	94.4	6.45	3.77	0.27
CFRP (cross ply)	95.4	$= E_{11}$	3.87	0.023
GFRP (cross ply)	23.8	$= E_{11}$	3.41	0.11
AFRP (cross ply)	34.7	$= E_{11}$	1.88	0.05

Table A.2: Elastic properties applied in calculations of chapter 5

	E_{11} [GPa]	E_{22} [GPa]	G_{12} [GPa]	ν_{12} [–]
Aluminium	73.1	$= E_{11}$	$= \frac{E_{11}}{2\left(1+n_{12}\right)}$	0.33
Copper	110	$= E_{11}$	$= \frac{E_{11}}{2\left(1+n_{12}\right)}$	0.35
Polyimide	3	$= E_{11}$	$= \frac{E_{11}}{2\left(1+n_{12}\right)}$	0.34
Steel	210	$= E_{11}$	$= \frac{E_{11}}{2\left(1+n_{12}\right)}$	0.3
CFRP (unidirectional ply)	100.0	8.0	5.0	0.28
GFRP (cross ply)	18	$= E_{11}$	3.5	0.13

Table A.3: Mass density values applied in the flutter calculations of chapter 5

	CFRP	GFRP	Aluminium
Mass density [kg/m^3]	1'550	1'800	2'780

Laminate properties

Table A.4: Lay-up and total thickness t of the laminates used for the different structural elements of the adaptive-twist airfoil based on thermomechanical coupling

Component	Ply material	Stacking angles [°]	t [mm]
Wing box flanges	CFRP (UD)	$[[0; 90]_s]_s$	1.2
Front spar	GFRP	[0/90; 0/90; ±45; 0/90; 0/90]	1.3
Rear spar	GFRP	[0/90; 0/90; ±45; 0/90; 0/90]	1.3
Skin	CFRP (UD)	$[0; 90]_s$	0.6
Ribs	CFRP (UD)	[90; 45; -45; 0; -45; 45; 90]	1.1

Table A.5: Lay-up of the laminates used for different structural elements of the adaptive-twist airfoil based on electromechanical coupling

Component	Ply material	Stacking angles [°]
Skin	CFRP	$[0; 60; -60]_s$
Ribs	GFRP	[0/90]

Detailed properties of experimental adaptive-twist airfoil based on thermomechanical coupling

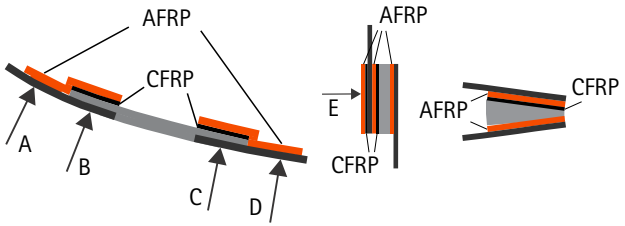

Figure A.1: Detail design of variable-stiffness interfaces in the experimental adaptive-twist airfoil based on thermomechanical coupling. For the according values see table A.6.

Table A.6: Total wall thickness and overlap width in mm at certain locations of the experimental adaptive-twist airfoil based on thermomechanical coupling. The locations are specified in figures A.2 and A.1.

Location	A	B	C	D	E	F	G	H	I
Thickness	2.7	3.8	3.7	2.7	7.9	3.1	3.0	3.0	4.3
Width	14.1	9.3	9.6	14.5	7.0	15.5	15.2	16.3	15.2

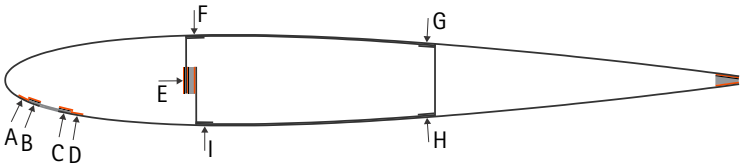

Figure A.2: Geometry of experimental adaptive-twist airfoil based on thermomechanical coupling. For the according values see table A.6.

A.2 Publications

Journal articles

1. Wolfram Raither, Andrea Bergamini, Farhan Gandhi, and Paolo Ermanni. Adaptive bending-twist coupling in laminated composite plates by controllable shear stress transfer. *Composites Part A: Applied Science and Manufacturing*, 43(10):1709–1716, 2012.

2. Wolfram Raither, Andrea Bergamini, and Paolo Ermanni. Profile beams with adaptive bending-twist coupling by adjustable shear center location. *Journal of Intelligent Material Systems and Structures*, 24(3): 334–346, 2013.

3. Wolfram Raither, Matthias Heymanns, Andrea Bergamini, and Paolo Ermanni. Morphing wing structure with controllable twist based on adaptive bending-twist coupling. *Smart Materials and Structures*, 22(6):065017, 2013.

4. Luigi Di Lillo, Wolfram Raither, Andrea Bergamini, Manuel Zündel, and Paolo Ermanni. Tuning the mechanical behaviour of structural elements by electric fields. *Applied Physics Letters*, 102(22):224106, 2013.

5. Izabela Kuder, Andres Arrieta, Wolfram Raither, and Paolo Ermanni. Variable stiffness material and structural concepts for morphing applications. *Progress in Aerospace Sciences*, 63:33–55, 2013.

Conference contributions

1. Wolfram Raither, Andrea Bergamini, and Paolo Ermanni. Adaptive Coupling in Composite Plates. In *5th International Conference on Composites Testing and Model Identification*, Lausanne, Switzerland, February 14–16, 2011.

2. Wolfram Raither, Andrea Bergamini, and Paolo Ermanni. Profile Beams with Adaptive Bending-Twist Coupling by Adjustable Shear Center Location. In *22nd International Conference on Adaptive Structures Technologies (ICAST)*, Corfu, Greece, October 10–12, 2011.

3. Wolfram Raither, Matthias Heymanns, Andrea Bergamini, and Paolo Ermanni. Morphing airfoil with adaptive bending-twist coupling. In *Deutscher Luft- und Raumfahrtkongress 2012*, Berlin, Germany, September 10–12, 2012.

4. Luigi Di Lillo, Wolfram Raither, Claudio Di Fratta, Andrea Bergamini, and Paolo Ermanni. Mechanical characterization of electro bonded laminates. In *ASME 2012 Conference on Smart Materials, Adaptive Structures and Intelligent Systems*, Stone Mountain, Georgia, USA, September 19–21, 2012.

5. Wolfram Raither, Matthias Heymanns, Andrea Bergamini, and Paolo Ermanni. Morphing wing structure based on variable coupling stiffness. In *23rd International Conference on Adaptive Structures Technologies (ICAST)*, Nanjing, China, October 11–13, 2012.

6. Wolfram Raither, Emian Furger, Manuel Zündel, Andrea Bergamini, and Paolo Ermanni. Variable-stiffness skin concept for camber-morphing airfoils. In *24th International Conference on Adaptive Structures Technologies (ICAST)*, Aruba, Netherlands, October 7–9, 2013.

7. Luigi Di Lillo, Wolfram Raither, Manuel Zündel, Andrea Bergamini, and Paolo Ermanni. Electrostatic tuning of the mechanical behaviour of structural elements. In *24th International Conference on Adaptive Structures Technologies (ICAST)*, Aruba, Netherlands, October 7–9, 2013.

8. Wolfram Raither, Luca De Simoni, Luigi Di Lillo, Andrea Bergamini, and Paolo Ermanni. Adaptive-Twist Airfoil Based on Electrostatic Stiffness Variation. In *22nd AIAA/ASME/AHS Adaptive Structures Conference*, National Harbor, Maryland, USA, January 13–17, 2014.

Related student theses

1. Matthias Heymanns, *Bending-twist coupled adaptive airfoil with a smart skin*. Master's thesis, ETH Zurich, 2012.

2. Urs Stebler, *Morphing structures with adaptive cross-sectional properties based on compliance and variable stiffness*. Bachelor's thesis, ETH Zurich, 2012.

3. Emian Furger, *Variable-camber morphing airfoils with adaptive stiffness.* Semester project, ETH Zurich, 2012.

4. Dario Carbonaro, *Compliant buckling mechanism for aeroelastic passive morphing of a wing structure.* Semester project, ETH Zurich, 2013.

5. Manuel Zündel, *Experimental investigation of morphing airfoils with variable-stiffness skin.* Semester project, ETH Zurich, 2013.

6. Andreas Reber, *Morphing wing box with integrated electro-bonded laminates.* Bachelor's thesis, ETH Zurich, 2013.

7. Cecilia Valluchi, *Realization of a morphing wing with adaptive bending-twist coupling based on electrostatic stiffness variation.* Master's thesis, ETH Zurich, 2013.

8. Luca de Simoni, *Aeroelastic behaviour of a morphing wing with adaptive bending-twist coupling based on electrostatic stiffness variation.* Master's thesis, ETH Zurich, 2013.

A.3 About the author

Wolfram Raither was born in 1984 in Filderstadt, Germany, and received his school education in the Lake Constance Area. He studied Mechanical Engineering and Aerospace Engineering at ETH Zurich and at the Technical University of Berlin. In 2008, he obtained the bachelor degree from ETH. Wolfram Raither graduated from ETH Zurich in 2010 with a Master's thesis entitled "Adaptive Coupling in Laminated Composite Plates" that was awarded the ETH Medal. He began his doctoral studies at the Centre of Structure Technologies of ETH Zurich in September 2010 and defended the thesis contained in this book on February 27th 2014.

List of figures

List of tables